Heat Transport Phenomenon in Fluid Flows over a Stretching Sheet

By

<u>Tanzila Hayat</u>

Department of Mathematics
Quaid-i-Azam University
Islamabad, Pakistan

2019

Heat Transport Phenomenon in Fluid Flows over a Stretching Sheet

By

Tanzila Hayat

Supervised By

Prof. Dr. Sohail Nadeem

Department of Mathematics
Quaid-i-Azam University
Islamabad, Pakistan

2019

Heat Transport Phenomenon in Fluid Flows over a Stretching Sheet

By

Tanzila Hayat

A Thesis Submitted for the Partial Fulfillment of the Requirements for the

Degree of

DOCTOR OF PHILOSOPHY

in

MATHEMATICS

Supervised By

Prof. Dr. Sohail Nadeem

Department of Mathematics
Quaid-i-Azam University
Islamabad, Pakistan

2019

Heat Transport Phenomenon in Fluid Flows over a Stretching Sheet

By

Tanzila Hayat

CERTIFICATE

A DISSERTATION SUBMITTED IN THE PARTIAL FULFILLMENT OF THE REQUIREMENTS FOR THE DEGREE OF THE DOCTOR OF

PHILOSOPHY

We accept this dissertation as conforming to the required standard

1. ____________________________
Prof. Dr. Sohail Nadeem
(Chairman)

2. ____________________________
Prof. Dr. Sohail Nadeem
(Supervisor)

3. Tanvir Akbar
Dr. Tanvir Akbar Kiani

Department of Mathematics
COMSATS University
Park Road Chak Shahzad,
Islamabad

4. ____________________________
Dr. Noreen Sher Akbar

Department of Basic Humanities
CE&ME, (NUST)
Peshawar Road Rawalpindi

Department of Mathematics
Quaid-I-Azam University
Islamabad, Pakistan
2019

Certificate of Approval

This is to certify that the research work presented in this thesis entitled **Heat Transport Phenomenon in Fluid Flows over a Stretching Sheet** was conducted by Mrs. **Tanzila Hayat** under the kind supervision of **Prof. Dr. Sohail Nadeem**. No part of this thesis has been submitted anywhere else for any other degree. This thesis is submitted to the Department of Mathematics, Quaid-i-Azam University, Islamabad in partial fulfillment of the requirements for the degree of Doctor of Philosophy in field of Mathematics from Department of Mathematics, Quaid-i-Azam University Islamabad, Pakistan.

Student Name: **Tanzila Hayat** Signature:____________

External committee:

a) **External Examiner 1**: Signature: Tanvir Akbar

Name: **Dr. Tanvir Akbar Kiani**

Designation: Assistant Professor

Office Address: Department of Mathematics, COMSATS University Park road Chak Shahzad, Islamabad.

b) **External Examiner 2**: Signature:____________

Name: **Dr. Noreen Sher Akbar**

Designation: Assistant Professor

Department of Basic Humanities

CE&ME, (NUST)

Peshawar Road Rawalpindi

c) **Internal Examiner** Signature:____________

Name: **Dr. Sohail Nadeem**

Designation: Professor

Office Address: Department of Mathematics, QAU Islamabad.

Supervisor Name: Signature:____________

Prof. Dr. Sohail Nadeem

Name of Dean/ HOD Signature:____________

Prof. Dr. Sohail Nadeem

Author’s Declaration

I Tanzila Hayat hereby state that my PhD thesis titled Heat Transport Phenomenon in Fluid Flows over a Stretching Sheet is my own work and has not been submitted previously by me for taking any degree from the Quaid-i-Azam University Islamabad, Pakistan or anywhere else in the country/world.

At any time if my statement is found to be incorrect even after my graduate the university has the right to withdraw my PhD degree.

Name of Student: Tanzila Hayat

Date: 8-09-2019

Plagiarism Undertaking

I solemnly declare that research work presented in the thesis titled "Heat Transport Phenomenon in Fluid Flows over a Stretching Sheet" is solely my research work with no significant contribution from any other person. Small contribution/help wherever taken has been duly acknowledged and that complete thesis has been written by me.

I understand the zero tolerance policy of the HEC and Quaid-i-Azam University towards plagiarism. Therefore, I as an Author of the above titled thesis declare that no portion of my thesis has been plagiarized and any material used as reference is properly referred/cited.

I undertake that if I am found guilty of any formal plagiarism in the above titled thesis even afterward of PhD degree, the University reserves the rights to withdraw/revoke my PhD degree and that HEC and the University has the right to publish my name on the HEC/University Website on which names of students are placed who submitted plagiarized thesis.

Student/Author Signature:

Name: Tanzila Hayat

Dedication

This work is dedicated to the one and only, ever flowing fountain of encouragement, love, support, belief and motivation

"My beloved Dad"

ACKNOWLEDGEMENT

*This task would never have been accomplished if the will of **Allah** and His blessings had not been with me. I am ever grateful to Allah Almighty for taking all the right choices through-out my life and bringing right people at the right juncture because of which I have been able to attain success. Intellectually I am indebted to my supervisor, **Dr. Sohail Nadeem**. He has been my mentor, an encouraging, guiding force who has helped me in my pursuit of knowledge.*

*My emotional life line has been my **Father.** Despite being a single parent and so many challenges in life including personal health, he has always been my guiding star. I am also thankful to my **siblings** for being patient with my hectic schedule and being supportive.*

*I am thankful to my sweet **husband** for being so understanding, cooperative and helpful through-out this task.*

*My respected Senior **Dr. Waqar Azeem** Bhai has proved to be a cooperative colleague, a friend and a guide through difficult times.*

*Some other positive influences during my thesis have been my seniors **Syed Tayyab Hussain**, **Hina**, **Rizwan ul Haq**, **Arif ullah Khan**, all my Lab Fellows, especially **Naeem Ullah**, my colleagues **Latif Bhai** and **Irfan** and special thanks to my dear best friends **Maryam**, **Sadia**,*

__Nuzhat__, __Aqsa__, __Humaira__ and __Madiha__ who are very close to my heart. I am thankful to all of them from the bottom of my heart.

My thesis is an outcome of the support system that consisted of all the above mentioned respected teachers, colleagues, friends and family. I owe this accomplishment to all of them.

Tanzila Hayat

TABLE OF CONTENTS

NOMENCLATURE

$2D$	Two dimensional
$3D$	Three dimensional
(u, v, w)	Velocity components
ODE	Ordinary differential equation
λ	Stretching parameter
PDE	Partial differential equation
HAM	Homotopy analysis method
T	Fluid's temperature
M	Magnetic parameter
T_w	Fluid's temperature at wall
β^0	Thermal expansion coefficient
T_∞	Ambient temperature
r	Gravity dependent parameter
$(\gamma_1, \gamma_2, \gamma_3, \gamma_4)$	Constants
Nc	Convective parameter
(a, b, c)	Stretching rates
α_{hnf}	Thermal diffusivity of hybrid nanofluid
ϕ	Nanoparticle volume fraction of hematite
$\Pr$	Prandtl number
ϕ_1	Nanoparticle volume fraction of copper oxide
$(\nu_f, \nu_{nf}, \nu_{hnf})$	Kinematic viscosity of (fluid, nanofluid, hybrid nanofluid)
ϕ_2	Nanoparticle volume fraction of silver
$((\mathrm{C}_p)_f, (\mathrm{C}_p)_{nf}, (\mathrm{C}_p)_{hnf})$	Specific heat capacity of (fluid, nanofluid, hybrid nanofluid)
Ec	Eckert number
$(\mathrm{K}_f, \mathrm{K}_{nf}, \mathrm{K}_{hnf})$	Thermal conductivity of (fluid, nanofluid, hybrid nanofluid)
$((\mathrm{C}_p)_{s1}, (\mathrm{C}_p)_{s2})$	Specific heat capacity of nanoparticles
$(\mathrm{K}_{s1}, \mathrm{K}_{s2})$	Thermal conductivity of nanoparticles
w^*	Angular velocity

Ω	Rotation parameter
$(\rho_f, \rho_{nf}, \rho_{hnf})$	Density of (fluid, nanofluid, hybrid nanofluid)
β_{hnf}	Concentration diffusivity of hybrid nanofluid
Q	Dimensional heat generation / absorption coefficient
ξ_1	Constant rate of 1^{st} order chemical reaction
$\vec{q}_r$	Radiation flux
σ^*	Stefan-Boltzman constant
ϱ	Mean absorption coefficient
R	Radiation parameter
Sc	Schmidt number for chemical reactions
R_{c1}	Chemical reaction constraint
k	Velocity slip factor
δ_1	Heat generation parameter
α	Velocity slip parameter
β	Thermal jump parameter
$\vec{\tau}_{ij}$	Extra stress tensor
(Ω_1, σ_1)	Properties of Eyring-Powell fluid
(A_1, A_2)	Chemical species
(a_1, a_2)	Concentrations of chemical species
(k_r, k_s)	Rate constants
$\vec{q}$	Heat flux
λ_e	Heat flux relaxation time
$(a_1)_0$	Positive dimensionless constant
$(\mathrm{F}_{A_1}, F_{A_2})$	Coefficients of diffusion species (A_1, A_2)
$(\gamma, \varepsilon_1, \varepsilon_2)$	Parameters of Eyring-Powell fluid
Le	Lewis number
l	Thermal slip factor
α_1	thermal relaxation parameter
χ	Ratio of diffusion coefficient

k_∞	Fluid's thermal conductivity far away from the plane
j	heterogeneous reaction strength
Λ	Dimensionless thermal relaxation time
$\vec{J}$	Mass flux
C	Concentration of the fluid
C_∞	Ambient Concentration
D_B	Brownian diffusivity
λ_c	Relaxation time of mass flux
σ_2	Homogeneous reaction strength
$k(T)$	Temperature dependent thermal conductivity
L	Reference length
Λ_1	Dimensionless relaxation time of concentration
Sc_b	Schmidt number
$(a_1)_0$	Positive dimensional constant
Θ	Variable thermal conductivity parameter
Re	Local Reynolds number

Chapter 1

Introduction

Heat transfer is an ubiquitous process occurring in nature. In an incompressible fluid, this phenomenon has attained broad consideration because of its utilization and developments in industry. These developments include rolling the steel at high temperature, metal extrusion, metal working process, paper production, glass fiber production, crystal flowing. Ostrach [1] evaluated these applications. Crane [2] investigated 2D flow for a stretched surface. He analyzed Nusselt number and skin friction. Wang [3] considered the 3D flow by utilizing the stretched surface. Later on, this work is extended by many investigators $[4-15]$ by considering different geometries. Some other applications related to stretching surface may be found in $[16-19]$. However flow analyses over exponentially stretching sheets are examined sparsely $[20-24]$. Magyari and Keller [25] scrutinized the influence of viscous fluid induced by exponentially stretching surface. The heat transport phenomenon in a nanofluid flow produced by exponentially stretching sheet was beautifully analyzed by Nadeem and Lee [26].

Nanofluids are a classification of heat transfer fluids which are engineered suspension nanoparticles(1-100nm) dispersed in the fluid. Usually base fluids incorporate water, organic fluids (e.g. ethylene, triethylene and so on) engine oil, polymeric solutions, bio-fluids and other base fluids. Medium normally utilized as nanoparticles encompass carbon in different structures (e.g. carbon nanotubes, graphite, diamond) metals (e.g. copper, silver, gold), metal oxides (e.g titania, zirconia) and functionalized nanoparticles. Utilization of nanofluids has found an extensive variety of potential applications. Choi was the first one to study enhancement of thermal conductivity in nanofluids [27]. As indicated by applications, nanofluids are listed as heat transfer fluids, bio and pharmaceutical nanofluids, medicinal nanofluids, environmental nanofluids etc. Numerous analysts contemplated how the size, concentration, shape and other properties influence heat transfer rate of fluid. The fusion of specialized liquids which are designed to enhance performance of heat transfer has turned out to be progressively appealing lately. So this subject has tempted vast interest from analysts as a result of fascinating properties and applications [$28-37$]. Chen et al. [38] presented an approach to estimate thermal conductivity of liquid having nano-sized particles, depend on their rheological properties. Zhou et al. [39] examined aspects of conductivity for different variety of mixtures. Heat transfer enhancement and thermal conductivity in nanofluids had been studied by [40]. Kabeel et al. [41] examined the performance of heat transfer of plate with alumina-water nanofluid and water-water fluids. Significance and importance of nanofluids to increase the heavy duty engine and automotive cooling rates was explained by Peyghambarzadeh et al. [42]. The improvement in heat transfer with the help of nanoparticles concentration and flow conditions was considered in [43]. Duangthongsuk and Wongwises [44] exposed difference among experimental data and computed thermophysical properties of nanofluids on heat transport phenomena. Quiet recently numerous experiments have been done with variety of nanoparticles suspended in base liquid named as "Hybrid Nanofluid", cutting edge nanofluid. These are reasonably a new class of nanofluids which have enormous applications in different heat transport phenomenon. When nano-sized particles are dispersed appropriately, hybrid nanoparticles offer colossal benefit having exceptional thermal conductivity. Particularly, nanofluid flow is well-known for high heat transport as compared to simple liquid. To improve it even more, hybrid nanofluid is instigated. Many experimental research articles have been published with the concept of hybrid nanofluid. Momin [45] carried out a study of mixed convection for laminar flow with $(Al_2O_3 - Cu/H_2O)$. Study on synthesize $(Al_2O_3 - Cu/H_2O)$ of hybrid nanofluid was examined by Suresh et al [46]. Further, Suresh et al. [47] explored effects of $(Al_2O_3 - Cu/H_2O)$ hybrid nanofluid in heat transfer. The pressure drop properties of hybrid nanofluid was scrutinized by suresh et al. [48].

Heat transport occurs due to temperature gradient in the medium. Later, Cattaneo [50] extended this law by adding relaxation time. Christov [51] had given detailed analysis of energy equation for the examination of heat transfer process. After that, researchers and analysts have demonstrated Cattaneo- Christov heat flux hypothesis for viscous as well as Non-Newtonian flows for different geometries presented in [52-56]. Study of liquid flows with chemical reaction has immensely attracted recent researchers. These flows are consequential in various procedures. For sure homogeneous-heterogeneous reactions occur in these procedures. These reactions in a time independent, viscous, boundary layer flow have been firstly considered by Chaudhary and Merkin [57]. Bachok et al. [58] examined the aspects of chemical mechanisms for stretched flow. Khan and Pop [59] studied impact of chemical mechanisms by considering viscoelastic liquid.

Study of non-Newtonian liquids has achieved considerable scrutiny in fluid mechanic's theory. The fluids which don't comply with Newtonian's law of viscosity are dropped into a class of non-Newtonian liquids. In perspective of the various attributes of these liquids, various non-Newtonian liquids model have been presented in literature. Eyring- Powell fluid model $[60-63]$ is one of non-Newtonian models. In 1944, a complete mathematical modelling of Eyring–Powell fluid [64] presented by Eyring and Powell. Mathematically, the Eyring-Powell fluid model is extra multiplex but this model has a lot of advantages because its equations can be extracted from the Kinematic theory of fluids relative to empirical relation. Also, for low and high shear stress it completely diminishes viscous flow conduct. Nadeem et al. [65] scrutinized Eyring-Powell liquid flow in an endoscope. Flow of Eyring-Powell liquid with shrinking surface was explored by Rosca and Pop [66]. Hayat et al. [67] studied effects of developed heat and mass flux models on 3D exponential flow of Eyring-Powell fluid.

The vigorous investigation on nanofluid got extraordinary improvement and it is applicable on different type of conditions, dimensions and surfaces by numerous analysts. But very few theoretical studies were published in field of hybrid nanofluid. Our basic aim is to enhance the present comprehension of the flow and heat transport of this new class of nanofluid called hybrid nanofluid. Moreover, existing data shows that investigation related to 3D flow of Eyring-Powell liquid with revised heat flux relation is not legitimately investigated. So, by considering different perspectives, this thesis explores the flow and heat transport phenomenon for hybrid nanofluid and Eyring-Powell fluid. The governing partial differential equations representing our problems are complicated, highly nonlinear and coupled in nature. After using suitable similarity transformations, system of these equations are converted into ODEs. But it is very challenging to find the exact solutions of these types of problems. Hence, the numerical and analytic series solutions will be achieved by using the BVP-4C and optimal HAM. Detail of these methods are provided in Chapter 2 and Chapter 3. Additionally, the impacts of various physical parameters will be considered for better understanding and to see the physics of the problem.

This thesis consists of EIGHT chapters containing diverse features of above mentioned fluids detailed below which have been already published in international peer reviewed journals of good impact factors. The order of the thesis is as follow:

Chapter 1 covers the introduction, motivation and methodology of the thesis.

In **Chapter 2,** aspects of time-independent 2D magnetohydrodynamic flow of Hematite–water nanofluid for a convective stretched surface is considered. The governing PDEs are converted into ODEs by using transformations. Then obtained mathematical data is tackled analytically by optimal HAM. Impacts of physical parameters are explored through graphical and tabular form. These contents are published in "**Neural Computing and Applications, (2017) 1-8, doi: 10.1007/s00521-017-3139-9**".

In **Chapter 3,** numerical treatment of rotating $Ag-CuO/water$ hybrid nanofluid flow with heat generation and absorption is examined. The comparison between heat transport properties of hybrid nanofluid and simple nanofluid is also investigated. The governing equations are solved numerically with BVP-4C technique. These contents are published in **"Canadian Journal of Physics, https://doi.org/10.1139/cjp-2018-0011"**.

In **Chapter 4,** we have studied the rotating hybrid nanofluid flow with radiation and heat source sink. Three dimensional stretching surface is considered in this chapter. Aspect of chemical reactions is also discussed. Solution is acquired numerically by using BVP-4C. Outcomes show that heat transport rate of hybrid nanofluid is higher than ordinary nanofluid and its efficiency can be increased by choosing different and proper portions of nanoparticles. These contents are published in **"Results in physics, 7 (2017) 2317-2324".**

In **Chapter 5,** impacts of partial slip and thermal slip on three dimensional rotating hybrid nanofluid are analyzed. Effects of thermal radiations are also considered here. BVP-4C technique is applied to solve the system of equations. Comparison of heat transport rate of old data with present outcomes is also provided. These contents are published in **"The European Physical Journal E, (2018) 41: 75".**

In **Chapter 6,** three dimensional Eyring-Powell fluid flow with revised heat flux relation and chemical processes with stretched surface are considered. The system of reduced ODEs are simplified by OHAM. These contents are published in **"J. Brazilian Society Mech. Sci. Eng., (2018) 40:538 "**.

Chapter 7 is associated to flow of Eyring-Powell fluid using revised heat flux relation and chemical reactions. Three dimensional exponential stretching surface is considered in this chapter. Numerical solution is obtained by using BVP-4C technique. These contents are published in **"Results in Physics, 8 (2018) 397-403".**

In **Chapter 8** three dimensional chemically reactive exponential flow of Eyring-Powell liquid subject to generalized relation is discussed. System of six highly coupled and non-linear equations is handled through BVP-4C. Comparison of our outcomes and previously published data for a limiting case is also taken into account. These contents are published in**"Results in Physics, 7 (2017) 3910-3917".**

Furthermore, probable extensions of the present study are discussed at the end.

Chapter 2

Magnetohydrodynamic aspects for 2D Hematite-water nanofluid over a convectively heated surface

Magneto-hydrodynamic aspects for two dimensional (2D) Hematite–water nanofluid with convective boundary conditions are considered. Governing PDEs of MHD nanofluid using hypothesis of boundary layer reduced into system of nonlinear ODEs. The solutions of these equations are found analytically with $OHAM$. Graphs are ploted for various physical parameters. It is anticipated that rate of transport rises as we boost volume fraction of nanoparticle and it decreases with Eckert number.

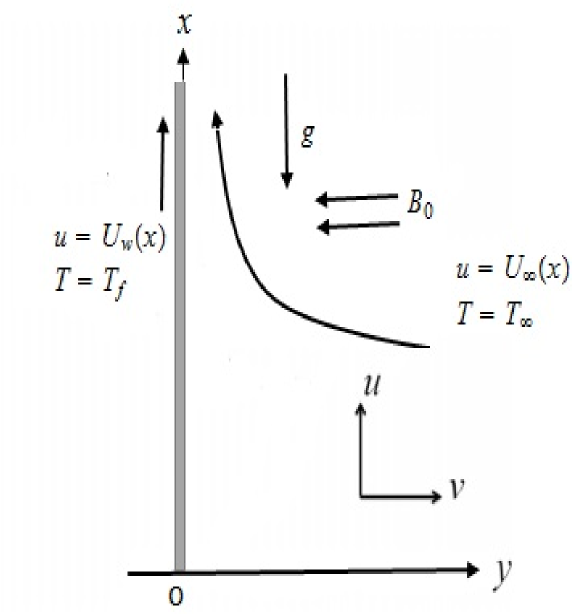

Figure 2.1: flow diagram

2.1 Formulation of the Problem

Let us suppose an incompressible 2D flow of a nanofluid. Fluid occupies $y > 0$ with $U_w = ax$ where $a > 0$ (See $Fig.$ 2.1). The surface is heated from hot fluid by a convective heat transfer at T_f . Further, fluid is electrically conducting with consistant mhd B_0 which is applied uniformly and perpendicularly to flow in absence of electric field. The aspects of induced mhd are negligible. The governing transport equations are written as [68-69]:

$$\nabla.\mathbf{V} = 0, \tag{2.1}$$

$$\rho_{nf}\mathbf{a}_j = \nabla.\mathbf{T_1}\rho_{nf}\mathbf{B} + \rho_f\mathbf{g}, \tag{2.2}$$

$$(\rho c_p)_{nf}\frac{dT}{dt} = \nabla.(K_{nf}\nabla T) + trac(\mathbf{T_1}.\mathbf{L}), \tag{2.3}$$

where

$$\mathbf{T_1} = -p\mathbf{I} + \mu_{nf}\mathbf{A}_{1,} \tag{2.4}$$

$$\mathbf{V} = [u(x,y),\ v(x,y),\ 0], \tag{2.5}$$

$$\mathbf{A}_{1,} = \mathbf{L} + \mathbf{L}^T, \tag{2.6}$$

First Rivilin-Ericksen tensor is

$$\mathbf{A}_{1,} = \begin{bmatrix} 2\frac{\partial u}{\partial x} & \frac{\partial u}{\partial y} + \frac{\partial v}{\partial x} \\ \frac{\partial u}{\partial y} + \frac{\partial v}{\partial x} & 2\frac{\partial v}{\partial y} \end{bmatrix} \tag{2.7}$$

The Cauchy stress tensor is given by

$$\mathbf{T_1} = \begin{bmatrix} -p + 2\mu_{nf}\frac{\partial u}{\partial x} & \mu_{nf}\frac{\partial u}{\partial y} + \mu_{nf}\frac{\partial v}{\partial x} & 0 \\ \mu_{nf}\frac{\partial u}{\partial y} + \mu_{nf}\frac{\partial v}{\partial x} & -p + 2\mu_{nf}\frac{\partial v}{\partial y} & 0 \\ 0 & 0 & -p \end{bmatrix} \tag{2.8}$$

Using Eqs. (2.4)-(2.6) in Eq. (2.2) we get

$$\rho_{nf}\mathbf{a}_j = -\nabla p + \mu_{nf}\nabla\cdot\mathbf{A}_1. \tag{2.9}$$

Due to MHD, an extra term $\mathbf{J}\times\mathbf{B}$ has been added in the equation (2.9) i.e.

$$\mathbf{J}\times\mathbf{B} = -\sigma_{nf}B_0^2\mathbf{V}, \tag{2.10}$$

Eq. (2.9), therefore

$$\rho_{nf}\mathbf{a}_j = -\nabla p + \mu_{nf}\nabla\cdot\mathbf{A}_{1,} - \sigma_{nf}B_0^2\mathbf{V}, \tag{2.11}$$

For $j = 1, 2$

$$a_1 = \frac{du}{dt} = u\frac{\partial u}{\partial x} + v\frac{\partial u}{\partial y}, \tag{2.12}$$

$$a_2 = \frac{dv}{dt} = u\frac{\partial v}{\partial x} + v\frac{\partial v}{\partial y}. \tag{2.13}$$

Using Eqs. (2.12)-(2.13) in Eq. (2.11), we get

For $j = 1$,

$$u\frac{\partial u}{\partial x} + v\frac{\partial u}{\partial y} = \frac{-1}{\rho_{nf}}\frac{\partial p}{\partial x} + 2\frac{\mu_{nf}}{\rho_{nf}}\frac{\partial^2 u}{\partial x^2} + \frac{\mu_{nf}}{\rho_{nf}}\frac{\partial^2 u}{\partial y^2} + \frac{\mu_{nf}}{\rho_{nf}}\frac{\partial^2 v}{\partial x \partial y} - \frac{\sigma_{nf} B_0^2 u}{\rho_{nf}}, \tag{2.14}$$

and for $j = 2$, we get the second equation that is

$$u\frac{\partial v}{\partial x} + v\frac{\partial v}{\partial y} = \frac{\mu_{nf}}{\rho_{nf}}\frac{\partial^2 u}{\partial x \partial y} + \frac{\mu_{nf}}{\rho_{nf}}\frac{\partial^2 v}{\partial x^2} - \frac{1}{\rho_{nf}}\frac{\partial p}{\partial y} + 2\frac{\mu_{nf}}{\rho_{nf}}\frac{\partial^2 v}{\partial y^2} - \frac{\sigma_{nf} B_0^2 v}{\rho_{nf}}. \tag{2.15}$$

Applying boundary layer phenomena

$$u = O(1),\ x = O(1),\ v = O(\delta),\ y = O(\delta),\ \nu = O(\delta^2). \tag{2.16}$$

Eq. (2.14) becomes

$$u\frac{\partial u}{\partial x} + v\frac{\partial u}{\partial y} = \frac{-1}{\rho_{nf}}\frac{\partial p}{\partial x} - \frac{\sigma_{nf} B_0^2 u}{\rho_{nf}} + \nu_{nf}\frac{\partial^2 u}{\partial y^2}, \tag{2.17}$$

while Eq. (2.15) reduce to

$$\frac{\partial p}{\partial y} = 0. \tag{2.18}$$

Boundary condition are

$$u(x,y) = U_w(x) = ax,\ v(x,y) = 0, -K_{nf}\left(\frac{\partial T}{\partial y}\right) = h_f\left(T_f - T\right) \quad at \ \ y = 0, \tag{2.19}$$

$$u(x,y) \to U_\infty(x) = cx,\ T(x,y) \to T_\infty \quad as \ \ y \to \infty. \tag{2.20}$$

Using Eq. (2.20) in Eq. (2.17), we have

$$\frac{-1}{\rho_{nf}}\frac{\partial p}{\partial x} = U_\infty \frac{\partial U_\infty}{\partial x} + \frac{\sigma_{nf} B_0^2 U_\infty}{\rho_{nf}}. \tag{2.21}$$

Subtituting Eq. (2.21) in Eq. (2.17), we get To derive the Equation of thermal energy,

$$u\frac{\partial u}{\partial x} + v\frac{\partial u}{\partial y} = U_\infty \frac{\partial U_\infty}{\partial x} + \nu_{nf}\frac{\partial^2 u}{\partial y^2} - \frac{\sigma_{nf} B_0^2}{\rho_{nf}}(u - U_\infty) + \frac{1}{\rho_{nf}}[\rho_f \beta^0 g(T - T_\infty)]. \tag{2.22}$$

we need the following quantities

$$\frac{dT}{dt} = (u\frac{\partial}{\partial x} + v\frac{\partial}{\partial y})T, \tag{2.22}$$

$$\nabla.(K_{nf}\nabla T) = K_{nf}\left(\frac{\partial^2 T}{\partial x^2} + \frac{\partial^2 T}{\partial y^2}\right), \tag{2.24}$$

$$\mathbf{T_1}.\mathbf{L}=\begin{bmatrix} \begin{array}{c} -p\frac{\partial u}{\partial x} + 2\mu_{nf}\left(\frac{\partial u}{\partial x}\right)^2 \\ + \left(\frac{\partial v}{\partial x}\right)\left(\mu_{nf}\frac{\partial u}{\partial y} + \mu_{nf}\frac{\partial v}{\partial x}\right) \end{array} & \begin{array}{c} \left(\frac{\partial u}{\partial y}\right)(-p + 2\mu_{nf}\frac{\partial u}{\partial x}) \\ + \left(\frac{\partial v}{\partial y}\right)\left(\mu_{nf}\frac{\partial u}{\partial y} + \mu_{nf}\frac{\partial v}{\partial x}\right) \end{array} & 0 \\ \begin{array}{c} \left(\frac{\partial u}{\partial x}\right)\left(\mu_{nf}\frac{\partial u}{\partial y} + \mu_{nf}\frac{\partial v}{\partial x}\right) \\ + \left(\frac{\partial v}{\partial x}\right)\left(-p + 2\mu_{nf}\frac{\partial v}{\partial y}\right) \end{array} & \begin{array}{c} \left(\frac{\partial u}{\partial y}\right)(\mu_{nf}\frac{\partial u}{\partial y} + \mu_{nf}\frac{\partial v}{\partial x}) \\ + \left(\frac{\partial v}{\partial y}\right)\left(-p + 2\mu_{nf}\frac{\partial v}{\partial y}\right) \end{array} & 0 \end{bmatrix}, \tag{2.25}$$

$$\begin{aligned} trac(\mathbf{T_1}.\mathbf{L}) =& (\frac{\partial u}{\partial x})(-p + 2\mu_{nf}\frac{\partial u}{\partial x}) + (\frac{\partial v}{\partial x})(\mu_{nf}\frac{\partial u}{\partial y} + \mu_{nf}\frac{\partial v}{\partial x}) \\ & + (\frac{\partial u}{\partial y})(\mu_{nf}\frac{\partial u}{\partial y} + \mu_{nf}\frac{\partial v}{\partial x}) + (\frac{\partial v}{\partial y})(-p + 2\mu_{nf}\frac{\partial v}{\partial y}). \end{aligned} \tag{2.26}$$

Using Eqs. (2.23), (2.24) and (2.26) in Eq. (2.3), we get

$$\begin{aligned} u\frac{\partial T}{\partial x} + v\frac{\partial T}{\partial y} =& \frac{K_{nf}}{(\rho c_p)_{nf}}(\frac{\partial^2 T}{\partial x^2} + \frac{\partial^2 T}{\partial y^2}) - \frac{p}{(\rho c_p)_{nf}}(\frac{\partial u}{\partial x} + \frac{\partial v}{\partial y}) \\ & + \frac{2\mu_{nf}}{(\rho c_p)_{nf}}[(\frac{\partial u}{\partial x})^2 + (\frac{\partial v}{\partial y})^2] + \frac{2\mu_{nf}}{(\rho c_p)_{nf}}(\frac{\partial u}{\partial y})(\frac{\partial v}{\partial x}) + \frac{\mu_{nf}}{(\rho c_p)_{nf}}(\frac{\partial v}{\partial x})^2 \\ & + \frac{\mu_{nf}}{(\rho c_p)_{nf}}(\frac{\partial u}{\partial y})^2. \end{aligned} \tag{2.27}$$

The above equation in simplified form is

$$
\begin{aligned}
&u\frac{\partial T}{\partial x}+v\frac{\partial T}{\partial y}=(\alpha_{nf})(\frac{\partial^2 T}{\partial x^2}+\frac{\partial^2 T}{\partial y^2})-\frac{(\alpha_{nf})p}{K_{nf}}(\frac{\partial u}{\partial x}+\frac{\partial v}{\partial y})\\
&+\frac{2\mu_{nf}(\alpha_{nf})}{K_{nf}}[(\frac{\partial u}{\partial x})^2+(\frac{\partial v}{\partial y})^2]+\frac{2\mu_{nf}(\alpha_{nf})}{K_{nf}}(\frac{\partial u}{\partial y})(\frac{\partial v}{\partial x})+\frac{\mu_{nf}(\alpha_{nf})}{K_{nf}}(\frac{\partial v}{\partial x})^2\\
&+\frac{\mu_{nf}(\alpha_{nf})}{K_{nf}}(\frac{\partial u}{\partial y})^2. \qquad (2.28)
\end{aligned}
$$

$$u=O(1),\ x=O(1),\ T=O(1),\ v=O(\delta),\ y=O(\delta),\ \upsilon_{nf}=O(\delta^2),\ \alpha_{nf}=O(\delta^2).$$

Eq. (2.28) becomes,

$$u\frac{\partial T}{\partial x}+v\frac{\partial T}{\partial y}=(\alpha_{nf})\frac{\partial^2 T}{\partial y^2}+\frac{\mu_{nf}(\alpha_{nf})}{K_{nf}}(\frac{\partial u}{\partial y})^2. \qquad (2.29)$$

The governing equations in simplified form are

$$\frac{\partial u}{\partial x}+\frac{\partial v}{\partial y}=0, \qquad (2.30)$$

$$u\frac{\partial u}{\partial x}+v\frac{\partial u}{\partial y}=U_\infty\frac{\partial U_\infty}{\partial x}+\nu_{nf}\frac{\partial^2 u}{\partial y^2}-\frac{\sigma_{nf}}{\rho_{nf}}B_0^2(u-U_\infty)+\frac{1}{\rho_{nf}}[\rho_f\beta^0 g(T-T_\infty)], \qquad (2.31)$$

$$u\frac{\partial T}{\partial x}+v\frac{\partial T}{\partial y}=\alpha_{nf}\frac{\partial^2 T}{\partial y^2}+\frac{\mu_{nf}\alpha_{nf}}{K_{nf}}(\frac{\partial u}{\partial y})^2, \qquad (2.32)$$

where α_{nf}, μ_{nf}, ρ_{nf} and K_{nf} are defined in Table. 2.1.

$$u(x,y)=U_w(x)=ax,\ v(x,y)=0,\ -K_{nf}\left(\frac{\partial T}{\partial y}\right)=h_f\left(T_f-T\right)\quad at\quad y=0, \qquad (2.33)$$

$$u(x,y)\to U_\infty(x)=cx,\ T(x,y)\to T_\infty\quad as\quad y\to\infty, \qquad (2.34)$$

We introduce following conversions

$$\eta=y\sqrt{\frac{a}{\nu}},\ u=axf'(\eta),\ v=-\sqrt{a\nu}f(\eta),\ \theta\left(\eta\right)=\frac{T-T_\infty}{T_w-T_\infty}. \qquad (2.35)$$

Utilizing Eq. (2.35), Eq. (2.30) is disappeared and Eqs. (2.31-2.32) yield:

$$\gamma_1 f''' + ff'' - f'^2 + \lambda^2 - \gamma_2[M(f' - \lambda) + r\theta] = 0, \tag{2.36}$$

$$\gamma_3\theta'' + \Pr(f\theta' + \gamma_4 Ecf''^2) = 0, \tag{2.37}$$

with boundary conditions

$$f = 0,\ f' = 1,\ \theta' = -Nc[1 - \theta] \ \text{ at } \eta = 0, \tag{2.38}$$
$$f' = \lambda,\ \theta = 0, \ \text{ as } \eta \to \infty, \tag{2.39}$$

where the physical parameters are defined as

$$\lambda = \frac{c}{a},\ ,r = \frac{T_f - T_\infty}{a^2 x}\ M = \frac{\sigma_{nf}B_0^2}{\rho_f a}\ \Pr = \frac{\nu}{\alpha_f},\ Nc = \sqrt{\frac{\nu}{a}}\frac{h_f}{K_{nf}}\ Ec = \frac{(ax)^2\rho_f\alpha_f}{K_f(T_f - T_\infty)},$$
$$\gamma_1 = \frac{1}{(1-\phi)^{2.5}[(1-\phi) + \phi\frac{\rho_s}{\rho_f}]}, \gamma_2 = \frac{1}{[(1-\phi) + \phi\frac{\rho_s}{\rho_f}]},\ \gamma_3 = \frac{(\frac{K_{nf}}{K_f})}{[(1-\phi) + \phi\frac{(\rho C_p)_s}{(\rho C_p)_f}]},$$
$$\gamma_4 = \frac{1}{(1-\phi)^{2.5}[(1-\phi) + \phi\frac{(\rho C_p)_s}{(\rho C_p)_f}]}.$$

The Skin friction C_f and transport rate Nu_x are defined as

$$C_f = \frac{\tau_w}{\rho_f U_w^2},\ Nu_x = \frac{q_f x}{K_f(T_f - T_\infty)}. \tag{2.41}$$

Making use of Eq. (2.35), Eq. (2.41) is as

$$\sqrt{\mathrm{Re}}C_f = \frac{1}{(1-\phi)^{2.5}}f''(0),\ \frac{Nu_x}{\sqrt{\mathrm{Re}}} = -\frac{K_{nf}}{K_f}\theta'(0), \tag{2.42}$$

where Re $= \frac{U_w x}{\nu_f}$.

2.2 Solution Technique

The coupled nonlinear system (2.36) to (2.39) is handled analytically with Optimal HAM (OHAM). Comprehensive description of OHAM is beautifully alaborated by Liao [70], therefore to avoid the repetition we skip the detail and just define the important quantities. Starting guesses and operator are defined as

$$f_0(\eta) = \eta\lambda + (1-\lambda)(1-e^{-\eta}), \quad \theta_0(\eta) = (\frac{Nc}{1+Nc})e^{-\eta}. \tag{2.45}$$

$$L_f(f) = \frac{d^3 f}{d\eta^3} - \frac{df}{d\eta}, \quad L_\theta(\theta) = \frac{d^2\theta}{d\eta^2} + \frac{d\theta}{d\eta}. \tag{2.46}$$

The convergence for the solution depends mainly on h_f and h_θ which are utilized to obtain analytic solution via OHAM. From $Fig.$ 2.2, we can visualize 11^{th} order approx. Convergent results are well presented in tabular form $(2.1-2.2)$. It has been witnessed that growth in the order of approximation lessens the total residual error (ϵ_m^t) consequently guarantees the solution convergence. So, we notice that OHAM gives appropriate procedure to pick parameters which gives convergent results.

Table 2.1: Individual residual square errors for ϵ_m^f and ϵ_m^θ.

$\frac{values\rightarrow}{order\downarrow}$	$h_f = -1.57809$	$h_\theta = -1.1836$
	ϵ_m^f	ϵ_m^θ
4	0.0000586612	0.00201884
8	3.46534×10^{-7}	0.0000158615
12	1.1515×10^{-7}	1.50674×10^{-6}
18	4.72789×10^{-8}	1.26305×10^{-8}
22	2.64815×10^{-8}	1.37207×10^{-9}
24	1.97362×10^{-8}	3.501×10^{-10}

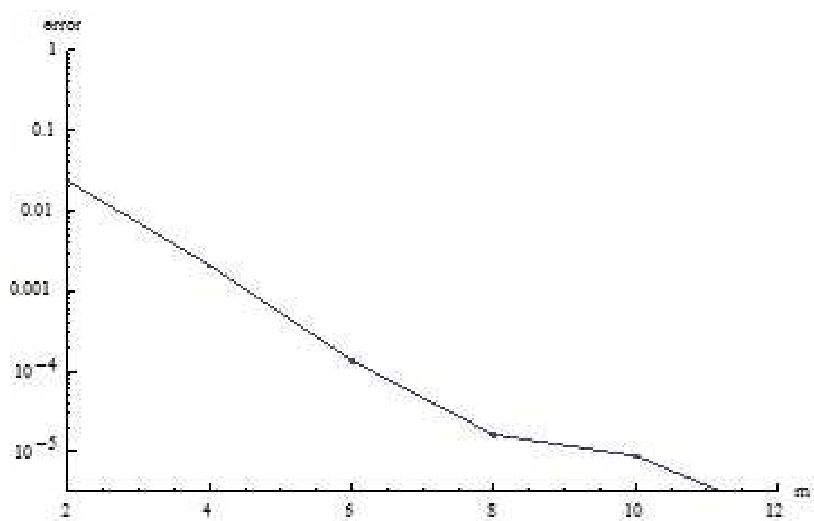

Figure 2.2: Graphical representation for 11^{th} order approximation.

Table 2.2: The convergence of parametric values for average residual square errors (ϵ_m^t) by OHAM.

$\frac{values\rightarrow}{order\downarrow}$	h_f	h_θ	ϵ_m^t
2	-1.70541	-1.00941	0.00770093
4	-1.27552	-0.792843	0.00154008
6	-1.65486	-1.05643	0.0000448689
8	-1.33777	-1.16387	2.47712×10^{-6}
10	-1.33284	-1.11819	1.43086×10^{-6}
12	-1.38412	-1.2082	2.52638×10^{-7}
14	-1.57772	-1.19275	1.43531×10^{-7}
16	-1.67855	-1.19196	8.84055×10^{-8}

2.3 Graphical Outcomes

For the better understanding of problem, graphical examination of aspects of physical parameters λ, M, Nc, Ec and ϕ on $f'(\eta)$ and $\theta(\eta)$ are elaborated in $Figs.$ $[2.3-2.9]$. $Fig.$ 2.3 represents influence of M on velocity field $f'(\eta)$. $Fig.$ 2.4 clarify the impacts of Ec on $\theta(\eta)$. Physically, an increment in the internal energy cause increase in temperature. $Fig.$ 2.5 show the effects of Nc on $\theta(\eta)$. There is a rise in temperature with increase in Nc. $Fig.$ 2.6 explain aspect of ϕ on $\theta(\eta)$. There is a rise in temperature with the enhancement in ϕ. Physically, with the increment in ϕ, heat energy increases which eventually boost the temperature. $Fig.$ 2.7 elucidate the impact of λ on $\theta(\eta)$. Increment in λ correlates with higher stretching rate so obviously reduce the temperature. Thermo-physical properties of hematite and water are in $Table$ 2.3. Aspects of parameters on friction factor and transport rate are provided in $Table$ 2.4. $Table$ 2.5 provide comparison of our results with Pop [6] (described in $[71-72]$).

Table 2.3: The Thermophysical properties of base fluid and Hematite nanoparticle.

Properties	H_2O	Hematite
$\rho(kg/m^3)$	997	5180
$C_p(J/kgK)$	4179	670
K(W/mK)	0.613	9.7
Pr(m^2/s)	6.2	-

.

Table 2.4: Comparison of $f''(0)$ for various λ values with literature.

λ	Pop et al. [6]	Our outcomes
0.1	-0.96938	-0.96937
0.3	-0.84942	-0.84940
1.0	0.0	0.0
2.0	2.01750	2.01750

.

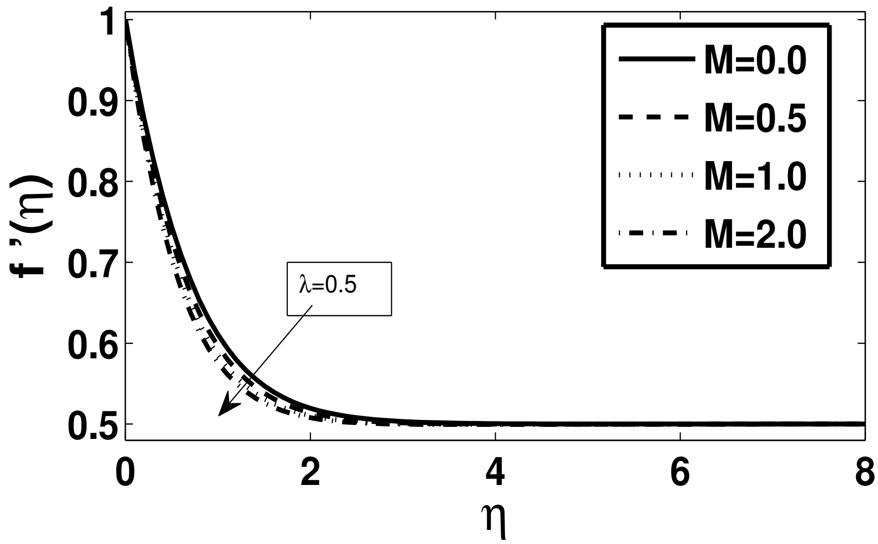

Figure 2.3: Effects of M on $f'(\eta)$.

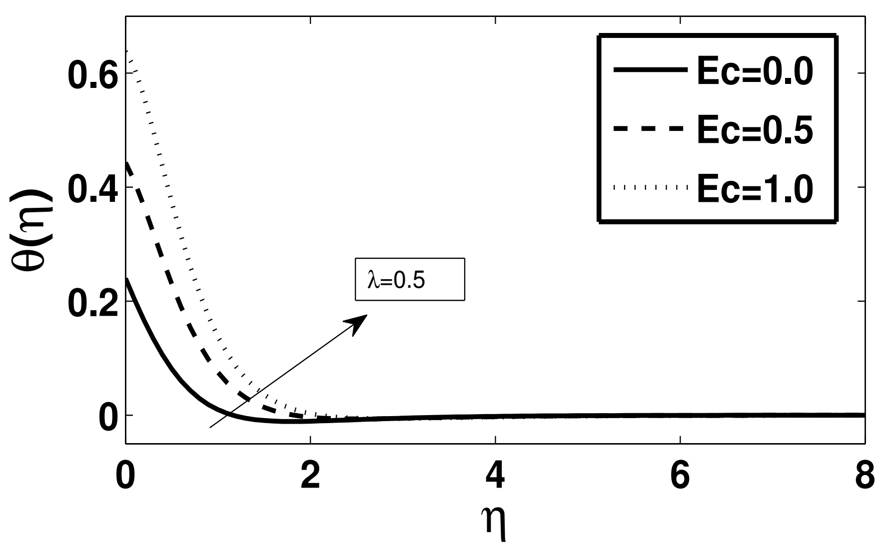

Figure 2.4: Effects of Ec on $\theta(\eta)$.

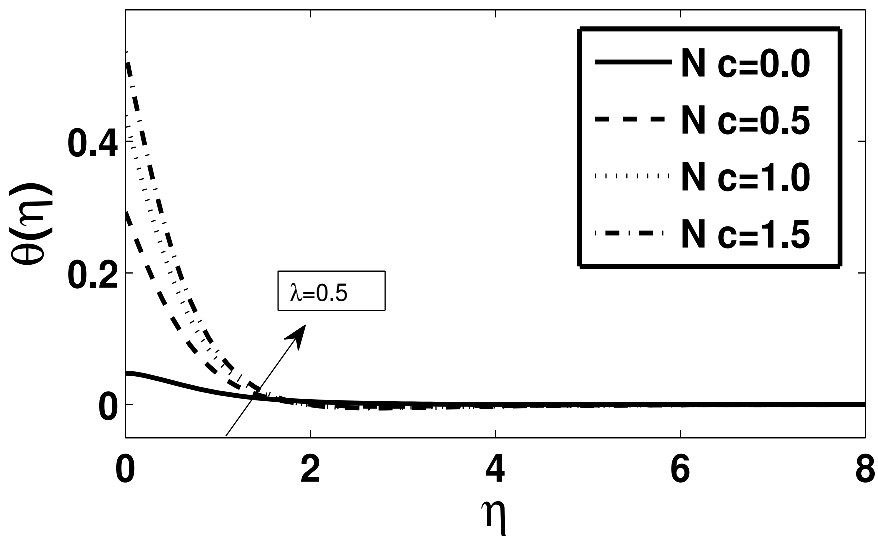

Figure 2.5: Effects of Nc on $\theta(\eta)$.

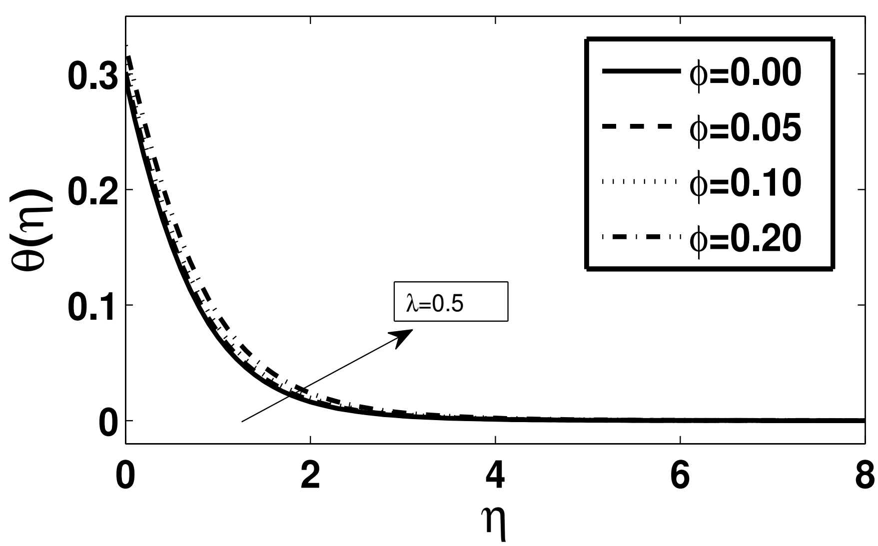

Figure 2.6: Effects of ϕ on $\theta(\eta)$.

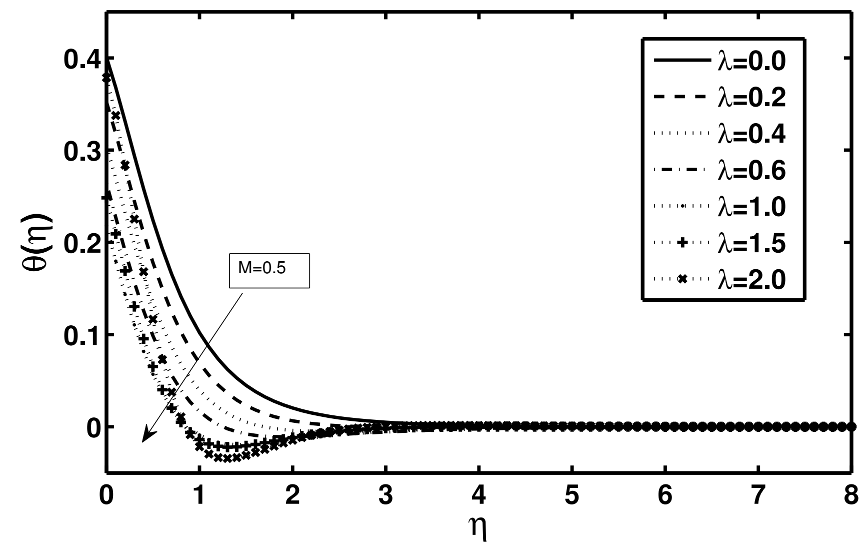

Figure 2.7: Effects of λ on $\theta(\eta)$.

Table 2.5: Aspects of physical parameters on friction factor and heat transport rate.

λ	M	Ec	Nc	$C_f\ Re^{\frac{1}{2}}$	$Nu_x\ Re^{\frac{-1}{2}}$
0.0	0.5	0.1	0.5	-0.768854	0.337401
0.1				-0.703101	0.346810
0.5				-0.353752	0.375481
0.5	0.0			-0.349361	0.375614
	0.5			-0.353752	0.375481
	1.0			-0.390326	0.374692
		0.1		-0.353752	0.375481
		0.5		-0.336012	0.342264
		1.0		-0.277429	0.311199
			0.1	-0.464620	0.0916735
			0.5	-0.353752	0.375481
			1.0	-0.351414	0.609997

2.4 Remarks

Effects of magnetohydrodynamic on Hematite-water nanofluid over a convectively heated stretched surface has been examined. The observation is as follows

- The velocity field f' declines when we boost M but it rises with λ.
- There is a rise in temperature as we enhance ϕ, Ec and Nc.
- The heat transport rate declines with the augmentation in Ec and M.
- Increase in convective parameter Nc helps the phenomenon of heat transport.

Chapter 3

Numerical analysis of rotating Hybrid nanofluid with heat absorption

This chapter is carried out to investigate aspects of (MHD), heat absorption/generation and nanoparticle's volume fraction on flow of hybrid nanofluid for a stretched surface. Comparison of heat transport properties of conventional nanofluid wit hybrid nanofluid is also taken into account. To study Lorentz force aspects on 3D stretching surface, a model of "thermophysical properties" is considered. Whole system including nanofluid and surface is in rigid body rotation about an axis normal to plane with constant angular velocity. Nonlinear PDEs has been solved using some transformations and sought out with an efficient numerical technique BVP-4C. Aspects of physical parameters have been explained through graphs and tables. From current

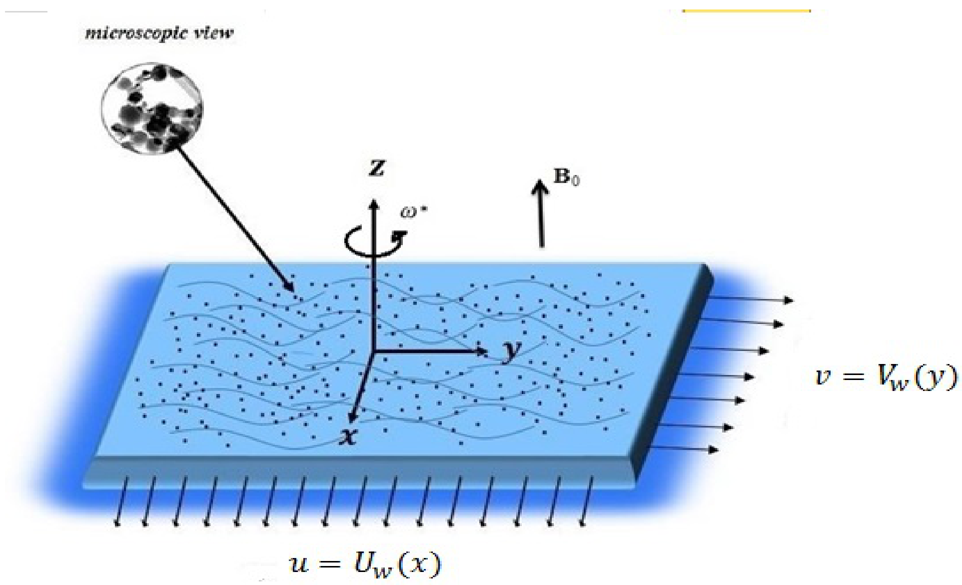

Figure 3.1: Physical regime of the problem.

analysis, heat transport rate of Hybrid nanofluid is very higher as nanofluid.

3.1 Mathematical Formulation of the Problem

Assume time-independent, 3-D, magnetohydrodynamic, viscous, electrically conducting, rotating flow of hybrid nanofluid. The fluid occupies $z > 0$. Also flow induction is due to stretching of surface at $z = 0$ (see Fig. 3.1).

Here (Ag) and (CuO) nano-size particle with (H_2O) as a base liquid are used. At beginning, $CuO(\phi_1)$ of 0.1 vol. is added in base liquid to form $CuO - water$. Thus, for $Ag - CuO/water$, $Ag(\phi_2)$ with many volume fractions are scattered in $CuO - water$. It is rotating in such a way along vertical axis that ω^* is constant. With these assumptions, the governing system is written as [73]:

$$u = U_w = ax,\ v = V_w = by,\quad w = 0,\quad T = T_w,\ at\ z = 0, \tag{3.5}$$

$$\frac{\partial u}{\partial x}+\frac{\partial v}{\partial y}+\frac{\partial w}{\partial z}=0, \tag{3.1}$$

$$u\frac{\partial u}{\partial x}+v\frac{\partial u}{\partial y}+w\frac{\partial u}{\partial z}-2\omega^{*}v=\nu_{hnf}\frac{\partial^2 u}{\partial z^2}-\frac{\sigma_{hnf}B_0^2}{\rho_{hnf}}u, \tag{3.2}$$

$$u\frac{\partial v}{\partial x}+v\frac{\partial v}{\partial y}+w\frac{\partial v}{\partial z}+2\omega^{*}u=\nu_{hnf}\frac{\partial^2 v}{\partial z^2}-\frac{\sigma_{hnf}B_0^2}{\rho_{hnf}}v, \tag{3.3}$$

$$u\frac{\partial T}{\partial x}+v\frac{\partial T}{\partial y}+w\frac{\partial T}{\partial z}=\alpha_{hnf}\frac{\partial^2 T}{\partial z^2}+\frac{Q}{(\rho C_p)_{hnf}}(T-T_\infty), \tag{3.4}$$

$$u\to 0, \quad v\to 0, \quad T\to T_\infty \quad \text{as} \quad z\to\infty. \tag{3.6}$$

By introduced transformations

$$u=axf'(\eta), \quad v=ayg'(\eta), \quad w=-\sqrt{a\nu_f}(f(\eta)+g(\eta)),$$
$$\eta=z\sqrt{\frac{a}{\nu_f}}, \quad \theta(\eta)=\frac{T-T_\infty}{T_w-T_\infty}. \tag{3.7}$$

Consequently, the above problem reduce to

$$f'''(\eta) - (1-\phi_1)^{2.5}(1-\phi_2)^{2.5}[(1-\phi_2)\{(1-\phi_1)+\phi_1(\frac{\rho_{s1}}{\rho_f})\}+\phi_2(\frac{\rho_{s2}}{\rho_f})]$$
$$\times[(f'(\eta))^2 - f''(\eta)(f(\eta)+g(\eta)) - 2\Omega\delta g'(\eta)] - (1-\phi_1)^{2.5}(1-\phi_2)^{2.5}M^2 f'(\eta) = 0, \tag{3.8}$$

$$g'''(\eta) - (1-\phi_1)^{2.5}(1-\phi_2)^{2.5}[(1-\phi_2)\{(1-\phi_1)+\phi_1(\frac{\rho_{s1}}{\rho_f})\}+\phi_2(\frac{\rho_{s2}}{\rho_f})]$$
$$\times[(g'(\eta))^2 - g''(\eta)(f(\eta)+g(\eta)) + 2\frac{\Omega}{\delta} f'(\eta)] - (1-\phi_1)^{2.5}(1-\phi_2)^{2.5}M^2 g'(\eta) = 0, \tag{3.9}$$

$$\begin{aligned} &\tfrac{K_{hnf}}{K_f}\theta''(\eta) + \Pr[(1-\phi_2)\{(1-\phi_1)+\phi_1(\tfrac{(\rho C_p)_{s1}}{(\rho C_p)_f})\} \\ &\quad +\phi_2(\tfrac{(\rho C_p)_{s2}}{(\rho C_p)_f})](f(\eta)+g(\eta))\theta'(\eta) + \delta_1\theta(\eta) = 0, \end{aligned} \tag{3.10}$$

$$f = 0, \quad f' = 1, \quad g = 0, \quad g' = \lambda, \quad \theta = 1 \quad \text{at} \quad \eta = 0,$$
$$f' \to 0, \quad g' \to 0, \quad \theta \to 0 \quad \text{as} \quad \eta \to \infty. \tag{3.11}$$

Where Ω, M, λ, δ_1 and Pr are defined as,

$$\Omega = \frac{\omega^*}{a},\ M = \sqrt{\frac{\sigma_{hnf}B_0^2}{a\rho_f}},\ \lambda = \frac{b}{a},\ \delta_1 = \frac{Q}{a(\rho C_p)_f}\ \Pr = \frac{\nu_f(\rho C_p)_f}{K_f}, \tag{3.12}$$

and

$$C_{fx} = \frac{\mu_{hnf}(\frac{\partial u}{\partial z})_{z=0}}{\rho_f(ax)^2}, \quad C_{fy} = \frac{\mu_{hnf}(\frac{\partial v}{\partial z})_{z=0}}{\rho_f(ax)^2}, \quad Nu_x = -\frac{xK_{hnf}}{K_f\,(T_w - T_\infty)}\left(\frac{\partial T}{\partial z}\right)\bigg|_{z=0}. \tag{3.13}$$

$$\mathrm{Re}^{\frac{1}{2}}\, C_{fx} = \frac{1}{(1-\phi_1)^{2.5}(1-\phi_2)^{2.5}} f''(0), \quad \delta^{-1}\,\mathrm{Re}^{\frac{1}{2}}\, C_{fy} = \frac{1}{(1-\phi_1)^{2.5}(1-\phi_2)^{2.5}} g''(0),$$
$$\mathrm{Re}^{-\frac{1}{2}}\, Nu_x = -\frac{K_{hnf}}{K_f}\theta'(0). \tag{3.14}$$

3.2 Numerical solution

The coupled non-linear ODEs $(3.8-3.10)$ with (3.11) are simplified using BVP-4C technique $[71-72]$. In MATLAB, BVP-4C is applied to handle Eqs because of its viability in solving BVPs which are very difficult than IVPs. In this procedure, system of equations $(3.8-3.10)$ escorted with boundary conditions is reduced to first order ODEs. Then appropriate starting guesses are opted that satisfy conditions. The procedure is as under:

let

$$\begin{aligned}
&p_1 = \frac{1}{(1-\phi_1)^{2.5}(1-\phi_2)^{2.5}},\ p_2 = (1-\phi_2)\{(1-\phi_1)+\phi_1(\frac{\rho_{s1}}{\rho_f})\}+\phi_2(\frac{\rho_{s2}}{\rho_f}),\\
&p_3 = (1-\phi_2)\{(1-\phi_1)+\phi_1(\frac{(\rho C_p)_{s1}}{(\rho C_p)_f})\}+\phi_2(\frac{(\rho C_p)_{s2}}{(\rho C_p)_f}),
\end{aligned} \tag{3.15}$$

also

$$f = y_1\ ,\ f' = y_2\ ,\ f'' = y_3\ ,\ f''' = y_3'\ , \tag{3.16}$$

$$g = y_4\ ,\ g' = y_5\ ,\ g'' = y_6\ ,\ g''' = y_6'\ , \tag{3.17}$$

$$\theta = y_7\ ,\ \theta' = y_8\ ,\ \theta'' = y_8'\ . \tag{3.18}$$

and

$$y_2 = y_1', \tag{3.19}$$

$$y_3 = y_2', \tag{3.20}$$

$$y_3' = \frac{p_2}{p_1}[y_2^2 - (y_1 + y_4)y_3 - 2\Omega\delta y_5], \tag{3.21}$$

$$y_5 = y_4', \tag{3.22}$$

$$y_6 = y_5', \tag{3.23}$$

$$y_6' = \frac{p_2}{p_1}[y_5^2 - (y_1 + y_4)y_6 + 2(\frac{\Omega}{\delta})y_2], \tag{3.24}$$

$$y_8 = y_7', \tag{3.25}$$

$$y_8' = \frac{-\Pr}{(\frac{K_{hnf}}{K_f})}[p_3(y_1 + y_4)y_8], \tag{3.26}$$

along with initial conditions that are given by

$$y_0(1) = 0,\ y_0(2) = 1,\ y_0(3) = a_1,$$
$$y_0(4) = 0,\ y_0(5) = \lambda,\ y_0(6) = a_2,$$
$$y_0(7) = 1,\ y_0(8) = a_3. \tag{3.27}$$

Here a_i are the un-known parameters. Now we pick appropriate guesses with the condition that solution satisfies at infinity boundary condition. Criterion to achieve the convergence is set to 10^{-6}. The acquired outcomes exhibit aspects of dimensionless parameters, Ω, M, λ, δ_1 and Pr on liquid velocity, temperature, drag forces and heat transport rate.

3.3 Results and Discussion

Graphical analyses of flow and heat transport have been carried out to perceive current situation. Comparison of velocity field for (H_2O), ($CuO - water$) and ($Ag - CuO/water$) is presented in $Fig.$ 3.2. Velocity of base fluid (H_2O) is greater than ($CuO - water$) and ($Ag - CuO/water$). $Figs.$ (3.3 − 3.4) demonstrate aspects of (M) on $f'(\eta)$ and $g'(\eta)$. By increasing M, for both ($CuO - water$) and ($Ag - CuO/water$), it is anticipated that there is enhancement in retarding force. Physically, the presence of transverse magnetic field creates Lorentz force which is resistive force and restricts the motion of fluid. So by increasing magnetic field the Lorentz force increases, that is why velocity and the associated boundary layer thickness diminish. Moreover, velocity profile decreases as (Ω) is augmented through $Figs.$ 3.5 and 3.6. The $Figs.$ 3.5 and 3.6 also explain that the velocity of hybrid nanofluid is always smaller than nanofluid velocity because addition of more colossal particle causes the flow of the fluid to decay. $Fig.$ 3.7 clarify aspects of λ on $g'(\eta)$. Physically, along y axis, as γ increases, there is an increase in "rate of stretching"which implies rise in velocity. Comparison for temperature profile for base liquid (H_2O),($CuO - water$) and ($Ag - CuO/water$) is exhibited in $Fig.$ 3.8. Temperature for ($Ag - CuO/water$) is higher than (H_2O) and nanofluid ($CuO - water$). $Fig.$ 3.9 represents aspects of M on temperature field. $Fig.$ 3.10 shows aspect of Ω on temperature field. Rotation enlarges thermal layer thickness. Additionally, instant increase in temperature is because of the hybrid nanofluid ($Ag - CuO/water$). The aspect of λ on $\theta(\eta)$ can be seen in Fig. 3.11. We noticed that temperature distribution is the diminishing function of λ. As $f'(\eta)$ rises, the thermal layer gets thinner which reduces temperature. Fig. 3.12 depict $\theta(\eta)$ with δ_1. Increase in δ_1 prompts an increase in temperature distribution because of the reason that energy is produced at thermal boundary layer. In $Figs$. $3.13 - 3.14$, by increasing Ω, with the non-zero λ, it is noticed that, in x-direction, a normal stress in the tangential direction is decreasing to a particular value but in y-direction, the same tangential stress enhances while hybridity increases skin friction in both directions. In $Table$ 3.1, thermophysical properties of nanofluid and hybrid nanofluid are given. For spheric nanoparticles we put $n = 3$. $Table$ 3.2 provides the thermophysical properties at 25^0C. From $Table$ 3.3, by adding ϕ_2, the velocity of the fluid increases which clearly reduces skin friction for both $(Ag - CuO/water)$ and $(CuO - water)$. From $Table$ 3.4, the Ω and M have decreasing impact but λ and ϕ_2 have increasing impact on the rate of heat transfer. Continuously addition of nanoparticles can exert more energy which increases the rate of heat transfer. Additionally, we have observed that hybrid nanofluid $(Ag - CuO/water)$ has higher rate of heat transport as $(CuO - water)$.

Thermophysical Properties of Hybrid Nanofluid $(Ag - CuO/water)$.

$$\rho_{hnf} = [(1-\phi_2)\{(1-\phi_1)\rho_f + \phi_1\rho_{s1}\}] + \phi_2\rho_{s2},$$
$$\mu_{hnf} = \frac{\mu_f}{(1-\phi_1)^{2.5}(1-\phi_2)^{2.5}},$$
$$(\rho C_p)_{hnf} = [(1-\phi_2)\{(1-\phi_1)(\rho C_p)_f + \phi_1(\rho C_p)_{s1}\}] + \phi_2(\rho C_p)_{s2},$$
$$\frac{K_{hnf}}{K_{bf}} = \frac{K_{s2} + (n-1)K_{bf} - (n-1)\phi_2(K_{bf} - K_{s2})}{K_{s2} + (n-1)K_{bf} + \phi_2(K_{bf} - K_{s2})},$$
$$\frac{K_{bf}}{K_f} = \frac{K_{s1} + (n-1)K_f - (n-1)\phi_1(K_f - K_{s1})}{K_{s1} + (n-1)K_f + \phi_1(K_f - K_{s1})}$$

Table 3.1: Thermophysical Properties of $(CuO - water)$.

Properties	Nanofluid $(CuO - water)$
Density (ρ)	$\rho_{nf} = (1-\phi)\rho_f + \phi\rho_s$
Viscosity (μ)	$\mu_{nf} = \frac{\mu_f}{(1-\phi)^{2.5}}$
Heat Capacity (ρC_P)	$(\rho C_p)_{nf} = (1-\phi)(\rho C_p)_f + \phi(\rho C_p)_s$
Thermal Conductivity (K)	$\frac{K_{nf}}{K_f} = \frac{K_s + (n-1)K_f - (n-1)\phi(K_f - K_s)}{K_s + (n-1)K_f + \phi(K_f - K_s)}$

Table 3.2: The Thermophysical Properties of CuO, Ag and H_2O.

Properties	CuO	Ag	H_2O
$\rho(\mathrm{kg/m^3})$	6320	10500	997.1
$C_p(\mathrm{J/kgK})$	531.80	235	4179.0
$K(\mathrm{W/mK})$	76.50	429	0.6130
$\mathrm{Pr}(\mathrm{m^2/s})$	–	–	6.20

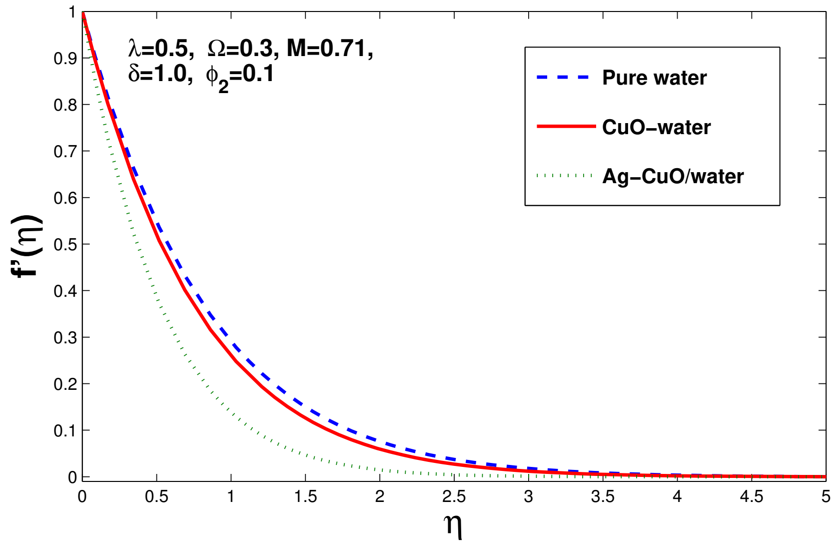

Figure 3.2: Comparison of velocity field for (H_2O), $(CuO - water\ )$ and $(Ag - CuO/water)$.

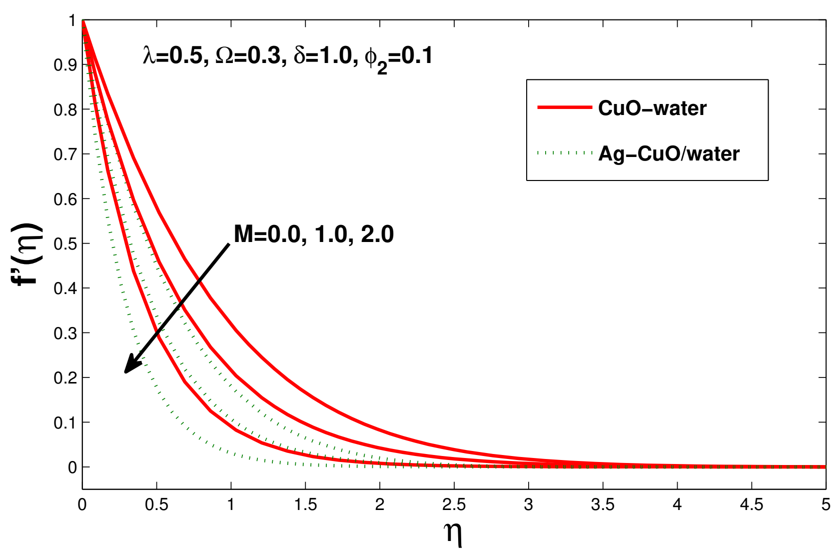

Figure 3.3: Velocity field for M in x direction.

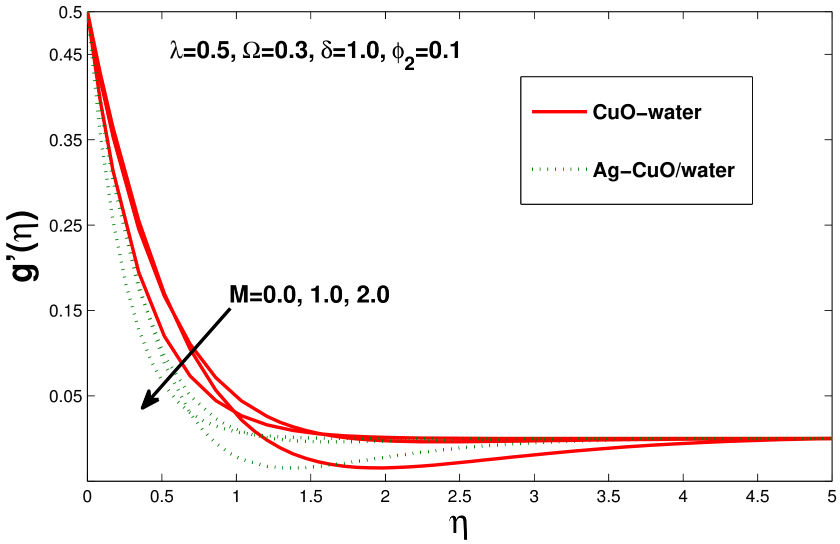

Figure 3.4: Velocity field for M in y direction.

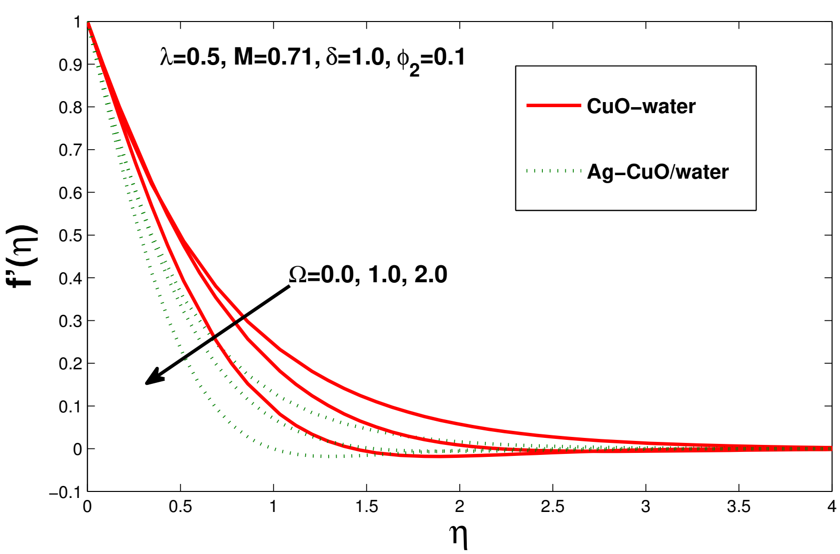

Figure 3.5: Velocity field for Ω in x direction.

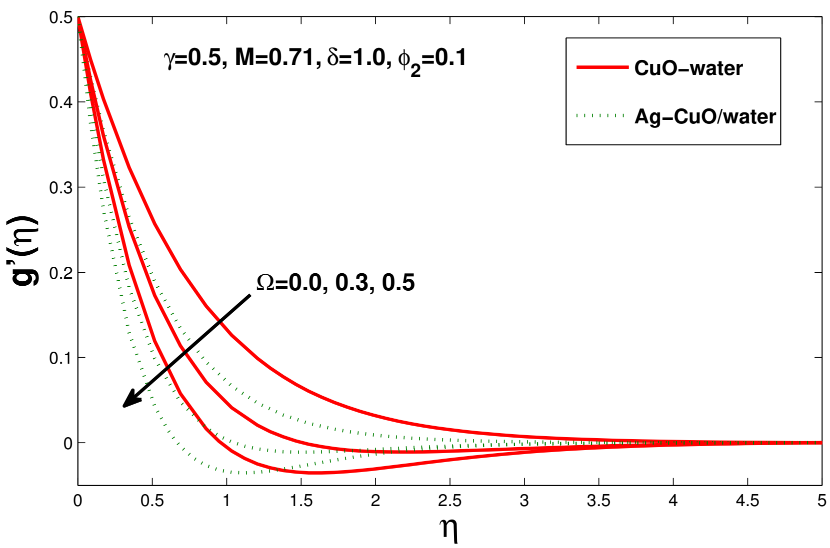

Figure 3.6: Velocity field for Ω in y direction.

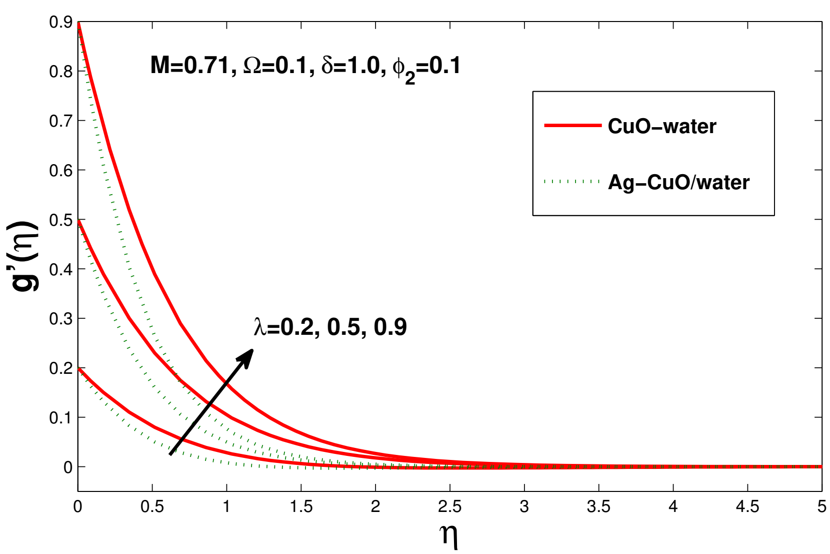

Figure 3.7: Velocity field for λ in y direction.

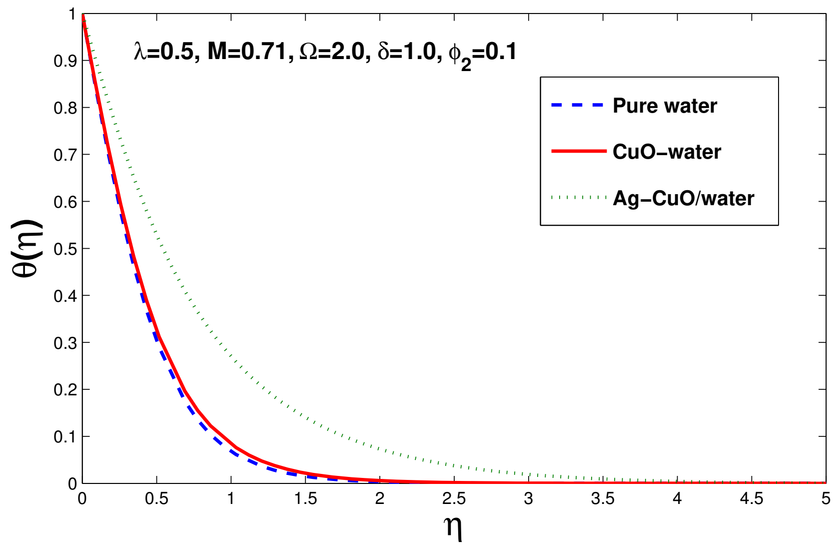

Figure 3.8: Comparison of temperature field for (H_2O), $(CuO - water)$ and $(Ag - CuO/water)$.

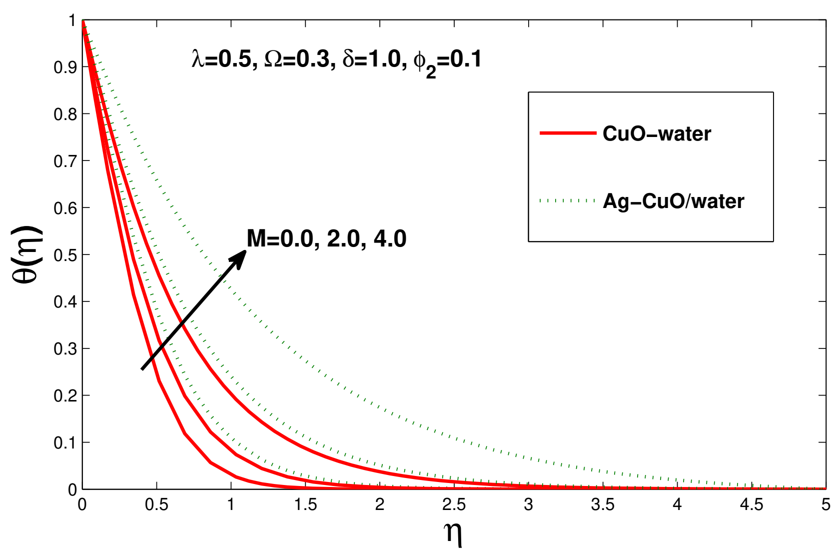

Figure 3.9: Temperature field for M.

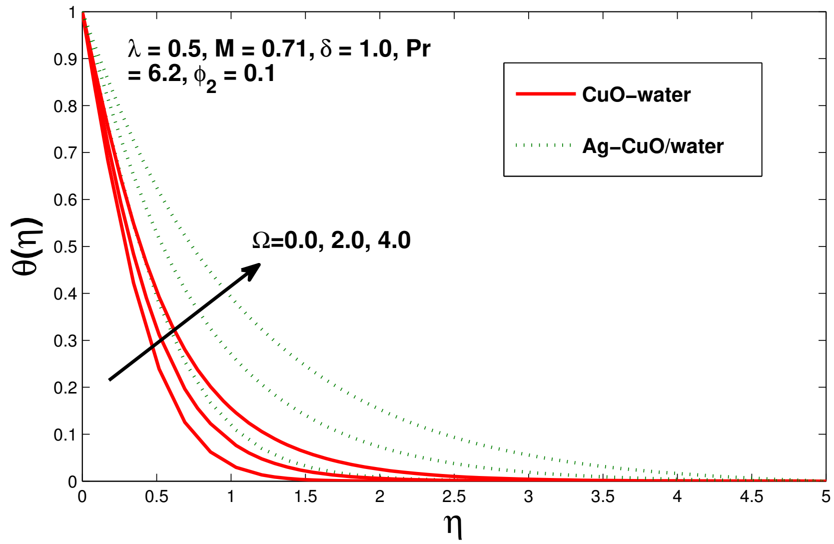

Figure 3.10: Temperature field for Ω.

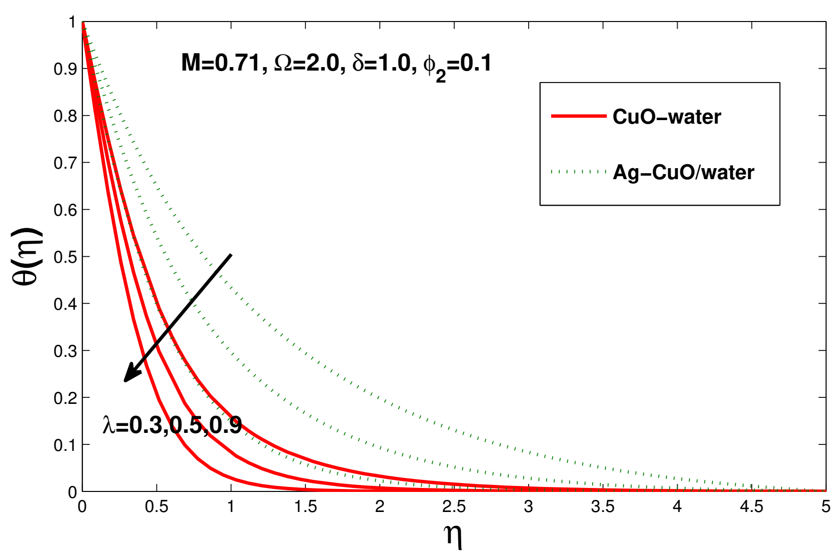

Figure 3.11: Temperature field for λ.

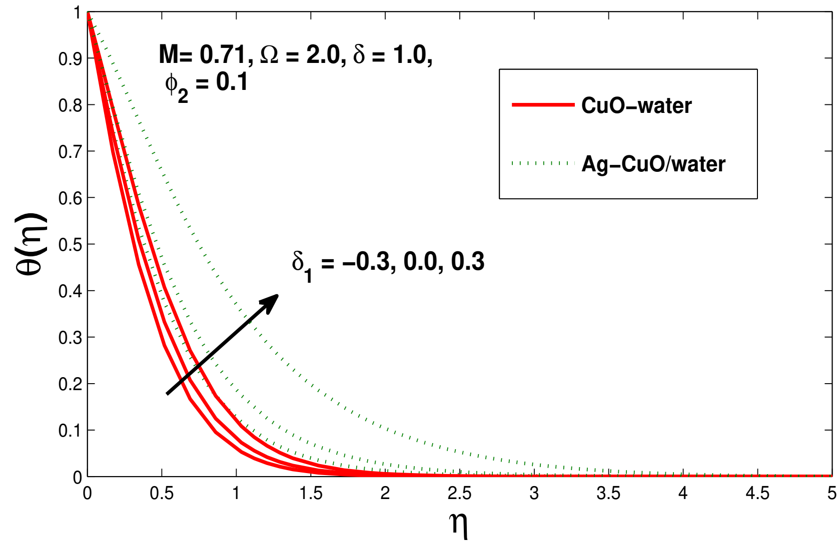

Figure 3.12: Temperature field for δ_1.

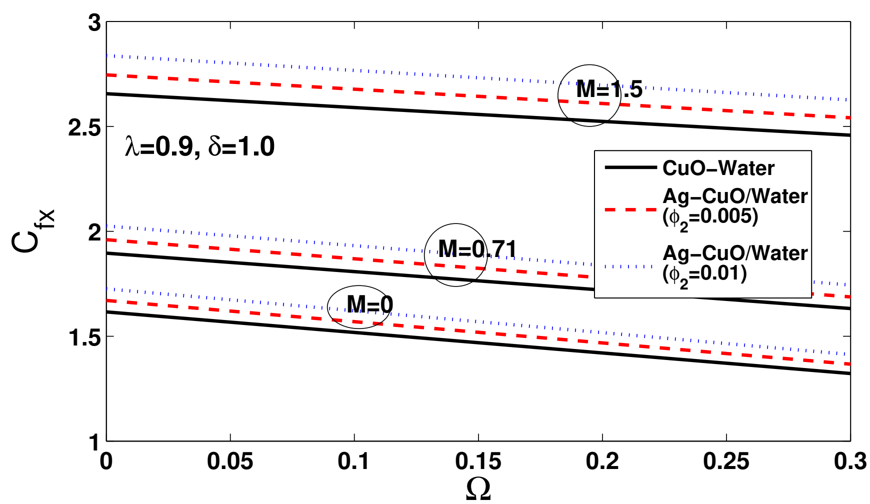

Figure 3.13: Skin friction for M in x direction.

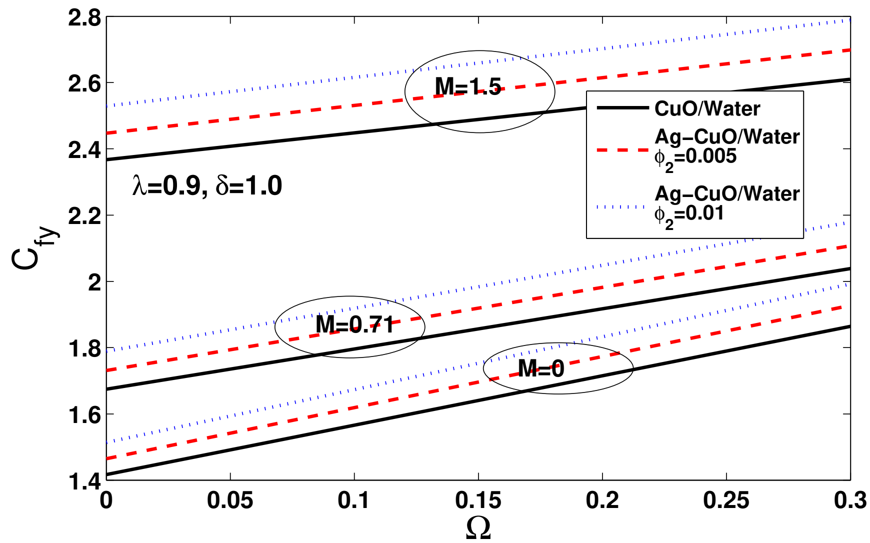

Figure 3.14: Skin friction for M in y direction.

Table 3.3: Variations of $-f''(0)$, $-g''(0)$ for $CuO - water$ and $Ag - CuO/water$ with $\phi_1 = 0.1$.

Ω	λ	M	ϕ_2	$-\frac{1}{(1-\phi_1)^{2.5}} f''(0)$	$-\frac{(1-\phi_1)^{-2.5}}{(1-\phi_2)^{2.5}} f''(0)$	$-\frac{1}{(1-\phi_1)^{2.5}} g''(0)$	$-\frac{(1-\phi_1)^{-2.5}}{(1-\phi_2)^{2.5}} g''(0)$
0.1	0.5	0.71	0.06	2.04364	2.38553	1.18579	1.38416
0.3				1.93741	2.26152	1.53247	1.78884
0.5				1.88474	2.20005	1.86815	2.18068
0.3	0.2			1.99092	2.32400	0.91252	1.06518
	0.5			1.93741	2.26152	1.53247	1.78884
	0.9			1.88373	2.19886	2.57639	3.00740
		0		1.74780	2.04020	1.44325	1.68470
		0.71		1.93741	2.26152	1.53247	1.78884
		1.5		2.51442	2.93507	1.86305	2.17473
			0.04	1.81933	2.01480	1.41764	1.56995
			0.08	2.05920	2.53647	1.65120	2.03390
			0.1	2.18521	2.84372	1.77456	2.30933

Table 3.4: Variations of heat flux at surface $-\theta'(0)$ for $CuO - water$ and $Ag - CuO/water$ with $\phi_1 = 0.1$.

Ω	λ	M	ϕ_2	$\frac{-K_{nf}}{K_f}\theta'(0)$	$\frac{-K_{hnf}}{K_f}\theta'(0)$
0.1	0.5	0.71	0.06	2.3941	2.1514
0.3				2.3486	2.1105
0.5				2.2881	2.0562
0.3	0.2			2.017	1.8126
	0.5			2.3486	2.1105
	0.9			2.7024	2.4285
		0		2.3827	2.1412
		0.71		2.3486	2.1105
		1.5		2.2262	2.0006
			0.04	1.6358	2.1781
			0.08	1.6975	2.2599
			0.1	1.7293	2.3021

3.4 Conclusion

In this chapter, numerical analysis is executed on magneto hydrodynamic 3-D flow of rotating hybrid nanofluid (Ag-CuO/Water) for a stretched surface. The results are as follow:

- Flow of hybrid nanofluid assumes extraordinary part in heat transport with magnetic field.
- Hybridity diminishes velocity; however, it increases temperature.
- Hybrid nanofluid would give preferable and better heat transfer execution when contrasted with nanofluid.
- The heat transport rate of hybrid nanofluid may be accomplished by picking distinctive and proper nanoparticle extents.

Chapter 4

Heat transfer enhancement with Ag-CuO/water hybrid nanofluid

Nanofluids are of great importance to researchers as they have significant uses industrially due to their high heat transfer rates. Recently, a new class of nanofluid, "hybrid nanofluid" is being used to further enhance the heat transfer rate. This new model in 3D is employed to examine the impact of thermal radiation and rotation over a stretched surface. Chemical reaction and heat absorption/generation effects are also considered. After employing similarity transformations, the system is solved numerically. Present outcomes shows that hybridity boosts heat transport rate at surface.

4.1 Formulation

Consider 3-D rotating flow of an incompressible hybrid nanofluid for stretching surface. The fluid occupy the half space at $z > 0$. We have considered Copper Oxide (CuO) and Silver(Ag) nano particles with base liquid as a water. Initially, $CuO(\phi_1)$ nanoparticle of 0.1 volume fraction is dissipated into water to make $(CuO - water)$. Thus, to formulate "$(Ag - CuO/water)$", Silver (ϕ_2) with different volume fractions is dispersed in nanofluid $(CuO - water)$. Using these assumptions, the governing system is

$$\frac{\partial u}{\partial x} + \frac{\partial v}{\partial y} + \frac{\partial w}{\partial z} = 0, \tag{4.1}$$

$$u\frac{\partial u}{\partial x} + v\frac{\partial u}{\partial y} + w\frac{\partial u}{\partial z} - 2\omega^* v = \nu_{hnf}\frac{\partial^2 u}{\partial z^2}, \tag{4.2}$$

$$u\frac{\partial v}{\partial x} + v\frac{\partial v}{\partial y} + w\frac{\partial v}{\partial z} + 2\omega^* u = \nu_{hnf}\frac{\partial^2 v}{\partial z^2}, \tag{4.3}$$

$$u\frac{\partial T}{\partial x} + v\frac{\partial T}{\partial y} + w\frac{\partial T}{\partial z} = \alpha_{hnf}\frac{\partial^2 T}{\partial z^2} + \frac{Q}{(\rho C_p)_{hnf}}(T - T_\infty) - \frac{\partial q_r}{\partial z}, \tag{4.4}$$

$$u\frac{\partial c}{\partial x} + v\frac{\partial c}{\partial y} + w\frac{\partial c}{\partial z} = \beta_{hnf}\frac{\partial^2 c}{\partial z^2} - \xi_1(c - c_\infty)^n. \tag{4.5}$$

Using Roseland approximation $[74 - 76]$, q_r is given by

$$q_r = \frac{-4\sigma^*}{3\varrho}\frac{\partial T^4}{\partial z}. \tag{4.6}$$

Expanding the Taylor series about T_∞ we have [77]

$$T^4 \approx 4TT_\infty^3 - 3T_\infty^4. \tag{4.7}$$

Related conditions for three dimensional flow are

$$u = U_w = ax,\ v = V_w = by,\ w = 0,\ T = T_w,\ c = c_w, \ \text{ at } z = 0,$$

$$u \to 0, \quad v \to 0, \quad T \to T_\infty,\ c \to c_\infty \ \text{ as } \ z \to \infty. \tag{4.8}$$

Given issue can be stated in a more straightforward form by using the suitable similarity transformation defined as

$$u = axf'(\eta),\ v = ayg'(\eta),\ w = -\sqrt{a\nu_f}(f(\eta)+g(\eta)),\ \eta = z\sqrt{\frac{a}{\nu_f}},$$
$$\theta(\eta) = \frac{T-T_\infty}{T_w-T_\infty},\ \xi(\eta) = \frac{c-c_\infty}{c_w-c_\infty}\ . \tag{4.9}$$

With Eq. (4.9), Eq. (4.1) is satisfied while Eqs. (4.2-4.8) transformed into following coupled nonlinear differential equations.

$$f'''(\eta) - (1-\phi_1)^{2.5}(1-\phi_2)^{2.5}[(1-\phi_2)\{(1-\phi_1)+\phi_1(\frac{\rho_{s1}}{\rho_f})\}+\phi_2(\frac{\rho_{s2}}{\rho_f})]$$
$$\times[(f'(\eta))^2 - f''(\eta)(f(\eta)+g(\eta)) - 2\Omega\delta g'(\eta)] = 0, \tag{4.10}$$
$$g'''(\eta) - (1-\phi_1)^{2.5}(1-\phi_2)^{2.5}[(1-\phi_2)\{(1-\phi_1)+\phi_1(\frac{\rho_{s1}}{\rho_f})\}+\phi_2(\frac{\rho_{s2}}{\rho_f})]$$
$$\times[(g'(\eta))^2 - g''(\eta)(f(\eta)+g(\eta)) + 2\frac{\Omega}{\delta}f'(\eta)] = 0, \tag{4.11}$$
$$(\frac{K_{hnf}}{K_f}+\frac{4}{3}R)\theta''(\eta) + \Pr[(1-\phi_2)\{(1-\phi_1)+\phi_1(\frac{(\rho C_p)_{s1}}{(\rho C_p)_f})\}$$
$$+\phi_2(\frac{(\rho C_p)_{s2}}{(\rho C_p)_f})](f(\eta)+g(\eta))\theta'(\eta) + \delta_1\theta(\eta) = 0, \tag{4.12}$$
$$\xi''(\eta) + \frac{Sc}{(1-\phi_1)(1-\phi_2)}[(f(\eta)+g(\eta)]\xi'(\eta) - R_{c1}\xi(\eta) = 0, \tag{4.13}$$

$$f=0,\quad f'=1,\quad g=0,\quad g'=\lambda,\quad \theta=1,\ \ \xi=1,\quad \text{at}\quad \eta=0,$$
$$f'\to 0,\quad g'\to 0,\quad \theta\to 0,\ \xi\to 0\quad \text{as}\quad \eta\to\infty, \tag{4.14}$$

where

$$\Omega = \frac{\omega^*}{a},\ \lambda = \frac{b}{a}, \Pr = \frac{\nu_f(\rho C_p)_f}{K_f},\ R = \frac{4\sigma^* T_\infty^3}{\varrho K_f},\ \delta_1 = \frac{Q}{a(\rho C_p)_f},$$
$$Sc = \frac{\nu_f}{\beta_f},\ R_{c1} = \frac{\xi_1(c-c_\infty)^{n-1}}{a}. \tag{4.15}$$

The physical quantities of the given problem are defined by

$$C_{fx}=\frac{\mu_{hnf}(\frac{\partial u}{\partial z})_{z=0}}{\rho_f(ax)^2},\ C_{fy}=\frac{\mu_{hnf}(\frac{\partial v}{\partial z})_{z=0}}{\rho_f(ax)^2},\ Nu_x=-\frac{xK_{hnf}}{K_f\left(T_w-T_\infty\right)}\left.\left(\frac{\partial T}{\partial z}\right)\right|_{z=0}+(q_r)_w\ ,$$
$$Sh_x=-\frac{xK_{hnf}}{K_f\left(c_w-c_\infty\right)}\left.\left(\frac{\partial c}{\partial z}\right)\right|_{z=0}. \tag{4.16}$$

With the use of similarity transformations, Eq. (4.16) take the form

$$\mathrm{Re}^{\frac{1}{2}}\,C_{fx}=\frac{1}{(1-\phi_1)^{2.5}(1-\phi_2)^{2.5}}f''(0),\quad \delta^{-1}\,\mathrm{Re}^{\frac{1}{2}}\,C_{fy}=\frac{1}{(1-\phi_1)^{2.5}(1-\phi_2)^{2.5}}g''(0),$$
$$\mathrm{Re}^{-\frac{1}{2}}\,Nu_x=-(\frac{K_{hnf}}{K_f}+\frac{4}{3}R)\theta'(0),\ \ \mathrm{Re}^{-\frac{1}{2}}\,Sh_x=-\frac{K_{hnf}}{K_f}\xi'\left(0\right). \tag{4.17}$$

4.2 Results and discussion

Numerical evaluation of the non-linear equations has been carried out to get a better understanding of the problem. The complete detail is provided in chap 3. The influence of pertinent physical parameters namely rotation parameter, stretching ratio parameter, heat generation parameter, radiation parameter, chemical reaction and Schmidt number on flow, heat and mass transport is presented graphically in *Figs.* (4.2 − 4.13). From *Table* 4.1, friction factor of hybrid nanofluid is enhanced with nanoparticle volume fraction whereas declines as we increase λ. Chemical reaction and Sc have no impact on skin friction coefficient. Increment in rotation reduces friction factor in x-direction, but, it escalates in y-direction. From *Table* 4.2 we conclude that changes in stretching ratio parameter, rotation, Schmidt number and chemical reaction have no influence on heat transport rate. The heat transport rate amplifies in presence of ϕ_2. We learnt that due to hybrid nanofluid ($Ag-CuO/water$) the heat transfer rate was further augmented. The mass transfer rate diminishes when we enhance rotation parameter and ϕ_2 but it elevates with λ, chemical reaction parameter and Schmidt number. To authenticate current numerical data, comparisons of $-f''(0)$ with published data for $\Omega = 0 = \phi_1 = \phi_2 = R$ is made through $Table$ 4.3.

4.2.1 Comparison of velocity and temperature profiles

The velocity profile comparison for H_2O, $CuO-water$ and $Ag-CuO/water$ is revealed in $Fig.$ (4.1). Since no magnetic field is being applied in the present study which accelerates nanoparticles, hence ($Ag-CuO/water$) reduces fluid's velocity. There is also a decrease in fluid velocity due to density and dynamic viscosity that rise because of hybridity and so there is a decline in velocity. We also observe that the velocity of hybrid nanofluid ($Ag-CuO/water$) is less than nanofluid's velocity. The reason being obvious that including further massive particles hurdles the normal fluid flow. $Fig.$ (4.2) depicts the comparison of temperature profile amid hybrid nanofluid ($Ag-CuO/water$), $CuO-water$ and H_2O. We noticed ($Ag-CuO/water$) reaches higher temperature than nanofluid ($CuO-water$). A sudden rise in temperature is a result of hybrid nanofluid ($Ag-CuO/water$).

4.2.2 Impact of rotation parameter (Ω)

It is demonstrated through $Figs.$ (4.3−4.4) the aspect of rotation on $f'(\eta)$ and $g'(\eta)$ in x and y direction respectively. We observe that as (Ω) enhances, the liquid velocity

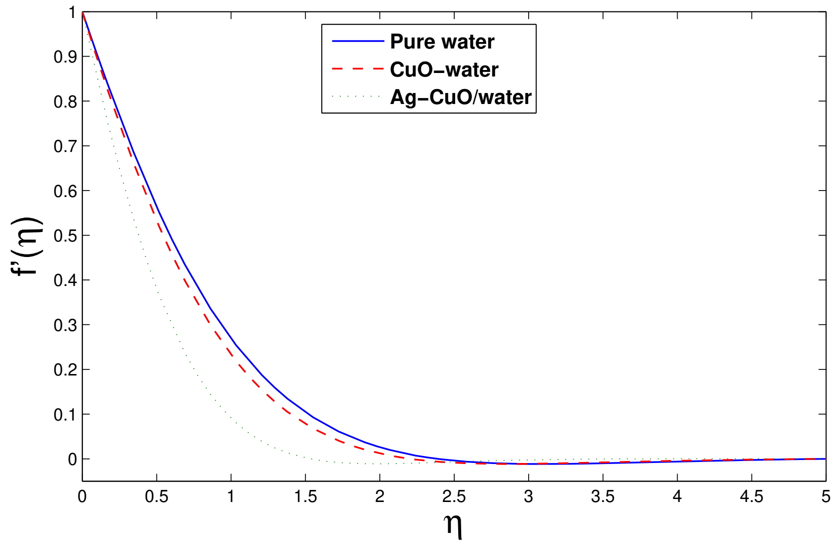

Figure 4.1: Comparison of $f'(\eta)$.

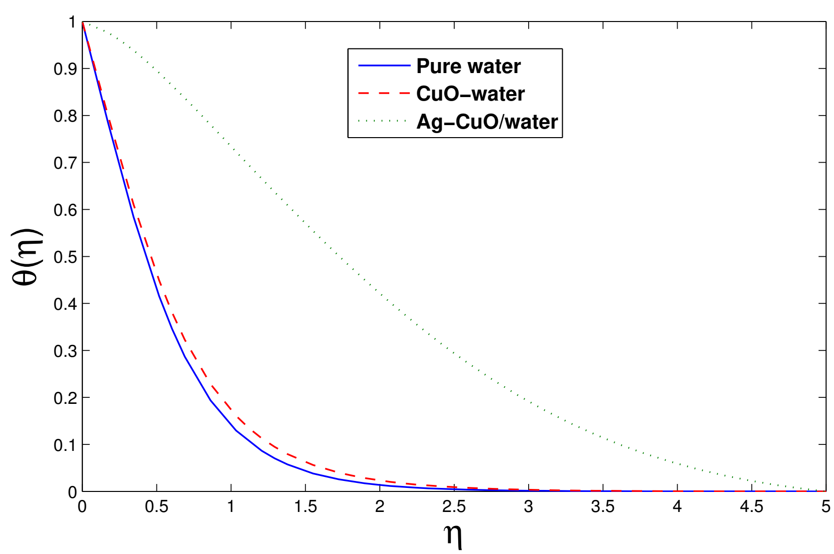

Figure 4.2: Comparison of $\theta(\eta)$.

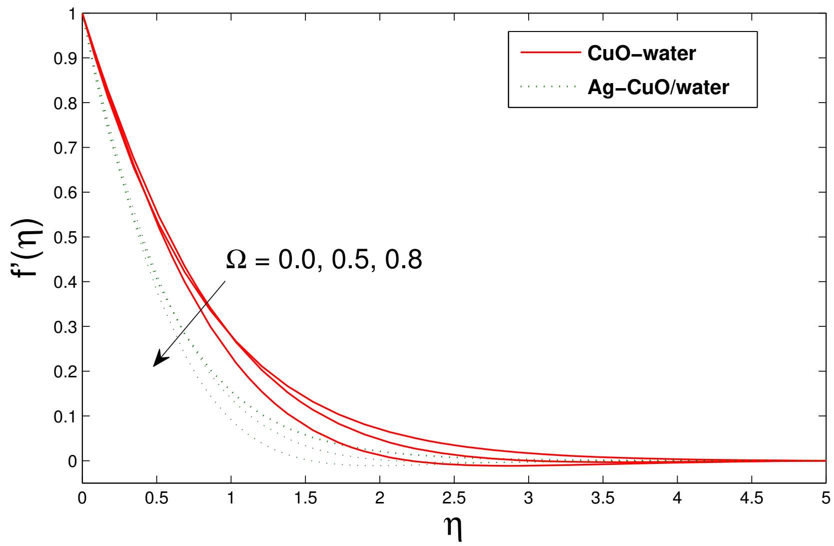

Figure 4.3: variation of Ω on $f'(\eta)$.

decelerate along with boundary layer thickness. The temperature distribution for $Ag - CuO/water$ and $CuO - water$ is displayed in $Fig.$ (4.5). Here we observe that immediate improvement in temperature is due to the hybrid nanofluid $Ag - CuO/water$. In $Fig.$ (4.6) the concentration, $\xi(\eta)$, has been plotted to see the effects against rotation. Rotation boosts the concentration.

4.2.3 Impact of (λ)

$Fig.$ (4.7) elucidates aspect of (λ) on velocity in y-direction. Increment in stretching ratio parameter correlates with higher stretching rate in y-axis so obviously there is a rise in velocity field. Aspects of (λ) on temperature distribution is depicted through $Fig.$ (4.8). It is discovered from the graph, as λ there is a reduction in the temperature profile. Through $Fig.$ (4.9) we observe the variation of concentration with respect to

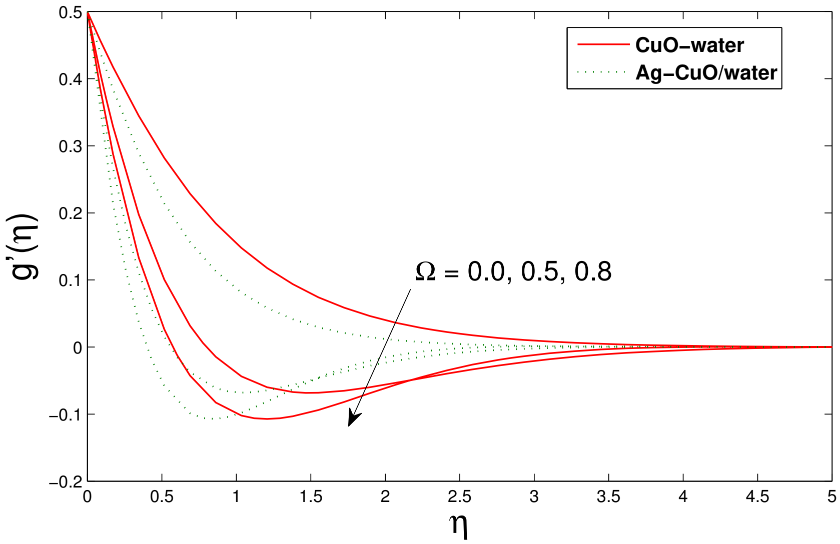

Figure 4.4: variation of Ω on $g'(\eta)$.

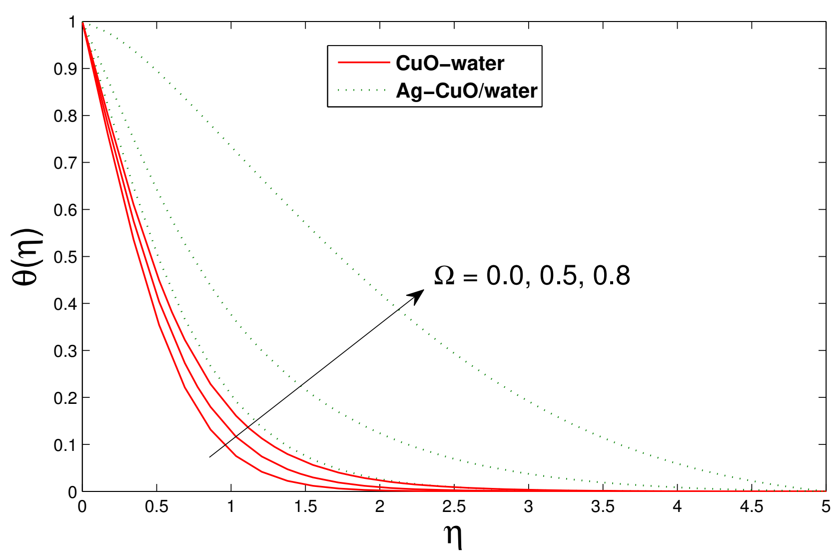

Figure 4.5: variation of Ω on $\theta(\eta)$.

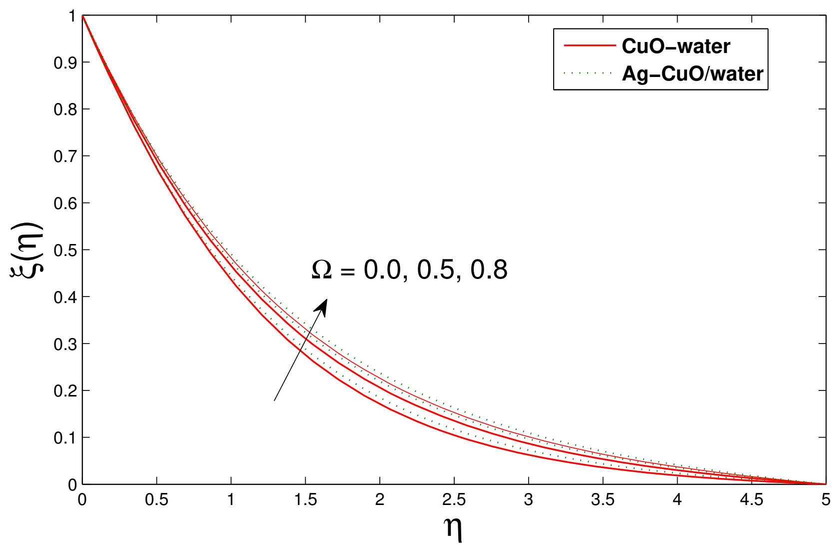

Figure 4.6: variation of Ω on $\xi(\eta)$.

stretching ratio parameter λ. Larger of λ declines concentration profile.

4.2.4 Impact of (δ_1)

Fig. (4.10) illustrates nature of temperature profile with the variation of heat generation/absorption parameter. Increase in δ_1 prompts an increase in the temperature field since energy is produced at thermal boundary layer.

4.2.5 Impact of (R)

Impact of R over the θ profile is demonstrated in *Fig.* (4.11). Physically we analyze higher values of this quantity $\frac{\varrho K_f}{4\sigma^* T_\infty^3}$ exhibit that thermal radiation is dominate over conduction. Hence a great amount of heat energy due to radiation is being released in the system giving a rise to temperature.

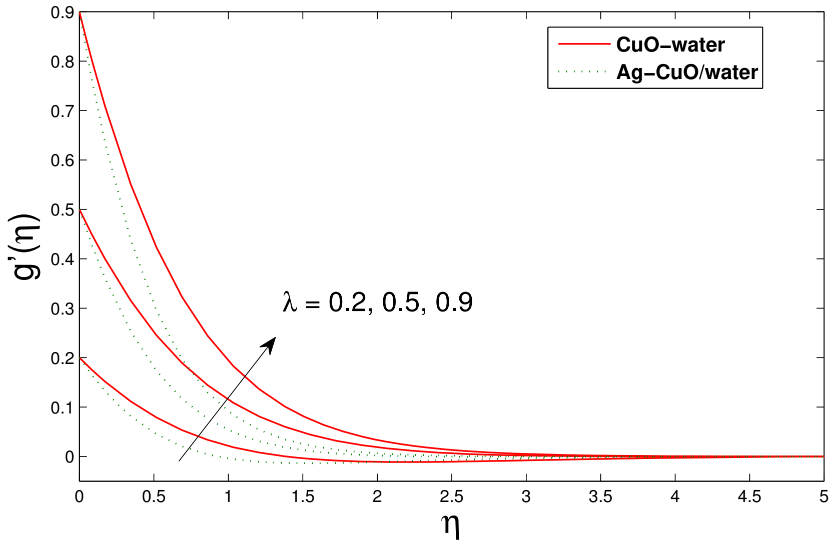

Figure 4.7: variation of λ on $g'(\eta)$.

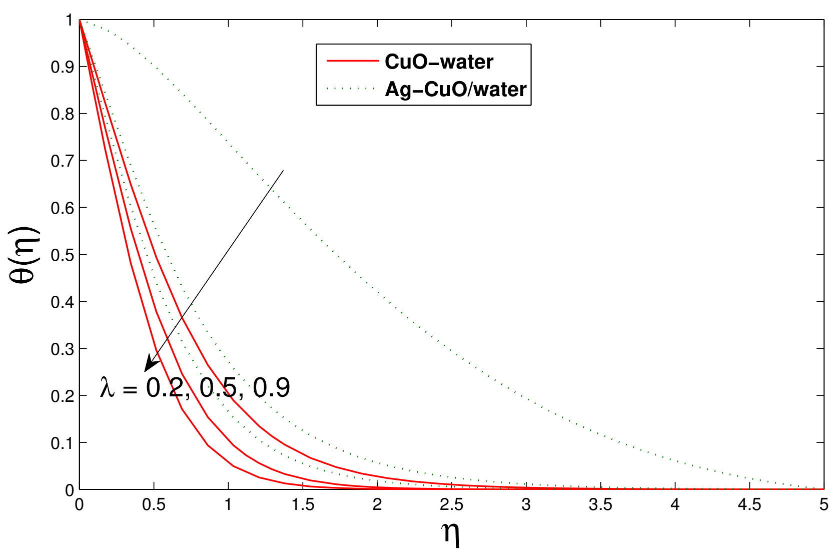

Figure 4.8: variation of λ on $\theta(\eta)$.

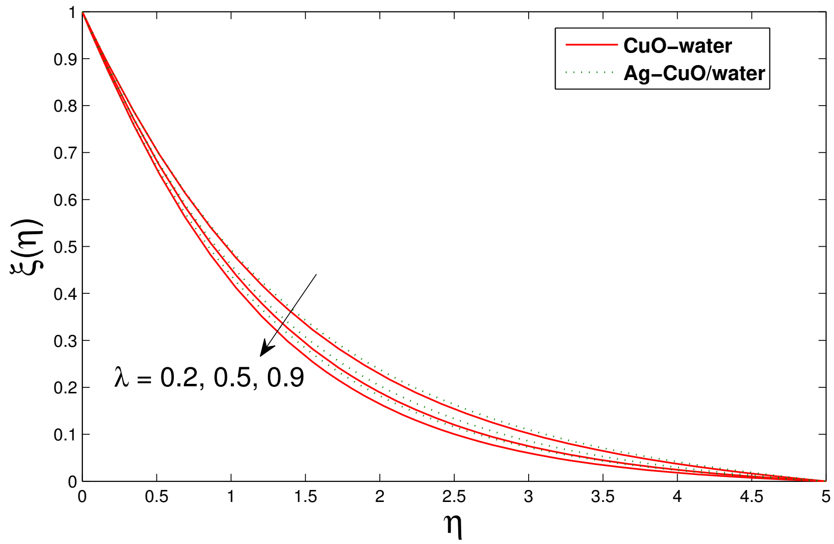

Figure 4.9: variation of λ on $\xi(\eta)$.

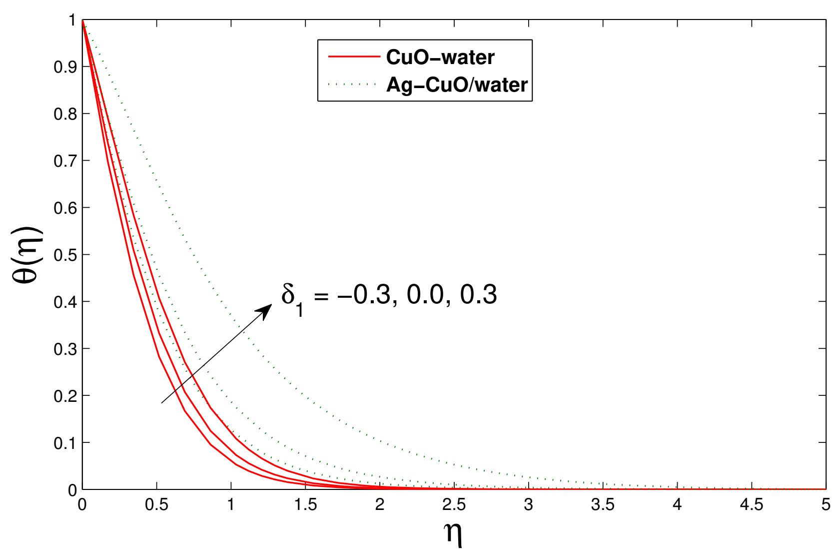

Figure 4.10: variation of δ_1 on $\theta(\eta)$.

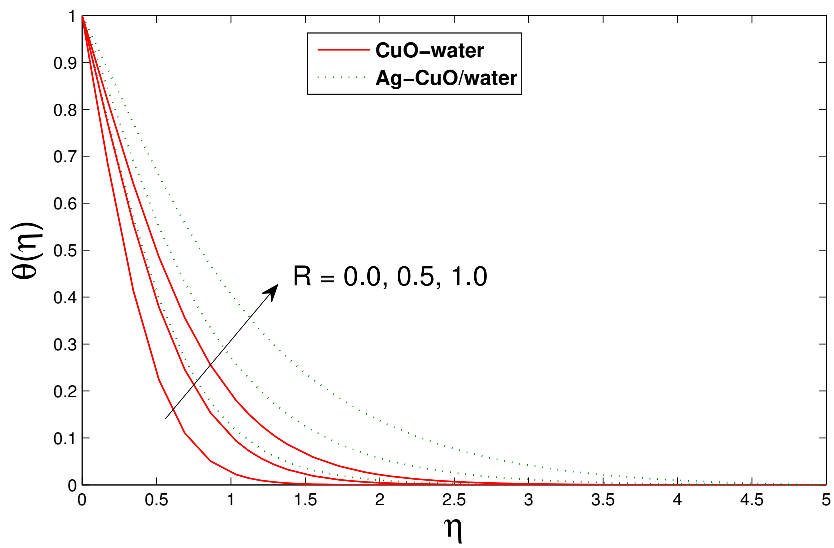

Figure 4.11: variation of R on $\theta(\eta)$.

4.2.6 Impact of chemical reaction parameter ($\mathbf{R}_{c1}$)

Fig. (4.12) demonstrate aspects of R_{c1} on the concentration profile. The raising values of chemical reaction lead to decline fluid's concentration. Consequently the concentration boundary layer thickness get increased.

4.2.7 Impact of (Sc)

Impact of Sc on ξ is exhibited in *Fig.* (4.13). Due to Sc, the diffusion is decreases consequently the fluid's concentration reduces.

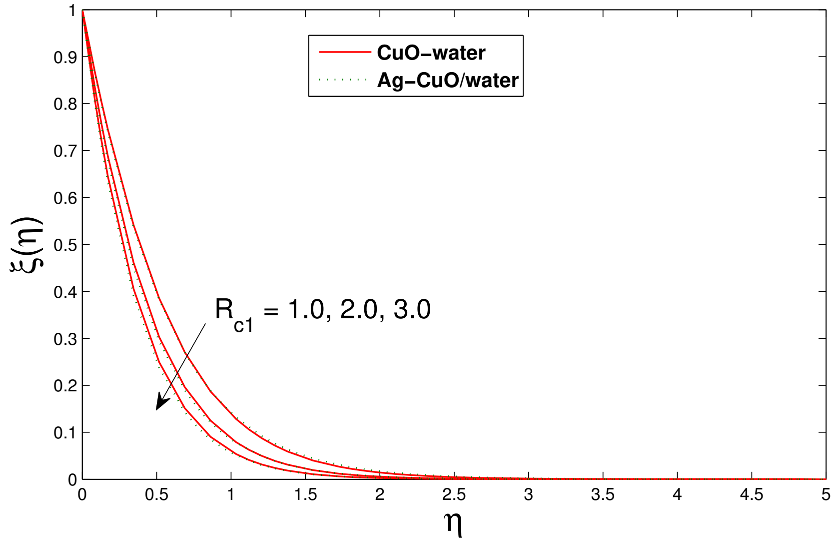

Figure 4.12: variation of R_{c1} on $\xi(\eta)$.

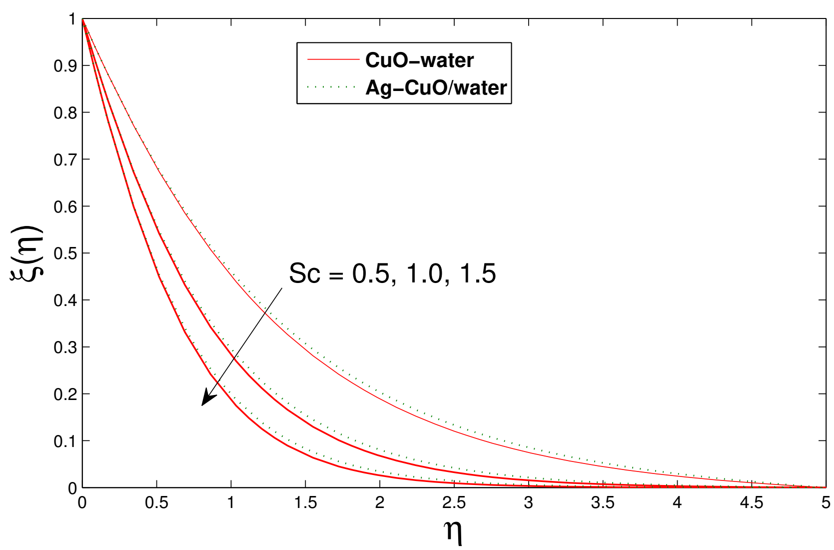

Figure 4.13: variation of Sc on $\xi(\eta)$.

Table 4.1: Effects of $-f''(0)$, $-g''(0)$ for $(CuO - water)$ and $(Ag - CuO/water)$.

Ω	λ	ϕ_2	R_{c1}	Sc	$\frac{-1}{(1-\phi_1)^{2.5}} f''(0)$	$\frac{-(1-\phi_1)^{-2.5}}{(1-\phi_2)^{2.5}} f''(0)$	$\frac{-1}{(1-\phi_1)^{2.5}} g''(0)$	$\frac{-(1-\phi_1)^{-2.5}}{(1-\phi_2)^{2.5}} g''(0)$
0.1	0.5	0.07	0.5	0.5	1.91658	2.29784	1.06164	1.27283
0.3					1.80930	2.16922	1.49397	1.79116
0.5					1.77585	2.12912	1.88764	2.26314
0.3	0.2				1.88714	2.26254	1.00655	1.20679
	0.5				1.80930	2.16922	1.49397	1.79116
	0.9				1.74547	2.09269	2.44057	2.92606
		0.05			1.68693	1.91773	1.39306	1.58365
		0.07			1.80930	2.16922	1.49397	1.79116
		0.1			1.99913	2.60156	1.65059	2.14799
			0		1.80930	2.16922	1.49397	1.79116
			1		1.80930	2.16922	1.49397	1.79116
			2		1.80930	2.16922	1.49397	1.79116
				0.5	1.80930	2.16922	1.49397	1.79116
				1.0	1.80930	2.16922	1.49397	1.79116
				1.5	1.80930	2.16922	1.49397	1.79116

Table 4.2: Effects of $-\theta'(0)$ and $-\xi'(0)$ for $(CuO - water)$ and $(Ag - CuO/water)$.

Ω	λ	ϕ_2	R_{c1}	Sc	$\frac{-K_{nf}}{K_f}\theta'(0)$	$\frac{-K_{hnf}}{K_f}\theta'(0)$	$-(1-\phi_1)\xi'(0)$	$-(1-\phi_1)(1-\phi_2)\xi'(0)$
0.1	0.5	0.07	0.5	0.5	1.32460	1.22440	0.65733	0.61131
0.3					1.32460	1.22440	0.64297	0.59796
0.5					1.32460	1.22440	0.62757	0.58364
0.3	0.2				1.32460	1.22440	0.60094	0.55887
	0.5				1.32460	1.22440	0.64297	0.59796
	0.9				1.32460	1.22440	0.68567	0.63767
		0.05			1.32460	1.15700	0.64230	0.61019
		0.07			1.32460	1.22440	0.64297	0.59796
		0.1			1.32460	1.33120	0.64486	0.58038
			0		1.32460	1.22440	0.38047	0.35384
			1		1.32460	1.22440	0.82157	0.76406
			2		1.32460	1.22440	1.08770	1.01150
				0.5	1.32460	1.22440	0.64297	0.59796
				1.0	1.32460	1.22440	0.957580	0.89055
				1.5	1.32460	1.22440	1.209200	1.12460

Table 4.3: Comparison of $-\ f''(0)$ for λ as $(\Omega = 0 = \phi_1 = \phi_2 = R)$.

λ	Wang [35]	Arial [36]	Butt et al [37]	Our Outcomes
0.0	1	1	1	1
0.1	1.020902	1.017027	1.020260	1.02137
0.2	1.041804	1.034587	1.039495	1.0404
0.3	1.062705	1.052470	1.057955	1.05871
0.4	1.083607	1.070529	1.075788	1.07643
0.5	1.104509	1.088662	1.093095	1.09364

4.3 Conclusion

The three dimensional steady rotating flow of "hybrid nanofluid $(Ag - CuO/water)$" is examined on a linearly stretching surface. The main conclusion of the work is as follows:

- Thermal boundary of "hybrid nanofluid $(Ag - CuO/water)$" increases by incrementing the heat generation parameter δ_1.
- There is an enhancement in rate of mass transport at surface by increasing Schmidt number Sc and chemical reaction R_{c1}.
- There is an increment in concentration profile with Ω where as it declines concentration at surface.

Chapter 5

Slip flow of 3-D rotating hybrid nanofluid with thermal jump

The comparison of properties of heat transport between $Ag-CuO/water$ and $CuO-water$ are studied in this chapter. Also the impacts of rotation, partial and thermal slip and radiation are examined. The numerical technique BVP-4C is used to tackle the solution of problem, the detailed method is presented in chapter three.

5.1 Problem formulation

Here $3D$ rotating flow of $Ag-CuO/water$ with surface temperature subject to partial slip and $(T_w + l\frac{\partial T}{\partial z})$ is considered. The fluid occupies $z > 0$. $U_w = ax$ and $V_w = by$, $a, b > 0$,. Nanofluid is moving about an axis normal to plane with the constant ω^*.

The representing system is:

$$\frac{\partial u}{\partial x} + \frac{\partial v}{\partial y} + \frac{\partial w}{\partial z} = 0, \tag{5.1}$$

$$u\frac{\partial u}{\partial x} + v\frac{\partial u}{\partial y} + w\frac{\partial u}{\partial z} - 2\omega^* v = \nu_{hnf}\frac{\partial^2 u}{\partial z^2}, \tag{5.2}$$

$$u\frac{\partial v}{\partial x} + v\frac{\partial v}{\partial y} + w\frac{\partial v}{\partial z} + 2\omega^* u = \nu_{hnf}\frac{\partial^2 v}{\partial z^2}, \tag{5.3}$$

$$u\frac{\partial T}{\partial x} + v\frac{\partial T}{\partial y} + w\frac{\partial T}{\partial z} = \alpha_{hnf}\frac{\partial^2 T}{\partial z^2} - \frac{1}{(\rho C_p)_{hnf}}\frac{\partial q_r}{\partial z}. \tag{5.4}$$

Using Roseland approximation

$$q_r = \frac{-4\sigma^*}{3\varrho}\frac{\partial T^4}{\partial z}, \tag{5.5}$$

$$T^4 \approx 4TT_\infty^3 - 3T_\infty^4. \tag{5.6}$$

So the equation (5.4) is

$$u\frac{\partial T}{\partial x} + v\frac{\partial T}{\partial y} + w\frac{\partial T}{\partial z} = \alpha_{hnf}\frac{\partial^2 T}{\partial z^2} + \frac{16\sigma^* T_\infty^3}{3\varrho(\rho C_p)_{hnf}}\frac{\partial^2 T}{\partial z^2}. \tag{5.6(a)}$$

The endpoint conditions are

$$u = U_w + k\nu_f\frac{\partial u}{\partial z}\ , \quad v = V_w + k\nu_f\frac{\partial v}{\partial z}\ , \quad w = 0, \quad T = T_w + l\frac{\partial T}{\partial z}, \quad \text{at } z = 0, \tag{5.7}$$

$$u \to 0, \quad v \to 0, \quad T \to T_\infty \quad \text{as} \quad z \to \infty. \tag{5.8}$$

As

$$\begin{aligned} &u = axf'(\eta), \quad v = ayg'(\eta), \quad w = -\sqrt{a\nu_f}(f(\eta) + g(\eta)), \\ &\eta = z\sqrt{\frac{a}{\nu_f}}, \quad \theta(\eta) = \frac{T - T_\infty}{T_w - T_\infty}, \end{aligned} \tag{5.9}$$

consequently, the above governing problem reduce to

$$f'''(\eta) - (1-\phi_1)^{2.5}(1-\phi_2)^{2.5}[(1-\phi_2)\{(1-\phi_1)+\phi_1(\frac{\rho_{s1}}{\rho_f})\}+\phi_2(\frac{\rho_{s2}}{\rho_f})]$$
$$\times[(f'(\eta))^2 - f''(\eta)(f(\eta)+g(\eta)) - 2\Omega\delta g'(\eta)] = 0, \tag{5.10}$$
$$g'''(\eta) - (1-\phi_1)^{2.5}(1-\phi_2)^{2.5}[(1-\phi_2)\{(1-\phi_1)+\phi_1(\frac{\rho_{s1}}{\rho_f})\}+\phi_2(\frac{\rho_{s2}}{\rho_f})]$$
$$\times[(g'(\eta))^2 - g''(\eta)(f(\eta)+g(\eta)) + 2\tfrac{\Omega}{\delta}f'(\eta)] = 0, \tag{5.11}$$
$$(\tfrac{K_{hnf}}{K_f} + \tfrac{4}{3}R)\theta''(\eta) + \Pr[(1-\phi_2)\{(1-\phi_1)+\phi_1(\tfrac{(\rho C_p)_{s1}}{(\rho C_p)_f})\} + \phi_2(\tfrac{(\rho C_p)_{s2}}{(\rho C_p)_f})](f(\eta)+g(\eta))\theta'(\eta) = 0, \tag{5.12}$$

$$f=0, \quad f' = 1+\alpha f''(0), \quad g=0, \quad g' = \lambda + \alpha g''(0), \quad \theta = 1+\beta\theta'(0) \qquad \text{at} \quad \eta = 0,$$
$$f' \to 0, \quad g' \to 0, \quad \theta \to 0 \quad \text{as} \quad \eta \to \infty. \tag{5.13}$$

These parameters are defined by

$$\Omega = \frac{\omega^*}{a}, \ \lambda = \frac{b}{a}, \alpha = k\sqrt{a\nu_f}, \ \beta = l\sqrt{\frac{a}{\nu_f}}, \ \Pr = \frac{\nu_f(\rho C_p)_f}{K_f}, \ R = \frac{4\sigma^* T_\infty^3}{\varrho K_f}. \tag{5.14}$$

And

$$C_{fx} = \frac{\mu_{hnf}(\frac{\partial u}{\partial z})_{z=0}}{\rho_f (ax)^2}, \ C_{fy} = \frac{\mu_{hnf}(\frac{\partial v}{\partial z})_{z=0}}{\rho_f (ax)^2}, \ Nu_x = -\frac{xK_{hnf}}{K_f\,(T_w - T_\infty)}\left(\frac{\partial T}{\partial z}\right)\bigg|_{z=0} + (q_r)_w.$$

$$\mathrm{Re}^{\frac{1}{2}}\, C_{fx} = \frac{1}{(1-\phi_1)^{2.5}(1-\phi_2)^{2.5}} f''(0), \quad \delta^{-1}\,\mathrm{Re}^{\frac{1}{2}}\, C_{fy} = \frac{1}{(1-\phi_1)^{2.5}(1-\phi_2)^{2.5}} g''(0),$$
$$\mathrm{Re}^{-\frac{1}{2}}\, Nu_x = -(\frac{K_{hnf}}{K_f} + \frac{4}{3}R)\theta'(0). \tag{5.16}$$

5.2 Discussion Section

This section scrutinizes aspects of flow imperatives on velocity and temperature fields. From *Figs.* (5.1 − 5.2), with the rise in α there is a clear decrease in velocity field

Table 5.1: Comparison of heat transport rate when $\alpha = \beta = \Omega = R = 0$.

λ	Our Outcomes $Ag-CuO/water$	SSUDevi & SPA Devi [73] $Cu-Al_2O_3/Water$
0.0	1.7603	0.25575
0.2	1.953	0.26006
0.4	2.121	0.26329

or both $(CuO - water)$ and $(Ag - CuO/water)$. Behaviour of β on temperature field is portrayed in $Fig.$ (5.3). From this figure, there is reduction in temperature with the rise in β. Impacts of Ω on velocity and temperature field are elucidated from $Figs.$ $(5.4 - 5.6)$. There is a noteworthy decay in velocity with the increase in Ω but on the other hand temperature rises significantly. Hybrid nanofluid $(Ag - CuO/water)$ has larger temperature than simple nanofluid $(CuO - water)$ due to its larger thermal conductivity which helps in enhancement in temperature. From $Fig.$ (5.7) the temperature distribution increases with R. This is due to reason that heat flux at surface increases with R which ultimately boost temperature. $Figs.$ $(5.8 - 5.9)$ displays the character of friction factor with Ω for two estimations of α. In $Fig.$ (5.8), friction factor decreases with Ω and α but in $Fig.$ (5.9) it rises with Ω and decreases with α. Also the friction factor of $Ag - CuO/water$ is more than simple nanofluid $(CuO - water)$. $Fig.$ (5.10) explore the effect of heat transport rate with Ω for two estimations of α. From this figure, heat transport rate diminishes with

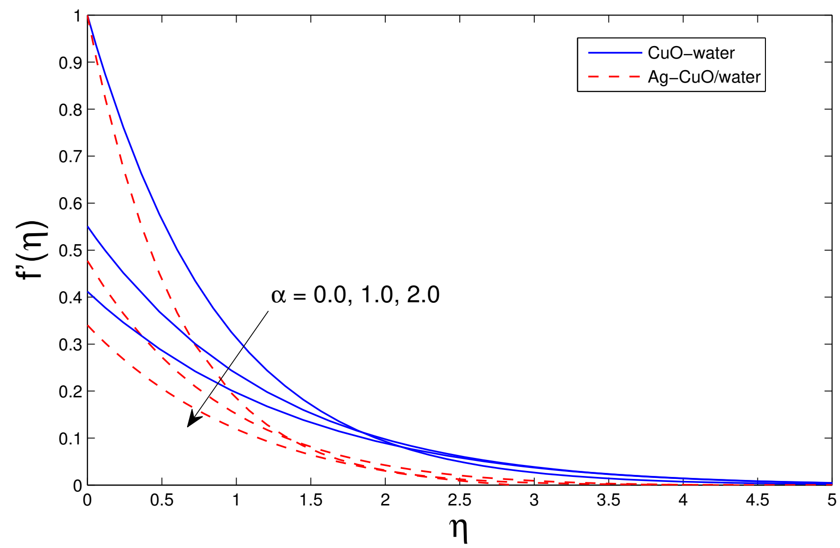

Figure 5.1: variation of α on $f'(\eta)$.

Ω and α. Additionally $Ag-CuO/water$ has larger heat transport rate than $CuO-water$. It could be accomplished by proper choice of proportions of nanoparticles. The comparison of the results of $Ag-CuO/water$ with nanoparticles composite $Cu-Al_2O_3/Water$ are shown in $Table$ 5.1. Also, effects of the parameters involved in present study on friction factor and heat transport rate are given in $Tables$ (5.2−5.3).

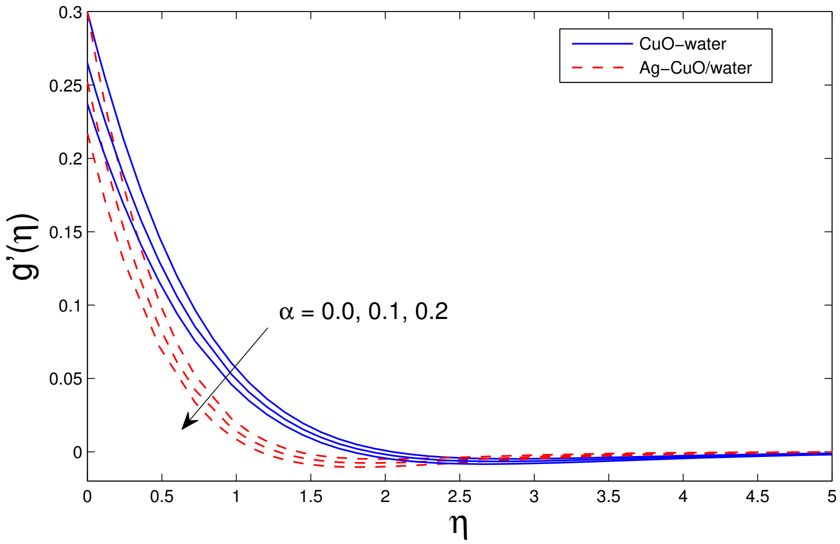

Figure 5.2: variation of α on $g'(\eta)$.

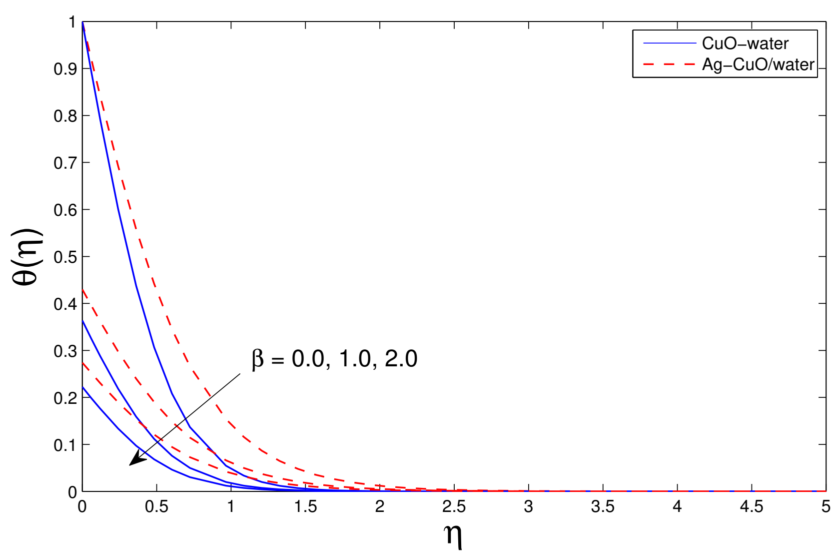

Figure 5.3: variation of β on $\theta(\eta)$.

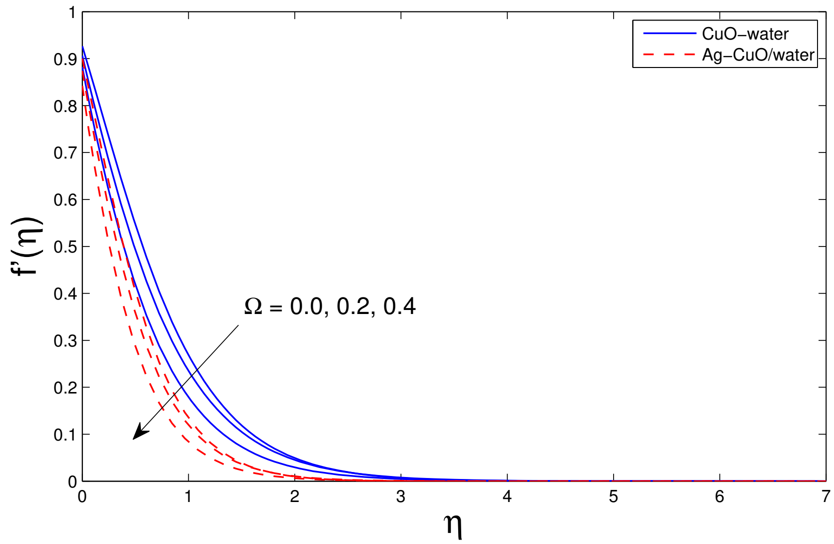

Figure 5.4: variation of Ω on $f'(\eta)$.

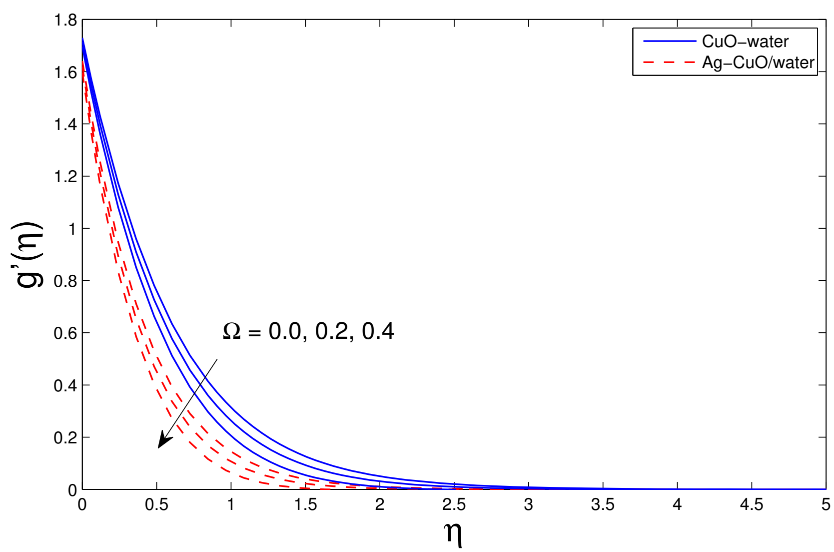

Figure 5.5: variation of Ω on $g'(\eta)$.

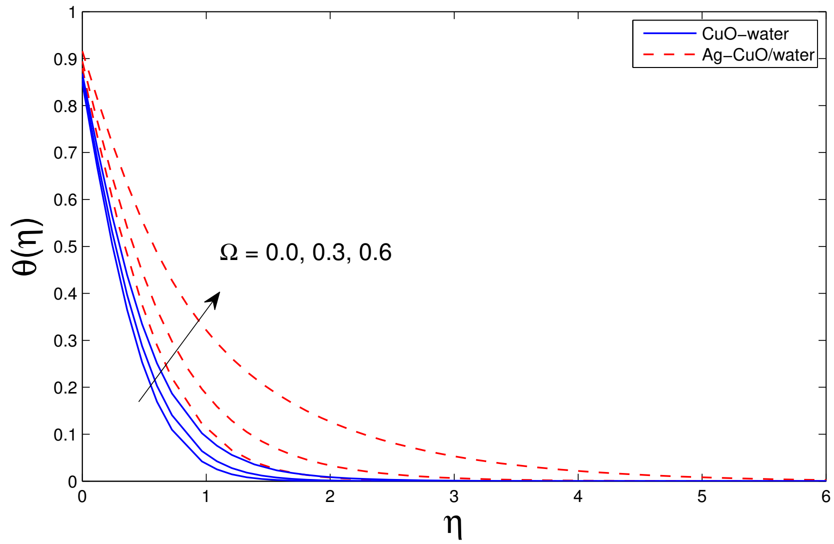

Figure 5.6: variation of Ω on $\theta(\eta)$.

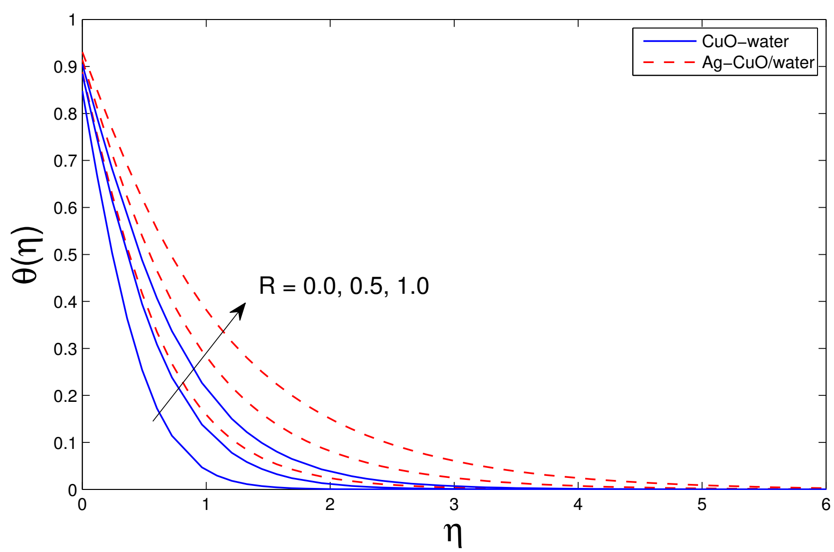

Figure 5.7: variation of R on $\theta(\eta)$.

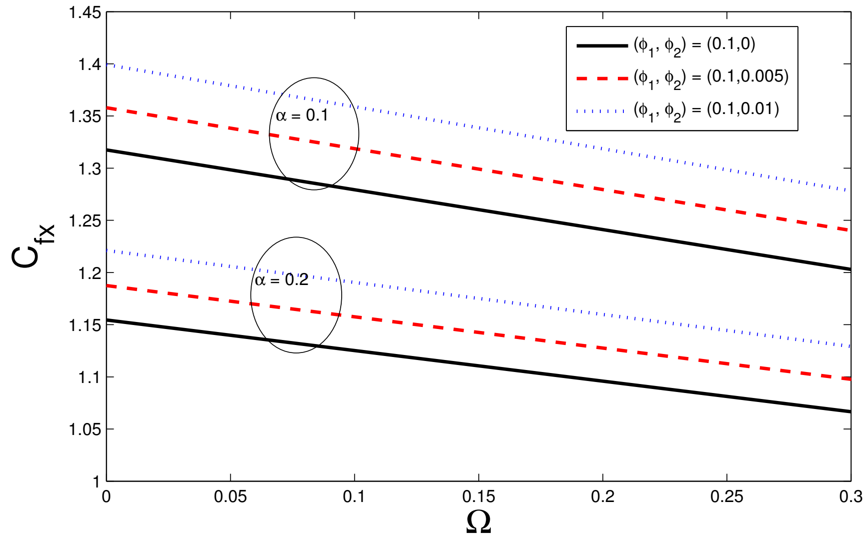

Figure 5.8: Skin-friction against Ω for α in x-direction.

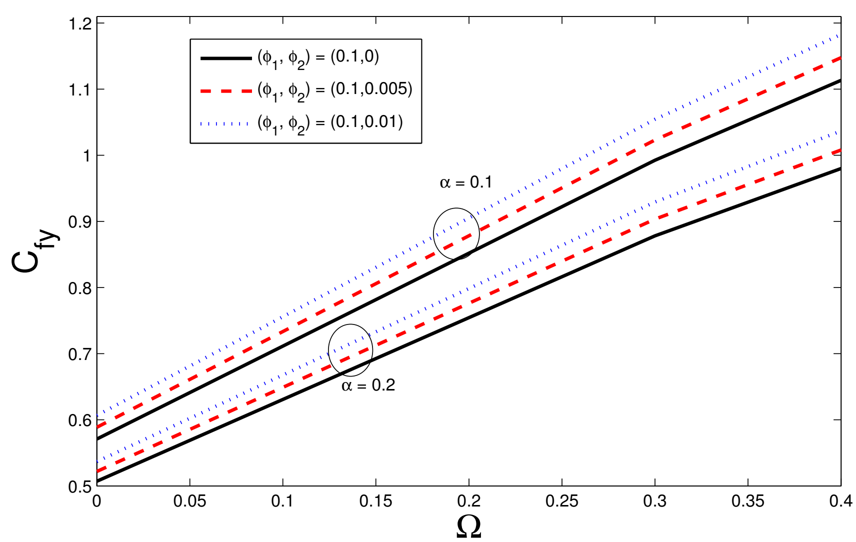

Figure 5.9: Skin-friction against Ω for α in y-direction.

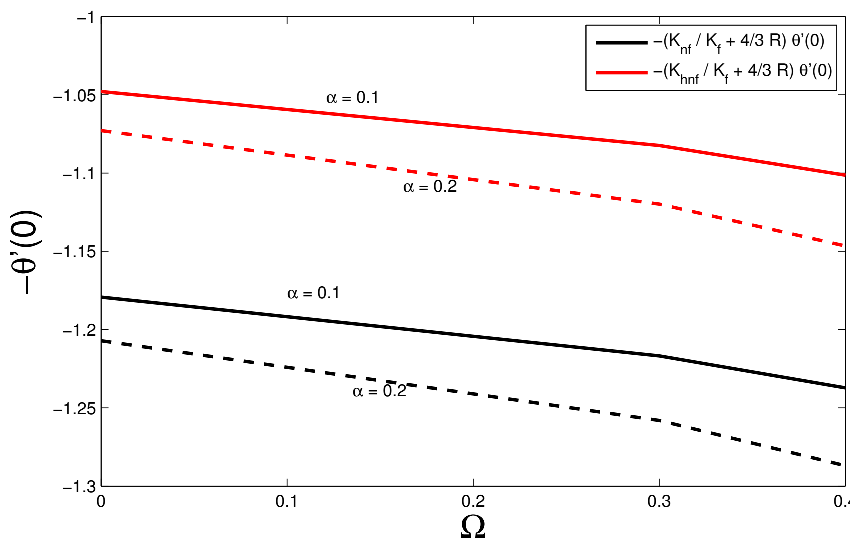

Figure 5.10: Rate of heat transport against Ω for α.

Table 5.2: Variations of $-f''(0)$, $-g''(0)$ for $CuO-water$ and $Ag-CuO/water$ with $\phi_1 = 0.1$.

α	β	Ω	λ	R	$-\frac{1}{(1-\phi_1)^{2.5}}f''(0)$	$-\frac{(1-\phi_1)^{-2.5}}{(1-\phi_2)^{2.5}}f''(0)$	$-\frac{1}{(1-\phi_1)^{2.5}}g''(0)$	$-\frac{(1-\phi_1)^{-2.5}}{(1-\phi_2)^{2.5}}g''(0)$
0	1	0.2	0.5	0.5	1.85063	2.21877	1.27913	1.53358
0.1					1.52545	1.8289	1.06515	1.27704
0.2					1.30868	1.56902	0.91979	1.10276
0.1	0				1.52545	1.8289	1.06515	1.27704
	1				1.52545	1.8289	1.06515	1.27704
	2				1.52545	1.8289	1.06515	1.27704
		0			1.64273	1.96951	0.715103	0.857356
		0.2			1.52545	1.8289	1.06515	1.27704
		0.4			1.50328	1.80232	1.40482	1.68427
			0		1.60783	1.92767	0.602434	0.722274
			0.5		1.52545	1.8289	1.06515	1.27704
			1		1.51305	1.81403	2.0322	2.43646
				0	1.52545	1.82891	1.06516	1.27704
				0.5	1.52545	1.82891	1.06516	1.27704
				1	1.52545	1.82891	1.06516	1.27704

5.3 Key Points

Important key points are given bellow:

- Temperature and rate of heat transport at surface in presence of hybrid nanofluid $(Ag - CuO/water)$ is noticed higher than simple nanofluid $(CuO - water)$.
- Temperature rises with Ω and R but decreases with α and β.

Table 5.3: Impact of $-\theta'(0)$ for $CuO-water$ and $Ag-CuO/water$ with $\phi_1 = 0.1$.

α	β	Ω	λ	R	$-(\frac{K_{nf}}{K_f} + \frac{4}{3}R)\theta'(0)$	$-(\frac{K_{hnf}}{K_f} + \frac{4}{3}R)\theta'(0)$
0	1	0.2	0.5	0.5	0.76136	1.087
0.1					0.73547	1.05
0.2					0.71339	1.0185
0.1	0				1.6537	2.3609
	1				0.73547	1.05
	2				0.4729	0.67515
		0			0.74932	1.0698
		0.2			0.73547	1.05
		0.4			0.71038	1.0142
			0		0.34789	0.49667
			0.5		0.73547	1.05
			1		0.79091	1.1292
				0	0.82359	0.76131
				0.5	1.1056	1.05
				1	1.3425	1.2919

Chapter 6

An optimal solution of Cattaneo-Christov heat flux model and chemical processes for 3D flow of Eyring-Powell fluid

This chapter investigates attributes of Eyring-Powell fluid with heterogeneous-homogenous processes. Moreover, investigation of heat conduction is carried out with revised heat flux relation. 3-D linearly stretching surface is considered. Analytical results are obtained by OHAM. Aspects of pertinent parameters are delineated through graphical illustrations. We found that temperature profile declines with enhancing the estimations of thermal relaxation parameter. Furthermore, the concentration increases with the augmented estimations of Lewis number.

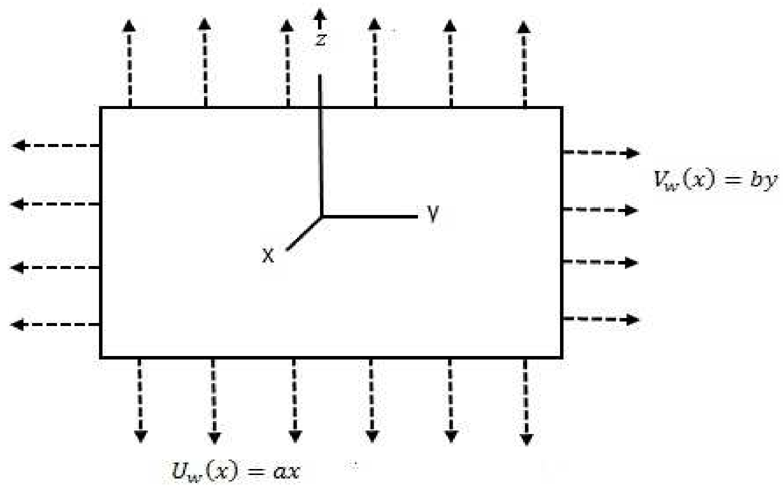

Figure 6.1: Flow representation.

6.1 Mathematical modeling

Consider $(3D)$ time independent flow of Eyring-powell liquid occupies $z > 0$ shown in $Fig.$ 6.1. U_w and V_w, are liquid velocities. In an Eyring-powell liquid,

$$\vec{S} = -p\vec{I} + \vec{\tau}_{ij}, \tag{6.1}$$

$$\rho\frac{d\vec{V}}{dt} = -\nabla p + \nabla.(\vec{\tau}_{ij}), \tag{6.2}$$

$$\vec{\tau}_{ij} = \mu\frac{\partial u_i}{\partial x_j} + \frac{1}{\Omega_1}sinh^{-1}(\frac{1}{\sigma_1}\frac{\partial u_i}{\partial x_j}). \tag{6.3}$$

Assuming 2nd order estimation of $sinh^{-1}$ i.e.

$$sinh^{-1}(\frac{1}{\sigma_1}\frac{\partial u_i}{\partial x_j}) \cong \frac{1}{\sigma_1}\frac{\partial u_i}{\partial x_j} - \frac{1}{6}(\frac{1}{\sigma_1}\frac{\partial u_i}{\partial x_j})^3, \quad |\frac{1}{\sigma_1}\frac{\partial u_i}{\partial x_j}| <<< 1. \tag{6.4}$$

For cubic autocatalysis, the homogeneous isothermal reaction can be written as:

$$A_1 + 2A_2 \to 3A_2, rate = k_r a_1 a_2^2, \tag{6.5}$$

while the first order, single isothermal reaction on catalyst is represented as follows:

$$A_1 \rightarrow A_2, \quad rate = k_s a_1. \tag{6.6}$$

Both reactions are supposed to be isothermal. In perspective of the theory of Cattaneo-Christov, $\vec{q}$ satisfies following equation [52]:

$$\vec{q} + \lambda_e(\frac{\partial \vec{q}}{\partial t} + \vec{V}.\nabla\vec{q} - \vec{q}.\nabla\vec{V} + (\nabla.\vec{V})\vec{q}) = -k\nabla T. \tag{6.7}$$

By putting λ_e=0, equation (6.7) deduces to basic law of Fourier. By supposing steady and incompressible flow, the above equation is as:

$$\vec{q} + \lambda_e(\vec{V}.\nabla\vec{q} - \vec{q}.\nabla\vec{V}) = -K_f\nabla T. \tag{6.8}$$

For under consideration problem, the boundary layer equations are $[78 - 80]$:

$$\frac{\partial u}{\partial x} + \frac{\partial v}{\partial y} + \frac{\partial w}{\partial z} = 0, \tag{6.9}$$

$$u\frac{\partial u}{\partial x} + v\frac{\partial u}{\partial y} + w\frac{\partial u}{\partial z} = (\nu + \frac{1}{\Omega_1\sigma_1\rho})\frac{\partial^2 u}{\partial z^2} - \frac{1}{2\Omega_1\sigma_1^3\rho}(\frac{\partial u}{\partial z})^2\frac{\partial^2 u}{\partial z^2}, \tag{6.10}$$

$$u\frac{\partial v}{\partial x} + v\frac{\partial v}{\partial y} + w\frac{\partial v}{\partial z} = (\nu + \frac{1}{\Omega_1\sigma_1\rho})\frac{\partial^2 v}{\partial z^2} - \frac{1}{2\Omega_1\sigma_1^3\rho}(\frac{\partial v}{\partial z})^2\frac{\partial^2 v}{\partial z^2}, \tag{6.11}$$

$$u\frac{\partial T}{\partial x} + v\frac{\partial T}{\partial y} + w\frac{\partial T}{\partial z} + \lambda_e\Gamma_e = \alpha_f\frac{\partial^2 T}{\partial z^2}, \tag{6.12}$$

$$u\frac{\partial a_1}{\partial x} + v\frac{\partial a_1}{\partial y} + w\frac{\partial a_1}{\partial z} = F_{A_1}\frac{\partial^2 a_1}{\partial z^2} - k_r a_1 a_2^2, \tag{6.13}$$

$$u\frac{\partial a_2}{\partial x} + v\frac{\partial a_2}{\partial y} + w\frac{\partial a_2}{\partial z} = F_{A_2}\frac{\partial^2 a_2}{\partial z^2} + k_r a_1 a_2^2. \tag{6.14}$$

The prescribed B.C are

$$u = U_w = ax,\ v = V_w = by,\ w = 0,\ T = T_w,\ F_{A_1}\frac{\partial a_1}{\partial z} = k_s a_1,\ F_{A_2}\frac{\partial a_2}{\partial z} = -k_s a_1, \quad \text{at } z = 0,$$

$$u \rightarrow 0,\ v \rightarrow 0,\ T \rightarrow T_\infty,\ a_1 \rightarrow (a_1)_0,\ a_2 \rightarrow 0, \qquad \text{as } z \rightarrow \infty. \tag{6.15}$$

Where

$$\Gamma_e = u^2\frac{\partial^2 T}{\partial x^2} + v^2\frac{\partial^2 T}{\partial y^2} + w^2\frac{\partial^2 T}{\partial z^2} + 2uv\frac{\partial^2 T}{\partial x\partial y} + 2vw\frac{\partial^2 T}{\partial y\partial z} + 2uw\frac{\partial^2 T}{\partial x\partial z}$$
$$+ (u\frac{\partial u}{\partial x} + v\frac{\partial u}{\partial y} + w\frac{\partial u}{\partial z})\frac{\partial T}{\partial x} + (u\frac{\partial v}{\partial x} + v\frac{\partial v}{\partial y} + w\frac{\partial v}{\partial z})\frac{\partial T}{\partial y}$$
$$+ (u\frac{\partial w}{\partial x} + v\frac{\partial w}{\partial y} + w\frac{\partial w}{\partial z})\frac{\partial T}{\partial z}, \tag{6.16}$$

Selecting

$$\eta = z\sqrt{\frac{a}{\nu}},\ u = axf'(\eta),\ v = ayg'(\eta),\ w = -\sqrt{a\nu}(f(\eta) + g(\eta)),$$
$$\theta\left(\eta\right) = \frac{T - T_\infty}{T_w - T_\infty},\ a_1 = (a_1)_0\xi(\eta),\ a_2 = (a_1)_0\Upsilon(\eta)\ . \tag{6.17}$$

Automatically continuity equation is verified and Eqs. (6.10-6.14) yield

$$(1+\gamma)f''' + (f+g)f'' - f'^2 - \gamma\varepsilon_1(f'')^2 f''' = 0, \tag{6.18}$$

$$(1+\gamma)g''' + (f+g)g'' - g'^2 - \gamma\varepsilon_2(g'')^2 g''' = 0, \tag{6.19}$$

$$\theta'' + \Pr(f+g)\theta' - \Pr\alpha_1\{(f+g)(f'+g')\theta' + (f+g)^2\theta''\} = 0, \tag{6.20}$$

$$\frac{1}{(\Pr)(Le)}\xi'' + (f+g)\xi' - \sigma_2\xi\Upsilon^2 = 0, \tag{6.21}$$

$$\frac{\chi}{(\Pr)(Le)}\Upsilon'' + (f+g)\Upsilon' + \sigma_2\xi\Upsilon^2 = 0, \tag{6.22}$$

$$f = 0,\ f' = 1,\ g = 0,\ g' = \lambda,\ \theta = 1,\ \xi' = j\xi,\ \chi\Upsilon' = -j\xi, \quad \text{at } \eta = 0,$$

$$f' = 0,\ g' = 0,\ \theta = 0,\ \xi = 1,\ \Upsilon = 0, \quad \text{as } \eta \to \infty, \tag{6.23}$$

where

$$\gamma = \frac{1}{\mu\Omega_1\sigma_1},\ \varepsilon_1 = \frac{a^3x^2}{2\nu\sigma_1^2},\ \varepsilon_2 = \frac{a^3y^2}{2\nu\sigma_1^2},\ \lambda = \frac{b}{a},\ \Pr = \frac{\upsilon}{\alpha_f},$$
$$Le = \frac{\alpha_f}{F_{A_1}},\ \sigma_2 = \frac{k_r(a_1)_0^2}{a},\ \chi = \frac{F_{A_2}}{F_{A_1}},\ j = \frac{k_s}{F_{A_1}},\ \alpha_1 = \lambda_e a. \tag{6.24}$$

It is supposed that F_{A_1} and F_{A_2} of A_1 and A_2 are of comparable size i.e. F_{A_1} and F_{A_2} are equal so χ=1. Thus:

$$\xi(\eta) + \Upsilon(\eta) = 1. \tag{6.25}$$

Hence Eqs. (6.20-6.21) takes the form

$$\frac{1}{(\mathrm{Pr})(Le)}\xi'' + (f+g)\xi' - \sigma_2\xi(1-\xi)^2 = 0, \tag{6.26}$$

$$\xi' = j\xi(0), \quad \xi(\infty) \to 1. \tag{6.27}$$

6.2 Graphical Results and Discussion

This area exhibits aspects of different related parameters, for example, λ (0$\leq$ λ $\leq$1.5), γ (0$\leq$ γ $\leq$7),ε_1 (0$\leq$ ε_1 $\leq$12) and ε_2(0$\leq$ ε_2 $\leq$20), α_1 (0$\leq$ α_1 $\leq$0.2), σ_2 (0$\leq$ σ_2 $\leq$2), j (0.5$\leq$j$\leq$2.0), Pr (0.5$\leq$Pr$\leq$1.0), and Le (0.5$\leq$Le$\leq$1.5) on $\theta(\eta)$ and $\xi(\eta)$ profiles. Range has been referred to by [81]. Aspects of λ on $\theta(\eta)$ profile are shown in Fig. 6.2. We observe that, by increasing λ, $\theta(\eta)$ declines. Physically, liquid velocity increases by increasing λ so there is less viscosity of the fluid to its motion. Hence production of heat is low. Effects of γ, ε_1, ε_2 on $\theta(\eta)$ are portrayed in $Figs$. $6.3-6.5$. We observe that associated thermal boundary layer and $\theta(\eta)$ increase when γ, ε_1, ε_2 increase. Aspects of Pr on $\theta(\eta)$ temperature profile can be analyzed from Fig. 6.6. Effects of λ on concentration profile are shown in Fig. 6.7. By increasing λ, there is an increase in stretching along y-axis which in turn increases concentration. $Figs$. $6.8-6.10$ show the influence of γ, ε_1, ε_2 on concentration $\xi(\eta)$ profile. By increasing γ, ε_1, ε_2, $\xi(\eta)$ decreases. Behaviors of Pr on $\xi(\eta)$ are shown through Fig. 6.11. Increasing Pr

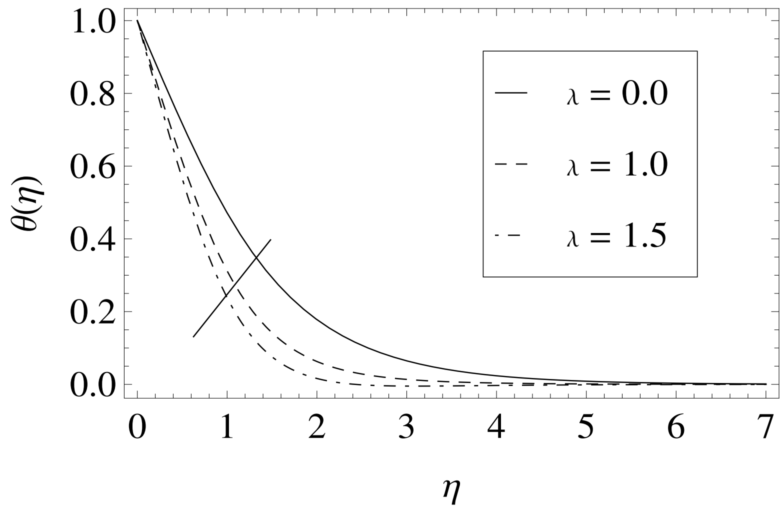

Figure 6.2: Aspect of λ on $\theta(\eta)$.

enhances the concentration profile. Physically, higher Pr boosts momentum diffusivity which results in increase in fluid concentration. *Fig.* 6.12 depicts the aspects of Le on $\xi(\eta)$ profile. Greater values of Le relate to enhancement in thermal diffusivity, that is why enhancement in concentration $\xi(\eta)$ profile is noticed. Properties of σ_2 and j on $\xi(\eta)$ are shown in *Figs.* $6.13 - 6.14$. By increasing σ_2 and j, the concentration profile decreases because more reactants are consumed which causes the concentration of a fluid to decrease.

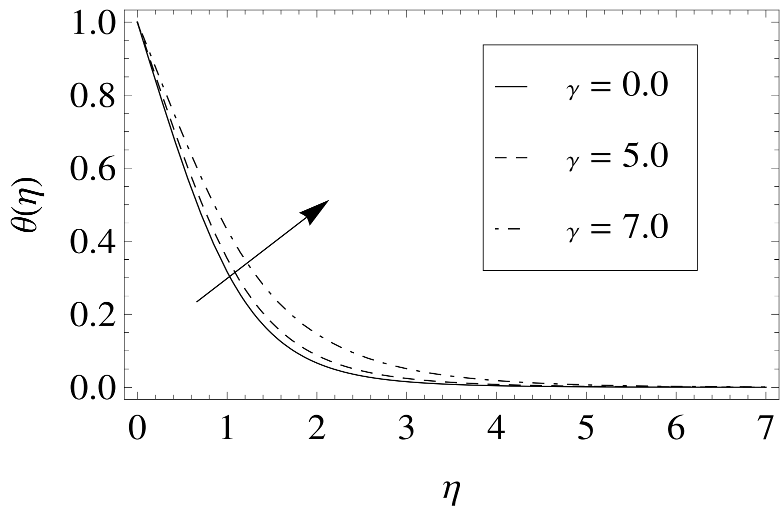

Figure 6.3: Aspect of γ on $\theta(\eta)$.

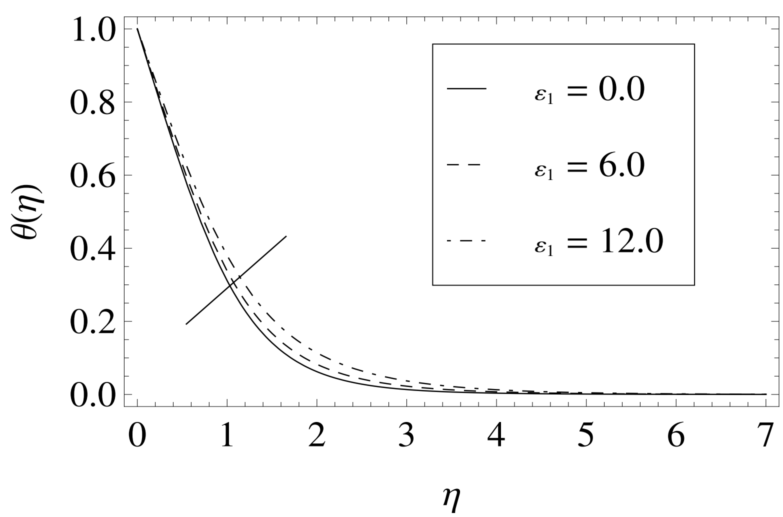

Figure 6.4: Aspect of ε_1 on $\theta(\eta)$.

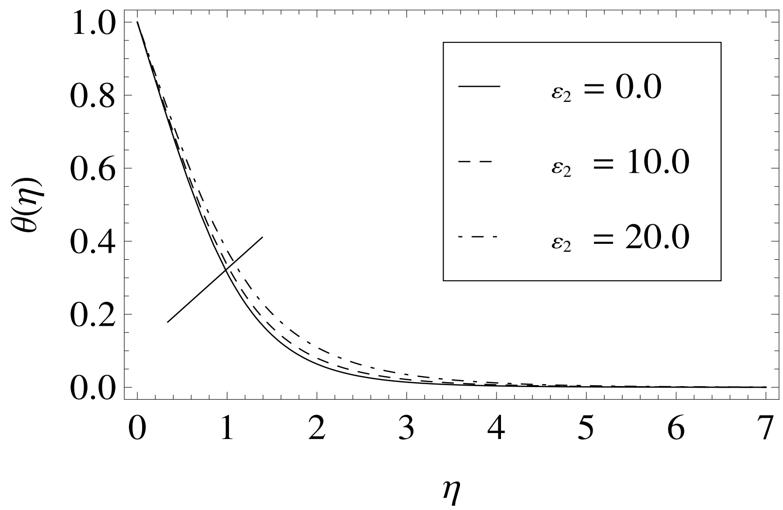

Figure 6.5: Aspect of ε_2 on $\theta(\eta)$.

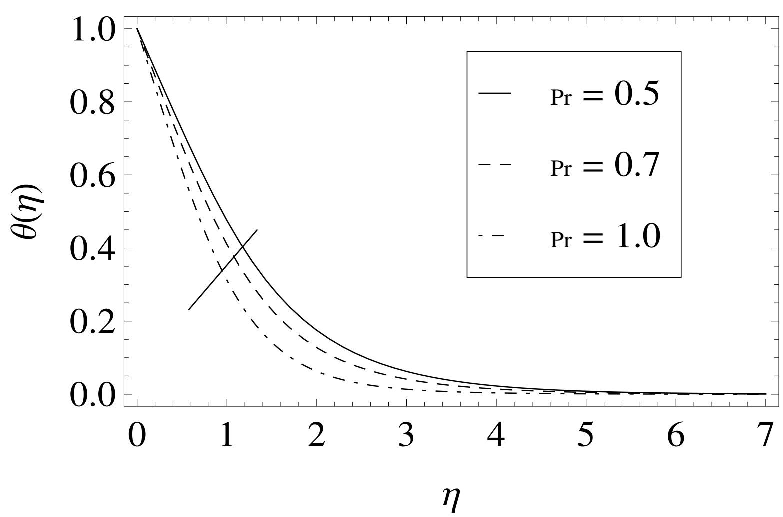

Figure 6.6: Aspect of Pr on $\theta(\eta)$.

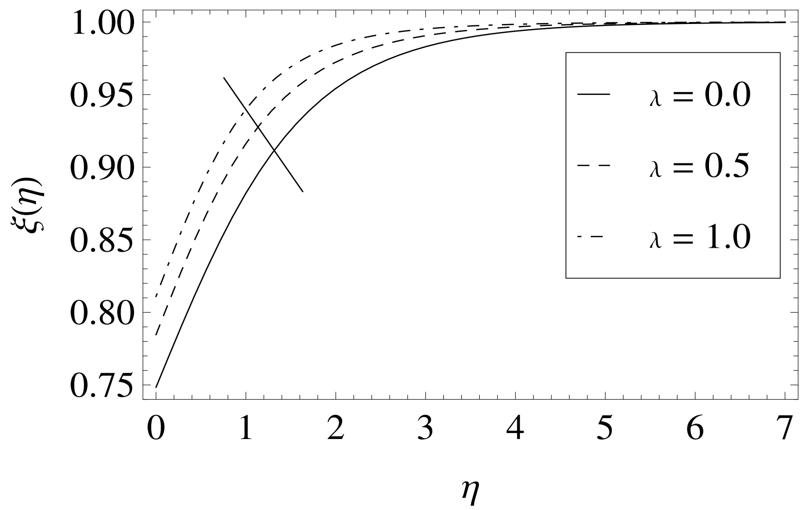

Figure 6.7: Aspect of λ on $\xi(\eta)$.

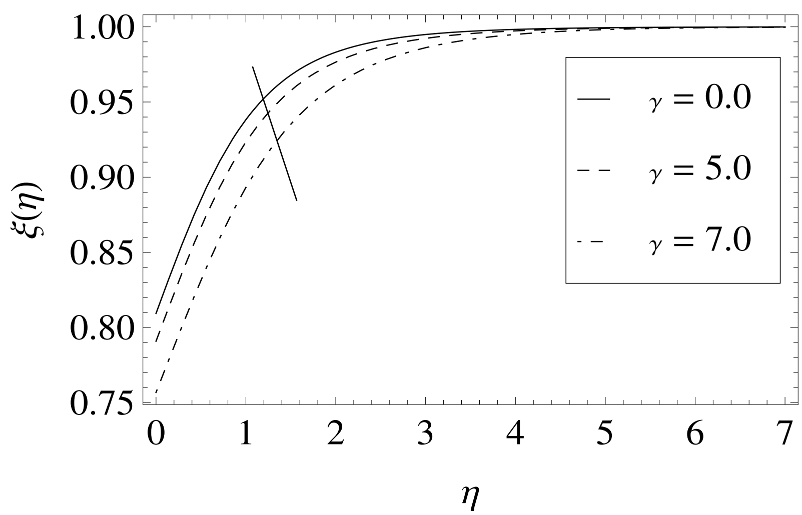

Figure 6.8: Aspect of γ on $\xi(\eta)$.

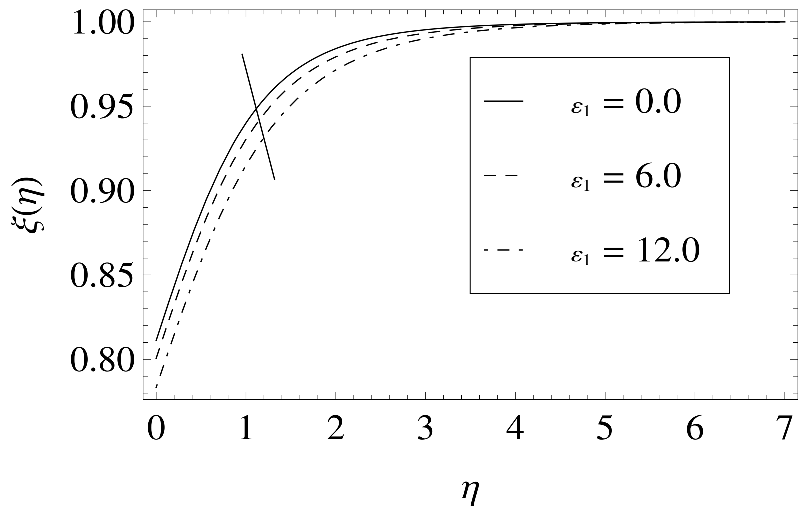

Figure 6.9: Aspect of ε_1 on $\xi(\eta)$.

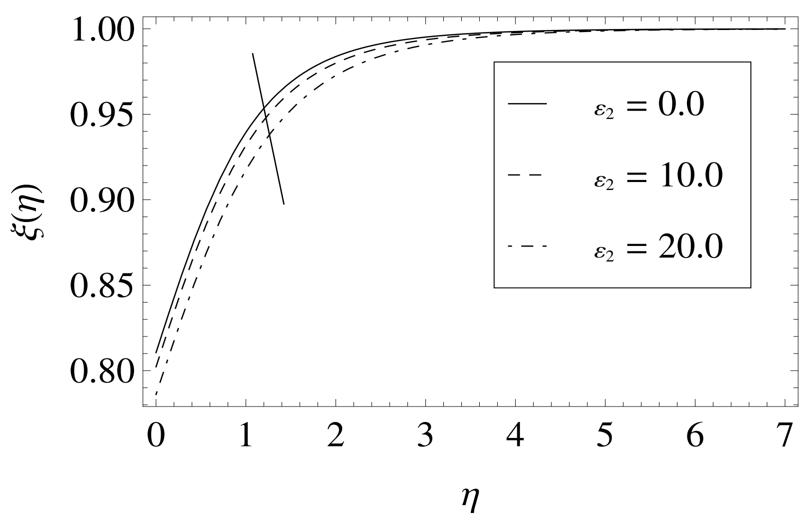

Figure 6.10: Aspect of ε_2 on $\xi(\eta)$.

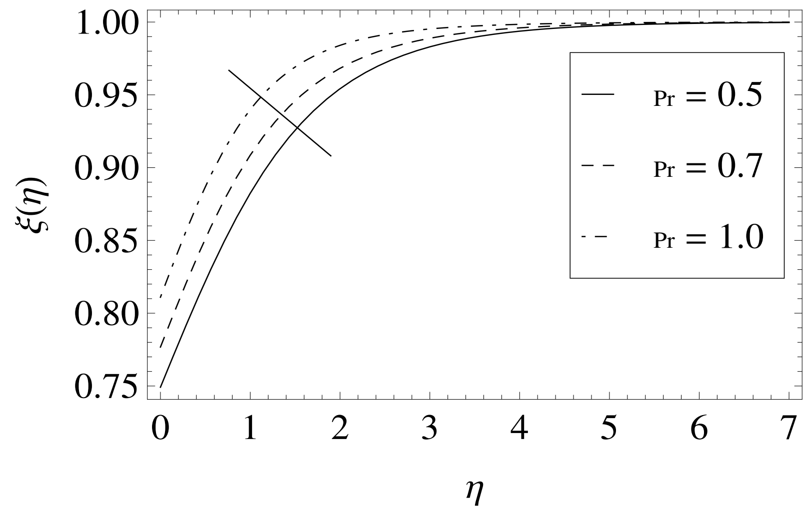

Figure 6.11: Aspect of Pr on $\xi(\eta)$.

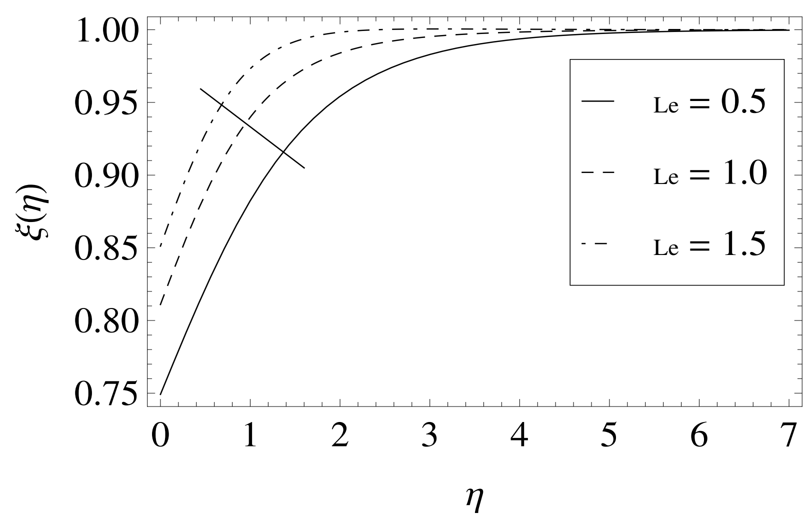

Figure 6.12: Aspect of Le on $\xi(\eta)$.

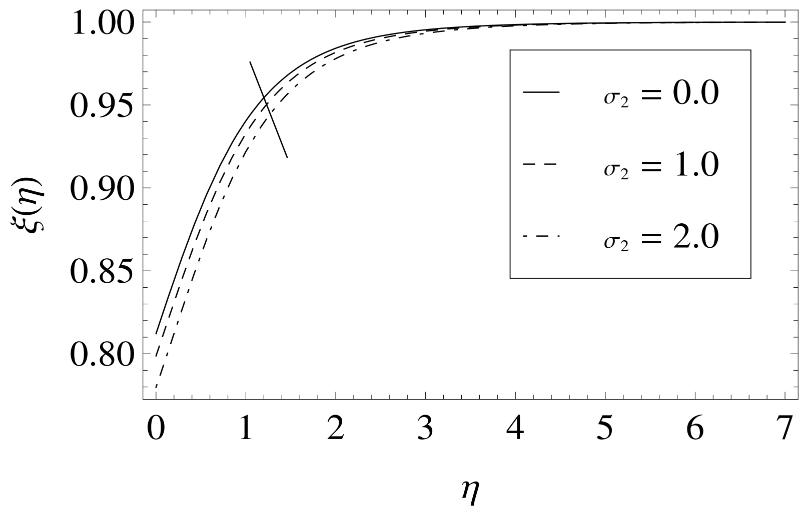

Figure 6.13: Aspect of σ_2 on $\xi(\eta)$.

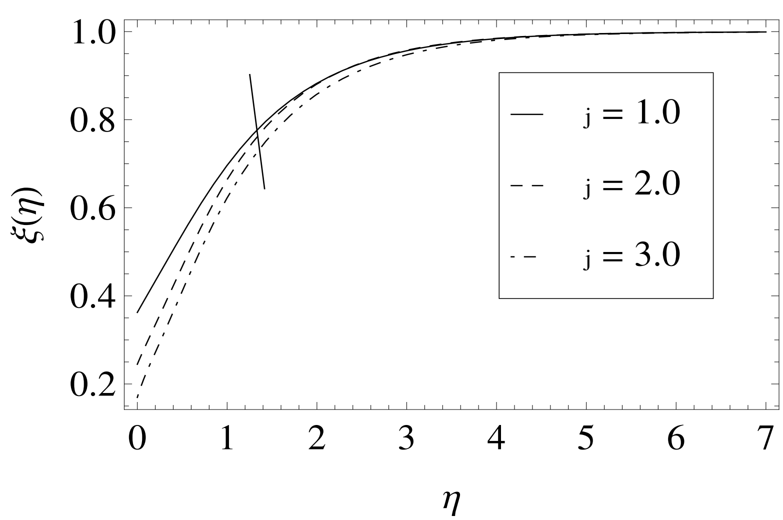

Figure 6.14: Aspect of j on $\xi(\eta)$.

6.3 Concluding remarks

An analysis is performed on 3-D Eyring-Powell liquid past a stretching surface in sight of homogeneous-heterogeneous processes. Heat transport study is effectuated in the thermal relaxation parameter by imposing new heat flux model. Results are achieved by employing OHAM. The main conclusions are as follows:

- $\theta(\eta)$ declines with the rising values of α_1.
- Concentration profile decreases for both Prandtl number and Lewis number due to the increase in momentum diffusivity and thermal diffusivity, respectively.
- Concentration profile is the decreasing function of both σ_2 and j. Reason is very clear that in reaction process, more reactants are consumed that is why concentration of a fluid declines.

Chapter 7

Flow of 3D Eyring-Powell fluid with revised heat flux relation and chemical processes over an exponentially stretching surface

This chapter examines 3-D Eyring-Powell liquid flow with chemical reactions. A new heat flux model is utilized to investigate properties of relaxation time. There is an inverse relationship between temperature and thermal relaxation time. Temperature inrevised heat flux relation is very less than classical Fourier's relation. In this study 3-D revised heat flux relation over an exponentially stretched surface is calculated first time. For negative A, temperature firstly intensifies to its extreme value and after that gradually declines to zero, which shows the occurrence of phe-

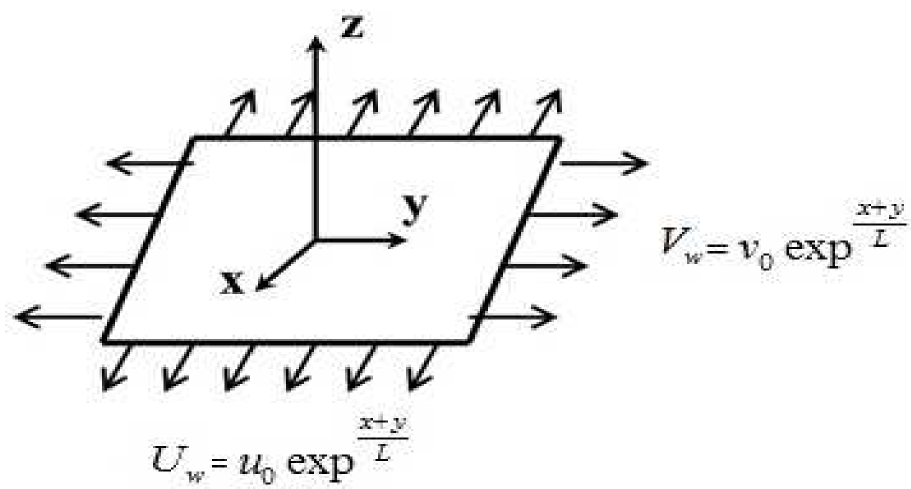

Figure 7.1: Physical configuration and coordinate system.

nomenon (SGH)"Sparrow-Gregg hill". Also, for higher values of strength of reaction parameters, the concentration profile decreases.

7.1 Mathematical modeling and flow analysis

Consider the three-dimensional, incompressible Eyring-Powell liquid flow on an exponentially stretched surface. The laminar flow is restricted in the domain $z > 0$ (see $Fig.$ 7.1). A simple model of chemical reactions suggested by Chaudhary and Merkin [57] is considered in the present chapter.

The principal equations are [82]:

$$\frac{\partial u}{\partial x}+\frac{\partial v}{\partial y}+\frac{\partial w}{\partial z}=0, \tag{7.1}$$

$$u\frac{\partial u}{\partial x}+v\frac{\partial u}{\partial y}+w\frac{\partial u}{\partial z}=(\nu+\frac{1}{\Omega_1\sigma_1\rho})\frac{\partial^2 u}{\partial z^2}-\frac{1}{2\Omega_1\sigma_1^3\rho}(\frac{\partial u}{\partial z})^2\frac{\partial^2 u}{\partial z^2}, \tag{7.2}$$

$$u\frac{\partial v}{\partial x}+v\frac{\partial v}{\partial y}+w\frac{\partial v}{\partial z}=(\nu+\frac{1}{\Omega_1\sigma_1\rho})\frac{\partial^2 v}{\partial z^2}-\frac{1}{2\Omega_1\sigma_1^3\rho}(\frac{\partial v}{\partial z})^2\frac{\partial^2 v}{\partial z^2}, \tag{7.3}$$

$$\rho c_p(u\frac{\partial T}{\partial x}+v\frac{\partial T}{\partial y}+w\frac{\partial T}{\partial z})=-\nabla.\vec{q}, \tag{7.4}$$

$$u\frac{\partial a_1}{\partial x}+v\frac{\partial a_1}{\partial y}+w\frac{\partial a_1}{\partial z}=F_{A_1}\frac{\partial^2 a_1}{\partial z^2}-k_r a_1 a_2^2, \tag{7.5}$$

$$u\frac{\partial a_2}{\partial x}+v\frac{\partial a_2}{\partial y}+w\frac{\partial a_2}{\partial z}=F_{A_2}\frac{\partial^2 a_2}{\partial z^2}+k_r a_1 a_2^2, \tag{7.6}$$

Now discard $\vec{q}$ from Eqs. (7.4) and (6.8), the following governing equation is as follows [83]:

$$\begin{aligned}u\frac{\partial T}{\partial x}+v\frac{\partial T}{\partial y}+w\frac{\partial T}{\partial z}&=\alpha_f\frac{\partial^2 T}{\partial z^2}-\lambda_e[u^2\frac{\partial^2 T}{\partial x^2}+v^2\frac{\partial^2 T}{\partial y^2}+w^2\frac{\partial^2 T}{\partial z^2}+2uv\frac{\partial^2 T}{\partial x\partial y}+2vw\frac{\partial^2 T}{\partial y\partial z}\\&+2uw\frac{\partial^2 T}{\partial x\partial z}+(u\frac{\partial u}{\partial x}+v\frac{\partial u}{\partial y}+w\frac{\partial u}{\partial z})\frac{\partial T}{\partial x}+(u\frac{\partial v}{\partial x}+v\frac{\partial v}{\partial y}+w\frac{\partial v}{\partial z})\frac{\partial T}{\partial y}\\&+(u\frac{\partial w}{\partial x}+v\frac{\partial w}{\partial y}+w\frac{\partial w}{\partial z})\frac{\partial T}{\partial z}],\end{aligned} \tag{7.7}$$

With relevant conditions

$$\begin{aligned}&u=U_w,\ v=V_w,\ w=0,\ T=T_w,\ F_{A_1}\frac{\partial a_1}{\partial z}=k_s a_1,\ F_{A_2}\frac{\partial a_2}{\partial z}=-k_s a_1,\quad \text{at } z=0,\\&u\to 0,\ v\to 0,\ T\to T_\infty,\ a_1\to (a_1)_0 e^{\frac{B(x+y)}{2L}},\ a_2\to 0,\qquad \text{as } z\to\infty.\end{aligned} \tag{7.8}$$

The velocities and temperature at the wall are given by

$$U_w=u_0 e^{\frac{x+y}{L}},\ V_w=v_0 e^{\frac{x+y}{L}},\ T_w=T_\infty+T_0 e^{\frac{A(x+y)}{2L}}.$$

Now transformations are [84]:

$$\eta = z\sqrt{\frac{u_0}{2\nu L}}e^{\frac{(x+y)}{2L}},\ u = u_0 e^{\frac{x+y}{L}} f'(\eta),\ v = u_0 e^{\frac{x+y}{L}} g'(\eta),$$
$$w = -\sqrt{\frac{\nu u_0}{2L}}e^{\frac{(x+y)}{2L}}(f(\eta)+g(\eta)+\eta(f'(\eta)+g'(\eta))),$$
$$T = T_\infty + T_0\ e^{\frac{A(x+y)}{2L}}\theta(\eta),\ a_1 = (a_1)_0 e^{\frac{B(x+y)}{2L}}\xi(\eta),\ a_2 = (a_1)_0 e^{\frac{B(x+y)}{2L}}\Upsilon(\eta). \tag{7.9}$$

Eq. (7.1) is automatically verified and Eqs. (7.2)-(7.7) yield

$$(1+\gamma)f''' + (f+g)f'' - 2(f'+g')f' - \gamma\varepsilon_1 (f'')^2 f''' = 0, \tag{7.10}$$

$$(1+\gamma)g''' + (f+g)g'' - 2(f'+g')g' - \gamma\varepsilon_2 (g'')^2 g''' = 0, \tag{7.11}$$

$$\frac{1}{\Pr}\theta'' - A(f'+g')\theta + (f+g)\theta' + \frac{\Lambda}{2}[\{\eta(f'+g') + (1+2A)(f+g)\}(f'+g')\theta'$$
$$-A\{(A+2)(f'+g')^2 - (f+g)(f'' + g'')\}\theta - (f+g)^2\theta''] = 0, \tag{7.12}$$

$$\frac{1}{Sc}\xi'' + (f+g)\xi' - B(f'+g')\xi - \sigma_2\xi\Upsilon^2 = 0, \tag{7.13}$$

$$\frac{\chi}{Sc}\Upsilon'' + (f+g)\Upsilon' + \sigma_2\xi\Upsilon^2 = 0, \tag{7.14}$$

$$f = 0,\ f' = 1,\ g = 0,\ g' = \lambda,\ \theta = 1,\ \xi' = j\xi,\ \chi\Upsilon' = -j\xi, \quad \text{at } \eta = 0,$$
$$f' = 0,\ g' = 0,\ \theta = 0,\ \xi = 1,\ \Upsilon = 0, \quad \text{as } \eta \to \infty, \tag{7.15}$$

where

$$\gamma = \frac{1}{\mu\Omega_1\sigma_1},\ \varepsilon_1 = \frac{u_0^3 e^{\frac{3(x+y)}{L}} x^2}{2\nu\sigma_1^2 L},\ \varepsilon_2 = \frac{u_0^3 e^{\frac{3(x+y)}{L}} y^2}{2\nu\sigma_1^2 L},\ \lambda = \frac{v_0}{u_0},\ \Pr = \frac{\upsilon}{\alpha_f},\ \Lambda = \frac{\lambda_e u_0 e^{\frac{x+y}{L}}}{L}$$
$$Sc = \frac{\upsilon}{F_{\mathrm{A}_1}},\ \sigma_2 = \frac{k_r (a_1)_0^2}{2u_0 L}e^{\frac{(B+1)(x+y)}{L}},\ \chi = \frac{F_{\mathrm{A}_2}}{F_{\mathrm{A}_1}},\ j = \frac{k_s}{F_{\mathrm{A}_1}}\sqrt{\frac{2\upsilon L}{u_0}}e^{\frac{-(x+y)}{2L}}. \tag{7.16}$$

Using Eq.(6.25), Eqs. (7.13-7.14) take the form

$$\frac{1}{Sc}\xi'' + (f+g)\xi' - B(f'+g')\xi - \sigma_2\xi(1-\xi)^2 = 0, \tag{7.17}$$

For engineering interest, C_f is demarcated as

$$C_f = \frac{\tau_w}{\rho u_w^2}, \tag{7.18}$$

where the wall shear stress τ_w is given by

$$\tau_w = (\mu + \frac{1}{\Omega_1 \sigma_1}) \frac{\partial u}{\partial z}_{z=0} - \frac{1}{6\Omega_1 \sigma_1^3} (\frac{\partial u}{\partial z})^3_{z=0}, \tag{7.19}$$

or

$$\sqrt{2\,\mathrm{Re}} C_f = (1+\gamma) f''(0) - \frac{\gamma \varepsilon_1}{3} (f''(0))^3. \tag{7.20}$$

7.2 Discussion section

The set of ODEs (7.10-7.12), (7.17) with (7.15) and (6.27) are implemented utilizing a solution technique named BVP-4C in MATLAB software. In this segment, the effect of relevant physical parameters i.e. Eyring-Powell fluid parameter γ, stretching ratio parameter λ, temperature exponent A, thermal relaxation time Λ, Prandtl number Pr, concentration exponent B, chemical reactions σ_2 and j and Sc on velocities, temperature and concentration profiles are represented in graphical and tabular form. $Fig.$ 7.2 describe the behavior of Eyring-Powell liquid parameter on f' and g'. This model explains properties of shear thinning liquid. From $Fig.$ 7.2, as γ increases, velocity component also increases. $Fig.$ 7.3 portrays aspect of λ on f' and g' distributions. One can notice that intensification in λ prompts reduction in f' distribution but an opposite trend is observed for g' profile. As stretching rate along y direction is higher because the adjacent surface starts to move in that direction rather than x direction. Due to this, f' profile decreases while g' profile increases. $Fig.$ 7.4 elucidates temperature exponent impact on temperature profile for both positive and negative values of temperature exponent A. For any under consideration value of A, there is a decrease in temperature distribution . $Fig.$ 7.5 portrays the impact of Eyring-Powell fluid parameter on temperature distribution. From $Fig.$ 7.5, one can observe that temperature is decreasing function of Eyring-Powell fluid parameter. In $Fig.$ 7.6, temperature distribution is plotted for different Λ. As $\Lambda = 0$ relates to traditional Fourier's law, therefore it is detected from graphical data that when we involve Λ in energy equation temperature is smaller. $Fig.$ 7.7 elucidates impacts of λ on temperature profile for both positive and negative values of temperature exponent . For any under consideration value of A, temperature distribution declines as λ increases. For negative A, temperature profile firstly intensifies to its extreme value and after that gradually declines to zero, which shows the occurrence of phenomenon (SGH)"Sparrow-Gregg hill". From this figure, for negative A, temperature distribution is concave down and for positive A, near the wall it is concave upward. Also, as λ increases, the thicknesses of thermal boundary declines. $Fig.$ 7.8 illustrates the impacts of Pr on $\theta(\eta)$. Physically, the relation between Prandtl and thermal diffusivity is inverse. As Prandtl number Pr increases, one can expect that there are less thermal impacts to infiltrate into the liquid. Consequently, with the enhancement in Pr, $\theta(\eta)$ decreases. $Fig.$ 7.9 describes the effects of concentration exponent B on ξ. Aspect of B on ξ is decreasing. Aspect of stretching ratio parameter on ξ is analyzed in $Fig.$ 7.10. By the intensification of λ, for any under consideration value of concentration exponent, the concentration distribution increases. This is due to the increment of stretching along y direction that is why concentration enhances. $Fig.$ 7.11 describes the aspect of γ on ξ. We observed that impact of γ on ξ is rising. Aspects of σ_2 and j on concentration distribution are depicted in $Figs.$ 7.12 and 7.13. With an increase in σ_2 and j, the concentration profiles depreciates. It may be the domination of diffusion coefficient than reaction rate. This shows the good agreement with Raju et al. [85]. $Fig.$ 7.14 elucidates the variation of Schmidt number Sc on ξ. For larger values of Sc, increasing behavior of ξ is observed. Physically, increasing values of Sc relate to high rate of viscous diffusion which causes the concentration of a fluid to increase. $Figs.$ $7.15 - 7.16$ are sketched to see the behavior of $gamma$ on shear stress versus stretching ratio parameter. These figures reveal that flow resistance boosts with variation of Eyring-Powell fluid parameter as well as with stretching ratio parameter , therefore, shear stress increases in both directions. From $Table$ 7.1, the magnitude of skin friction rises with an expansion in γ and λ. However it reduces when ε_1 increases.

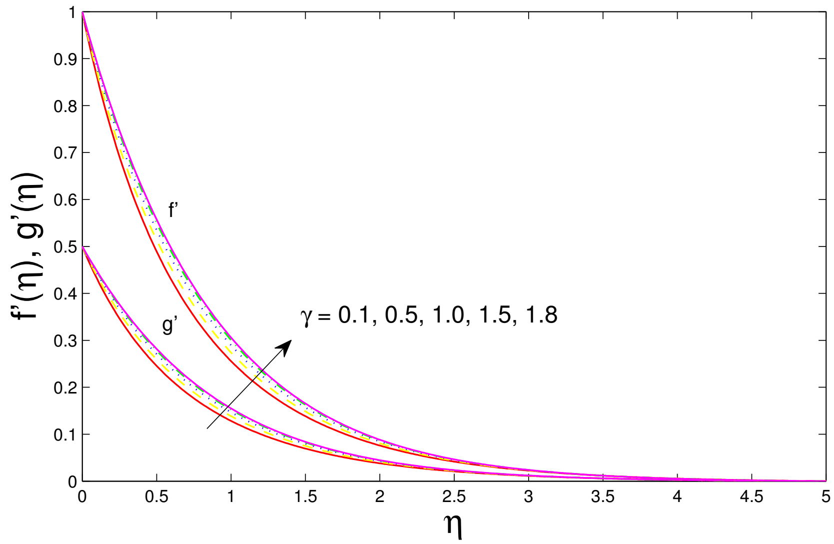

Figure 7.2: Impact of γ on f' and g'.

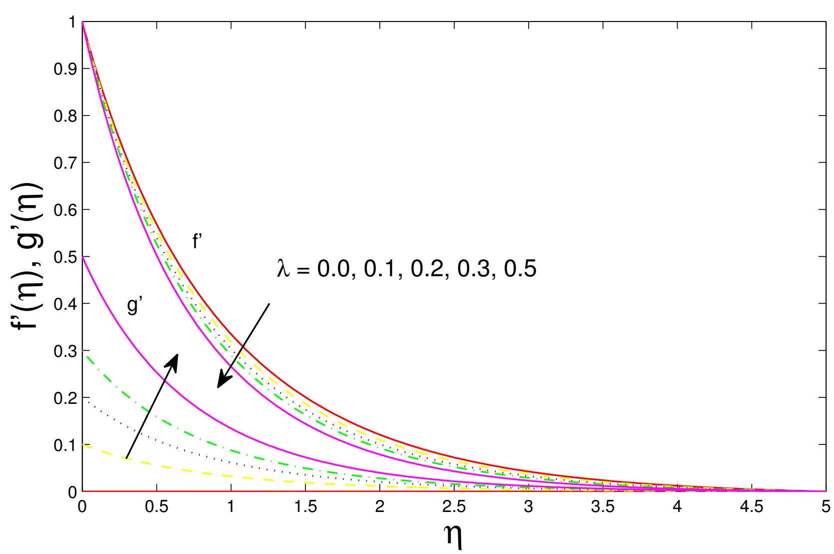

Figure 7.3: Impact of λ on f' and g'.

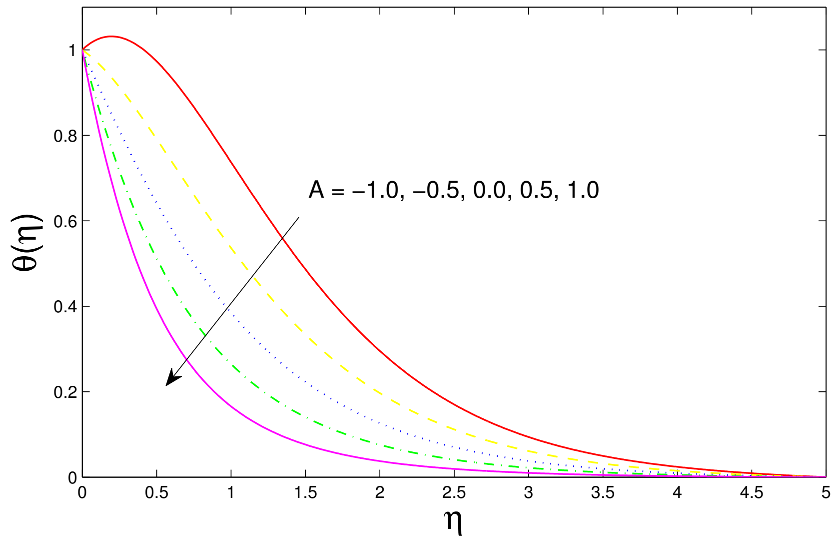

Figure 7.4: Impact of A on θ.

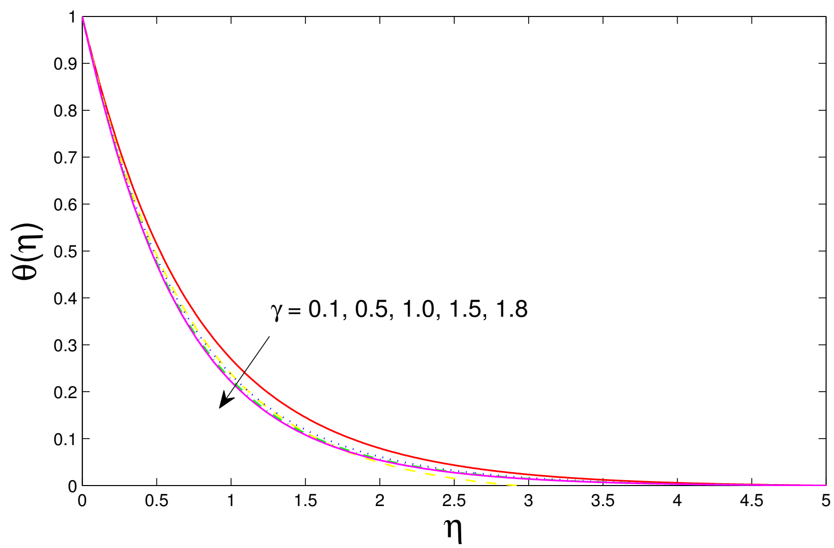

Figure 7.5: Impact of γ on θ.

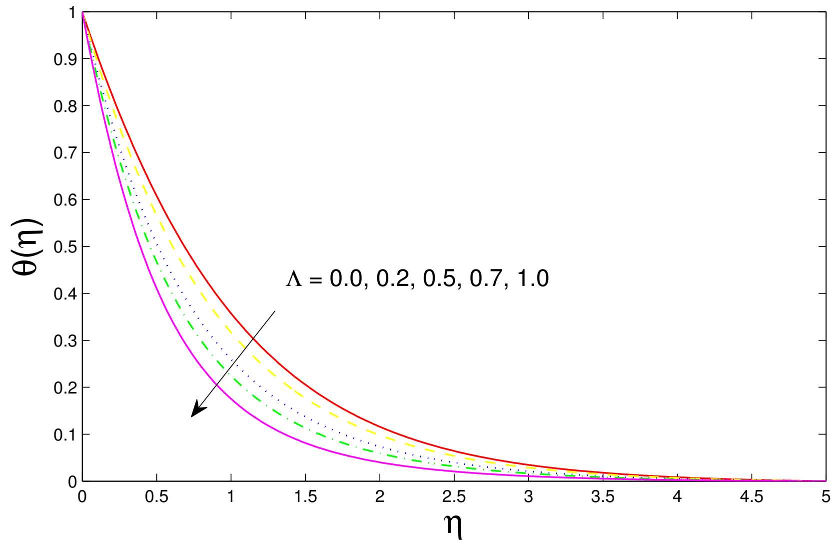

Figure 7.6: Impact of Λ on θ.

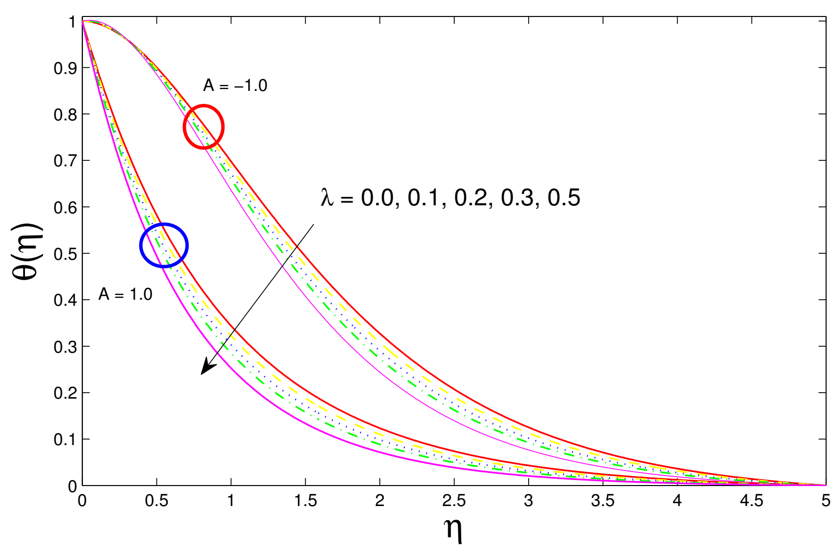

Figure 7.7: Impact of λ on θ.

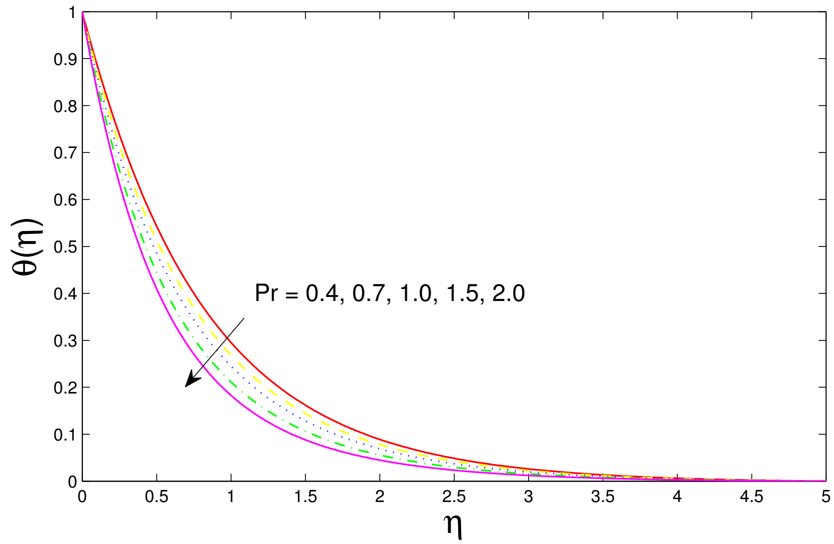

Figure 7.8: Impact of Pr on θ.

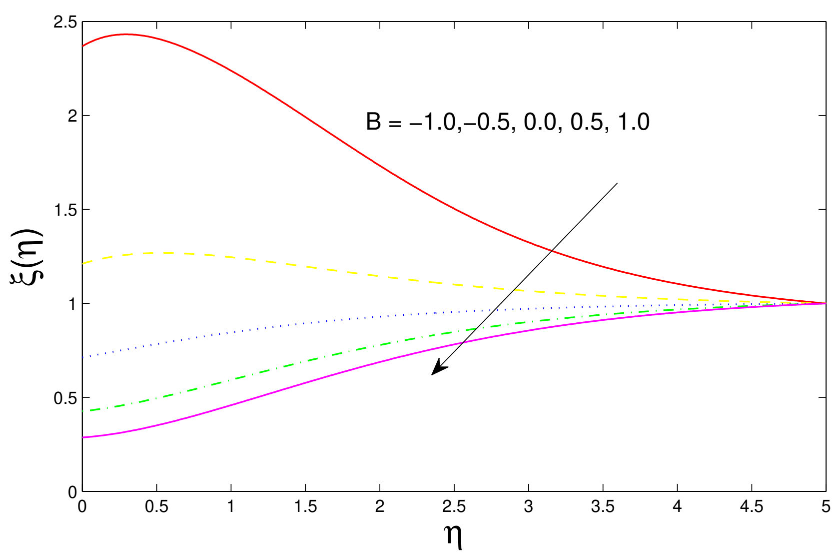

Figure 7.9: Impact of B on ξ.

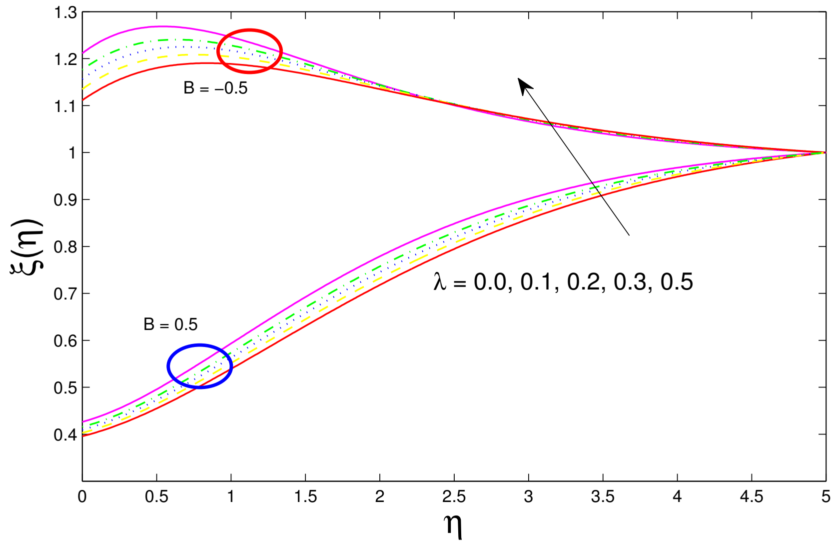

Figure 7.10: Impact of λ on ξ.

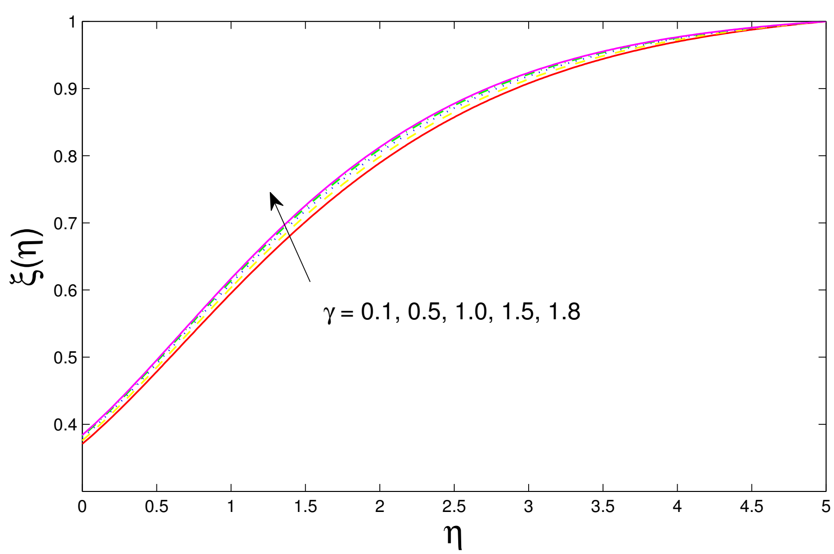

Figure 7.11: Impact of γ on ξ.

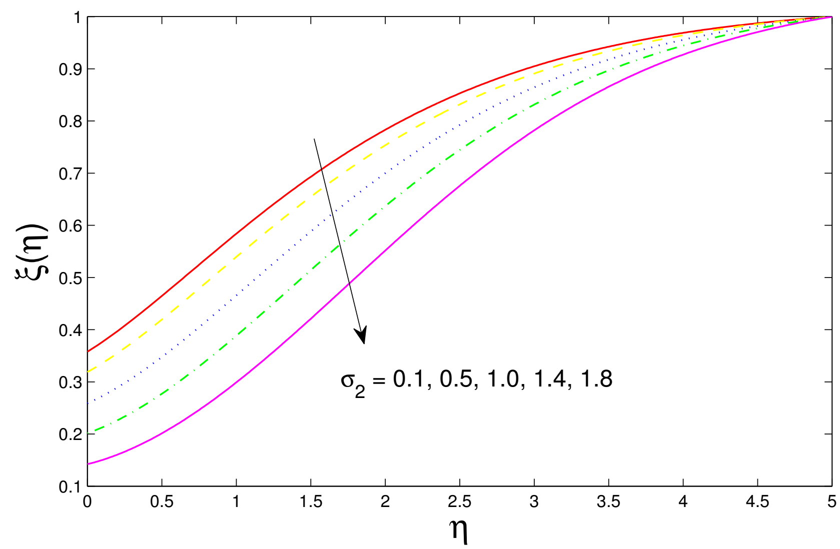

Figure 7.12: Impact of σ_2 on ξ.

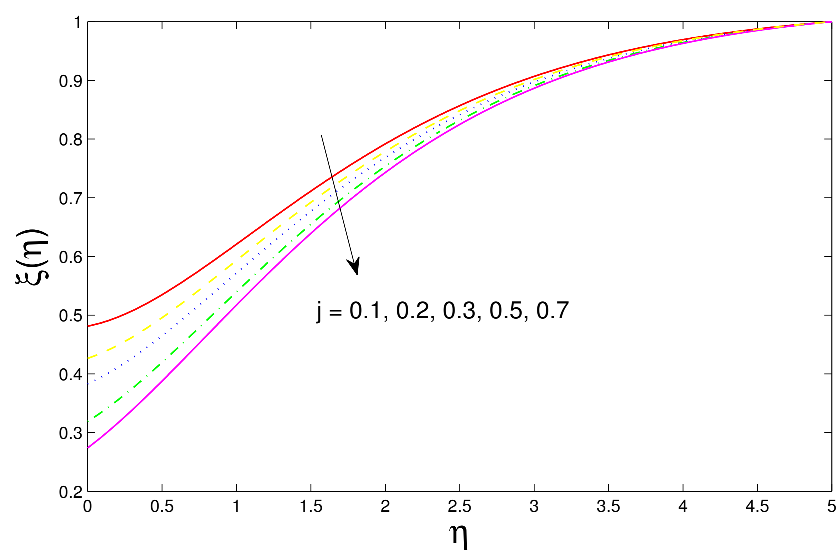

Figure 7.13: Impact of j on ξ.

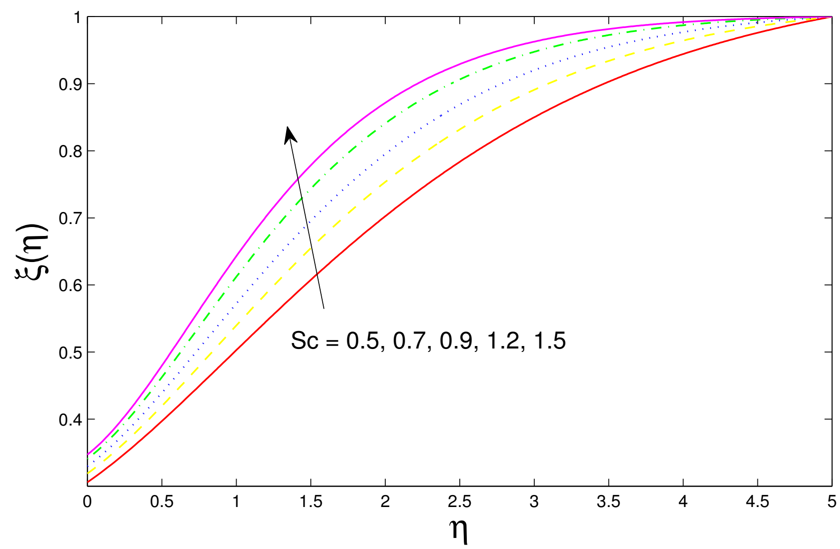

Figure 7.14: Impact of Sc on ξ.

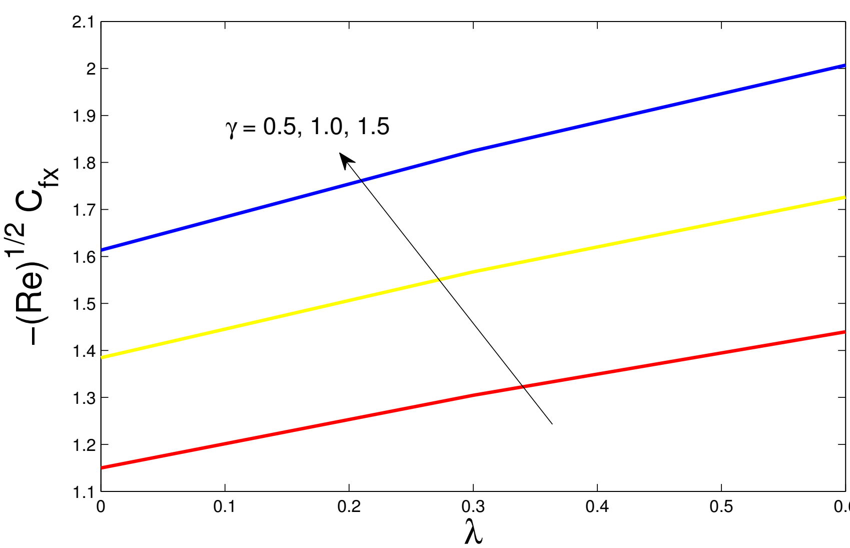

Figure 7.15: Impact of γ on skin friction along x direction.

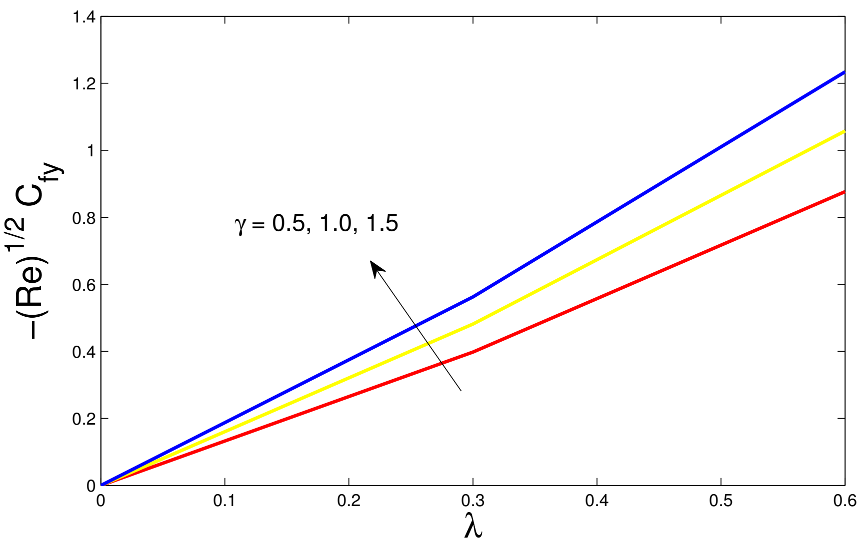

Figure 7.16: Impact of γ on skin friction along y direction.

Table 7.1: Effects of Skin friction C_f along x and y directions

γ	ε_1	λ	-$C_{fx}(\mathrm{Re})^{\frac{1}{2}}$	-$C_{fy}(\mathrm{Re})^{\frac{1}{2}}$
0.1	0.3	0.5	1.16824	0.586858
0.5			1.39662	0.709678
1.0			1.67553	0.85724
1.5			1.94891	1.00084
1.8			2.11098	1.08575
0.3	0.1		1.29827	0.651541
	0.2		1.29077	0.650262
	0.3		1.28308	0.648959
	0.5		1.2670	0.646263
	0.6		1.25854	0.644862
		0.0	1.05405	0.0
		0.1	1.10412	0.111621
		0.2	1.15183	0.233044
		0.3	1.19743	0.363538
		0.5	1.28309	0.648961

7.3 Concluding Remarks

- The three dimensional Eyring-Powell liquid flow using revised heat flux relation and chemical processes was intended to be investigated in this paper. The nonlinear ODEs are tackled with bvp-4c technique. Concluding remarks are:

- The intensification in stretching ratio parameter prompts reducing f' distribution.

- Temperature in revised heat flux relation is lesser as compared to classical Fourier's relation.

- Temperature distribution declines as *lambda* boosts.

- For negative values of At, $\theta(\eta)$ represent SGH phenomenon.

- By the intensification of stretching ratio parameter, for under consideration value of concentration exponent, the concentration distribution increases.

- The flow resistance increments with the variation of γ as well as with λ,therefore, shear stress increases.

Chapter 8

Consequences of improved heat-mass flux relations for 3D flow of Eyring-Powell fluid

Variable conductivity aspects and generalized Fourier's-Fick's laws are studied in this chapter. Properties of heat/mass transport mechanisms are reported with time dependent relaxation time in energy and concentration equations. Another heat flux idea involving mystery of heat conduction is exploited which is not quite the same as the usual literature. Such idea has been utilized as a part of perspective of Cattaneo-Christov heat flux theory. The characteristic of temperature and concentration relaxation features are described. Other than this, chemical reactions are additionally considered. A numerical technique bvp4c is adopted to simplify the highly complex six ODEs. The skin friction coefficient for three dimensional Eyring-Powell fluid model is calculated. From the present analysis we observe that for higher values of strength of reaction parameters, the concentration profile decreases. Current effort for three dimensional Cattaneo-Christov double diffusion and homogeneous-heterogeneous reactions over an exponentially stretching surface does not yet exist in the literature.

8.1 Mathematical modeling and flow analysis

We study 3-D, incompressible Eyring-powell liquid flow on an exponentially stretched surface. The laminar flow is restricted in the domain. A simple chemical reaction model is considered in the present analysis.For three dimensional flow, the principal equations are [20]:

$$\frac{\partial u}{\partial x}+\frac{\partial v}{\partial y}+\frac{\partial w}{\partial z}=0, \tag{8.1}$$

$$u\frac{\partial u}{\partial x}+v\frac{\partial u}{\partial y}+w\frac{\partial u}{\partial z}=(\nu+\frac{1}{\Omega_1\sigma_1\rho})\frac{\partial^2 u}{\partial z^2}-\frac{1}{2\Omega_1\sigma_1^3\rho}(\frac{\partial u}{\partial z})^2\frac{\partial^2 u}{\partial z^2}, \tag{8.2}$$

$$u\frac{\partial v}{\partial x}+v\frac{\partial v}{\partial y}+w\frac{\partial v}{\partial z}=(\nu+\frac{1}{\Omega_1\sigma_1\rho})\frac{\partial^2 v}{\partial z^2}-\frac{1}{2\Omega_1\sigma_1^3\rho}(\frac{\partial v}{\partial z})^2\frac{\partial^2 v}{\partial z^2}, \tag{8.3}$$

$$\rho c_p(u\frac{\partial T}{\partial x}+v\frac{\partial T}{\partial y}+w\frac{\partial T}{\partial z})=-\nabla.\vec{q}, \tag{8.4}$$

$$u\frac{\partial C}{\partial x}+v\frac{\partial C}{\partial y}+w\frac{\partial C}{\partial z}=-\nabla.\vec{J}, \tag{8.5}$$

$$u\frac{\partial a_1}{\partial x}+v\frac{\partial a_1}{\partial y}+w\frac{\partial a_1}{\partial z}=F_{A_1}\frac{\partial^2 a_1}{\partial z^2}-k_r a_1 a_2^2, \tag{8.6}$$

$$u\frac{\partial a_2}{\partial x}+v\frac{\partial a_2}{\partial y}+w\frac{\partial a_2}{\partial z}=F_{A_2}\frac{\partial^2 a_2}{\partial z^2}+k_r a_1 a_2^2, \tag{8.7}$$

The frame indifferent generalization regarding Fourier's and Fick's laws are derived as [51]:

$$\vec{q} + \lambda_e(\frac{\partial \vec{q}}{\partial t} + \vec{V}.\nabla\vec{q} - \vec{q}.\nabla\vec{V} + (\vec{\nabla}.\vec{V})\vec{q}) = -k\nabla T, \tag{8.8}$$

$$\vec{J} + \lambda_c(\frac{\partial \vec{J}}{\partial t} + \vec{V}.\nabla\vec{q} - \vec{J}.\nabla\vec{V} + (\vec{\nabla}.\vec{V})\vec{J}) = -D_B\nabla C, \tag{8.9}$$

replacing $\lambda_e = \lambda_c = 0$, in equation (8.8-8.9), we get the classical Fourier's law and Fick's law. By assuming steady state flow with ($\frac{\partial \vec{q}}{\partial t} = 0$) and ($\frac{\partial \vec{J}}{\partial t} = 0$), also due the incompressible flow ($\vec{\nabla}.\vec{V} = 0$), Eqs. (8.8-8.9) can be rewritten as:

$$\vec{q} + \lambda_e(\vec{V}.\nabla\vec{q} - \vec{q}.\nabla\vec{V}) = -k\nabla T, \tag{8.10}$$

$$\vec{J} + \lambda_c(\vec{V}.\nabla\vec{q} - \vec{J}.\nabla\vec{V}) = -D_B\nabla C, \tag{8.11}$$

now take the divergence of above equations,

$$\nabla.\vec{q} + \lambda_e(\nabla.(\vec{V}.\nabla\vec{q} - \vec{q}.\nabla\vec{V})) = -\nabla.(k\nabla T), \tag{8.12}$$

$$\nabla.\vec{J} + \lambda_c(\nabla.(\vec{V}.\nabla\vec{q} - \vec{J}.\nabla\vec{V})) = -\nabla.(D_B\nabla C), \tag{8.13}$$

as

$$\nabla.(\vec{V}.\nabla\vec{q} - \vec{q}.\nabla\vec{V}) = \vec{V}.\nabla(\nabla.\vec{q}) + (\vec{\nabla}.\vec{V})(\nabla.\vec{q}) = \vec{V}.((\nabla.\vec{q})\vec{V}), \tag{8.14}$$

$$\nabla.(\vec{V}.\nabla\vec{J} - \vec{J}.\nabla\vec{V}) = \vec{V}.\nabla(\nabla.\vec{J}) + (\vec{\nabla}.\vec{V})(\nabla.\vec{J}) = \vec{V}.((\nabla.\vec{J})\vec{V}), \tag{8.15}$$

Eqs. (8.12) and (8.13) can be rewritten as

$$\nabla.\vec{q} + \lambda_e[\vec{V}.\{(\nabla.\vec{q})\vec{V}\}] = -\nabla.(k\nabla T), \tag{8.16}$$

$$\nabla.\vec{J} + \lambda_c[\vec{V}.\{(\nabla.\vec{J})\vec{V}\}] = -\nabla.(D_B\nabla C), \tag{8.17}$$

Using Eqs. (8.4) and (8.5) in Eqs. (8.16) and (8.17), the three dimensional equations are [86]:

$$
\begin{aligned}
u\frac{\partial T}{\partial x}+v\frac{\partial T}{\partial y}+w\frac{\partial T}{\partial z} &= \frac{1}{\rho c_p}\frac{\partial}{\partial z}\left(k(T)\frac{\partial T}{\partial z}\right)-\lambda_e\left(u^2\frac{\partial^2 T}{\partial x^2}+v^2\frac{\partial^2 T}{\partial y^2}+w^2\frac{\partial^2 T}{\partial z^2}\right)\\
&-\lambda_e\left(2uv\frac{\partial^2 T}{\partial x\partial y}+2vw\frac{\partial^2 T}{\partial y\partial z}+2uw\frac{\partial^2 T}{\partial x\partial z}+\left(u\frac{\partial u}{\partial x}+v\frac{\partial u}{\partial y}+w\frac{\partial u}{\partial z}\right)\frac{\partial T}{\partial x}\right)\\
&-\lambda_e\left(u\frac{\partial v}{\partial x}+v\frac{\partial v}{\partial y}+w\frac{\partial v}{\partial z}\right)\frac{\partial T}{\partial y}+\left(u\frac{\partial w}{\partial x}+v\frac{\partial w}{\partial y}+w\frac{\partial w}{\partial z}\right)\frac{\partial T}{\partial z}
\end{aligned}
\tag{8.18}
$$

$$
\begin{aligned}
u\frac{\partial C}{\partial x}+v\frac{\partial C}{\partial y}+w\frac{\partial C}{\partial z} &= D_B\frac{\partial^2 C}{\partial z^2}-\lambda_e\left(u^2\frac{\partial^2 C}{\partial x^2}+v^2\frac{\partial^2 C}{\partial y^2}+w^2\frac{\partial^2 C}{\partial z^2}\right)\\
&-\lambda_e\left(2uv\frac{\partial^2 C}{\partial x\partial y}+2vw\frac{\partial^2 C}{\partial y\partial z}+2uw\frac{\partial^2 C}{\partial x\partial z}+\left(u\frac{\partial u}{\partial x}+v\frac{\partial u}{\partial y}+w\frac{\partial u}{\partial z}\right)\frac{\partial C}{\partial x}\right)\\
&-\lambda_e\left(u\frac{\partial v}{\partial x}+v\frac{\partial v}{\partial y}+w\frac{\partial v}{\partial z}\right)\frac{\partial C}{\partial y}+\left(u\frac{\partial w}{\partial x}+v\frac{\partial w}{\partial y}+w\frac{\partial w}{\partial z}\right)\frac{\partial C}{\partial z}
\end{aligned}
\tag{8.19}
$$

$$
\begin{aligned}
&u=U_w,\ v=V_w,\ w=0,\ T=T_w,\ C=C_w,\ F_{A_1}\frac{\partial a_1}{\partial z}=k_s a_1,\ F_{A_2}\frac{\partial a_2}{\partial z}=-k_s a_1, \quad \text{at } z=0,\\
&u\to 0,\ v\to 0,\ T\to T_\infty,\ C\to C_\infty,\ a_1\to (a_1)_0 e^{\frac{A(x+y)}{2L}},\ a_2\to 0, \qquad \text{as } z\to\infty.
\end{aligned}
\tag{8.20}
$$

Where $k(T)$ can be defined as:

$$
k(T)=k_\infty(1+\Theta\frac{T-T_\infty}{\Delta T})
\tag{8.21}
$$

The velocities, temperature and concentration at the wall are

$$
U_w=u_0 e^{\frac{x+y}{L}},\ V_w=v_0 e^{\frac{x+y}{L}},\ T_w=T_\infty+T_0 e^{\frac{A(x+y)}{2L}},\ C_w=C_\infty+C_0 e^{\frac{A(x+y)}{2L}}.
\tag{8.22}
$$

Now

$$\eta = z\sqrt{\frac{u_0}{2\nu L}}e^{\frac{(x+y)}{2L}},\ u = u_0 e^{\frac{x+y}{L}} f'(\eta),\ v = u_0 e^{\frac{x+y}{L}} g'(\eta),$$

$$w = -\sqrt{\frac{\nu u_0}{2L}}e^{\frac{(x+y)}{2L}}(f(\eta)+g(\eta)+\eta(f'(\eta)+g'(\eta))),\ T = T_\infty + T_0\ e^{\frac{A(x+y)}{2L}}\theta(\eta),$$

$$C = C_\infty + C_0\ e^{\frac{A(x+y)}{2L}}\Psi(\eta),\ a_1 = (a_1)_0 e^{\frac{B(x+y)}{2L}}\xi(\eta),\ a_2 = (a_1)_0 e^{\frac{B(x+y)}{2L}}\Upsilon(\eta). \quad (8.23)$$

Eq. (8.1) is automatically verified and Eqs. (8.6-8.12) yield

$$(1+\gamma)f''' + (f+g)f'' - 2(f'+g')f' - \gamma\varepsilon_1(f'')^2 f''' = 0, \quad (8.24)$$

$$(1+\gamma)g''' + (f+g)g'' - 2(f'+g')g' - \gamma\varepsilon_2(g'')^2 g''' = 0, \quad (8.25)$$

$$\frac{1}{\Pr}(1+\Theta\theta)\theta'' + \Theta(\theta')^2 - A(f'+g')\theta + (f+g)\theta' + \frac{\Lambda}{2}[\{\eta(f'+g') + (1+2A)(f+g)\}$$

$$\times(f'+g')\theta' - A\{(A+2)(f'+g')^2 - (f+g)(f''+g'')\}\theta - (f+g)^2\theta''] = 0, \quad (8.26)$$

$$\frac{1}{Sc_b}\Psi'' - A(f'+g')\Psi + (f+g)\Psi' + \frac{\Lambda_1}{2}[\{\eta(f'+g') + (1+2A)(f+g)\}(f'+g')\Psi'$$

$$-A\{(A+2)(f'+g')^2 - (f+g)(f''+g'')\}\Psi - (f+g)^2\Psi''] = 0, \quad (8.27)$$

$$\frac{1}{Sc}\xi'' + (f+g)\xi' - B(f'+g')\xi - \sigma_2\xi\Upsilon^2 = 0, \quad (8.28)$$

$$\frac{\chi}{Sc}\Upsilon'' + (f+g)\Upsilon' + \sigma_2\xi\Upsilon^2 = 0, \quad (8.29)$$

$$f = 0,\ f' = 1,\ g = 0,\ g' = \lambda,\ \theta = 1,\ \Psi = 1,\ \xi' = j\xi,\ \chi\Upsilon' = -j\xi, \quad \text{at } \eta = 0,$$

$$f' = 0,\ g' = 0,\ \theta = 0,\ \Psi = 0,\ \xi = 1,\ \Upsilon = 0, \quad \text{as } \eta \to \infty, \quad (8.30)$$

here the parameters are defined in the following expression as,

$$\gamma = \frac{1}{\mu\Omega_1\sigma_1},\ \varepsilon_1 = \frac{u_0^3 e^{\frac{3(x+y)}{L}} x^2}{2\nu\sigma_1^2 L},\ \varepsilon_2 = \frac{u_0^3 e^{\frac{3(x+y)}{L}} y^2}{2\nu\sigma_1^2 L},\ \lambda = \frac{v_0}{u_0},\ \Pr = \frac{\upsilon\rho c_p}{k_\infty},$$

$$\Lambda = \frac{\lambda_e u_0 e^{\frac{x+y}{L}}}{L},\ \Lambda_1 = \frac{\lambda_c u_0 e^{\frac{x+y}{L}}}{L},\ Sc_b = \frac{\upsilon}{D_B},\ Sc = \frac{\upsilon}{F_{\mathrm{A}_1}},\ \sigma_2 = \frac{k_r(a_1)_0^2}{2u_0 L}e^{\frac{(A+1)(x+y)}{L}},$$

$$\chi = \frac{F_{\mathrm{A}_2}}{F_{\mathrm{A}_1}},\ j = \frac{k_s}{F_{\mathrm{A}_1}}\sqrt{\frac{2\upsilon L}{u_0}}e^{\frac{-(x+y)}{2L}}. \quad (8.31)$$

Now using Eq. (7.22), we get Eq. (7.23) along with the boundary condition defined in Eq. (7.24).

8.2 Consequence

We characterize effect of relevant physical parameters on temperature and concentration distributions in graphical and tabular form. The given mathematical model is solved numerically by utilizing BVP-4C in MATLAB software $c.f.$[$chap$ 3]. $Fig.$ 8.1 describe the behavior of stretching ratio parameter on temperature profile . From $Fig.$ 8.1, we see that there is a reduction in temperature and thermal boundary thickness as stretching ratio parameter intensifications. $Fig.$ 8.2 portrays the impacts of variable thermal conductivity parameter on temperature distribution. One can notice that intensification in prompts increasing temperature distribution. Physically, the significant quantity of heat transfers from the surface to the substance results an increase in thermal conductivity that is why increases. In $Fig.$ 8.3, temperature distribution is plotted for various values of non-dimensional relaxation time. Physically, when we boost Λ, then the material elements need more time to transport heat to its neighboring elements and so temperature decays. For $\Lambda = 0$, the heat transports quickly all over the material and relates to traditional Fourier's law. $Fig.$ 8.4 elucidates temperature exponent impacts on temperature profile. For any under consideration value of A, we observe that there is a decrease in temperature distribution . $Fig.$ 8.5 illustrates aspect of Pr on $\theta(\eta)$. There are less thermal impacts as Pr raises, thus, the temperature declines. *Fig.* 8.6 illustrates the impacts of concentration relaxation parameter on concentration profile . There is a reduction in $\xi(\eta)$ when Λ_1 is increased. Here $\Lambda_1 = 0$ relates to traditional Fick's law. *Fig.* 8.7 explains the impacts of Schmidt number on concentration distribution . We conclude that $\xi(\eta)$ is decreasing function of Schmidt number. As molecular diffusivity declines when we increment the Schmidt number. *Fig.* 8.8 describes the effects of concentration exponent on concentration profile . From figure we note that the influence of concentration exponent on $\xi(\eta)$ is decreasing. Impact of stretching ratio parameter on $\xi(\eta)$ is analyzed in *Fig.* 8.9. By the intensification of λ, for any under consideration value of concentration exponent , the concentration distribution increases. Physically, this is due to the increment of stretching along y direction that is why concentration enhances. Aspects of σ_2 and j on concentration distribution are depicted in *Figs.* 8.10 and 8.11. With an increase in σ_2 and j, the concentration profiles depreciates. It may be the domination of diffusion coefficient than reaction rate. *Fig.* 8.12 elucidates the variation of Schmidt number Sc on $\xi(\eta)$. For larger Sc, we note increasing behavior of ξ. Physically, increasing values of Sc relate to high rate of viscous diffusion which causes the concentration of a fluid to increase. *Figs.* $8.13 - 8.14$ are sketched to see aspects of γ on shear stress versus stretching ratio parameter . From these figures, we observe that the flow resistance increments with the variation of Eyring-Powell fluid parameter as well as with stretching ratio parameter , therefore, shear stress increases in both directions. From *Table* 8.1, the magnitude of Skin friction increments with an expansion in γ and λ but decreases when ε_1 intensifies. *Table* 8.2 is prepared to compare present outcomes with those of Liu et al. [84] in a limiting case. Here good agreement is observed.

Table 8.1: Comparative values of $-f''(0)$ and $-g''(0)$ for various values of λ when γ=ε_1=0

	Present Results		Liu et al. [84]	
λ	-$f''(0)$	-$g''(0)$	-$f''(0)$	-$g''(0)$
0.0	1.281809	0.0	1.28180856	0.0
0.5	1.569888	0.784943	1.56988846	0.78494423
1.0	1.812750	1.812750	1.81275105	1.81275105

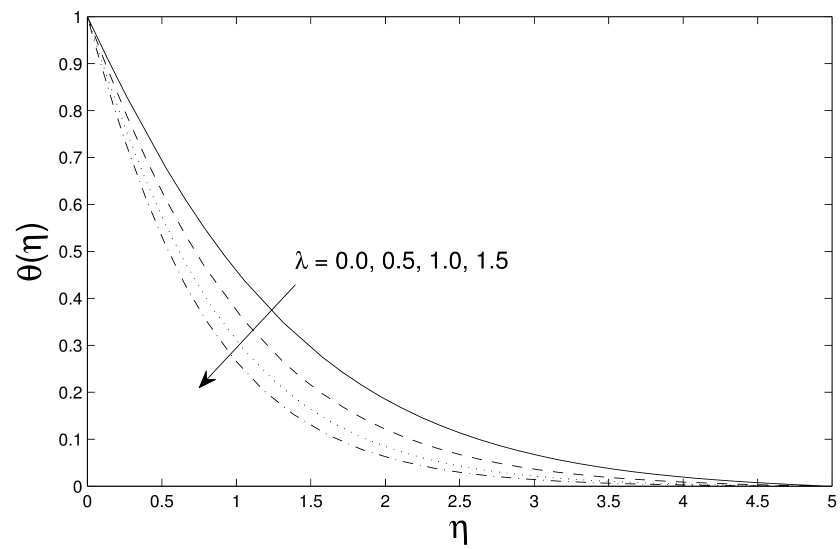

Figure 8.1: Impact of λ on $\theta(\eta)$.

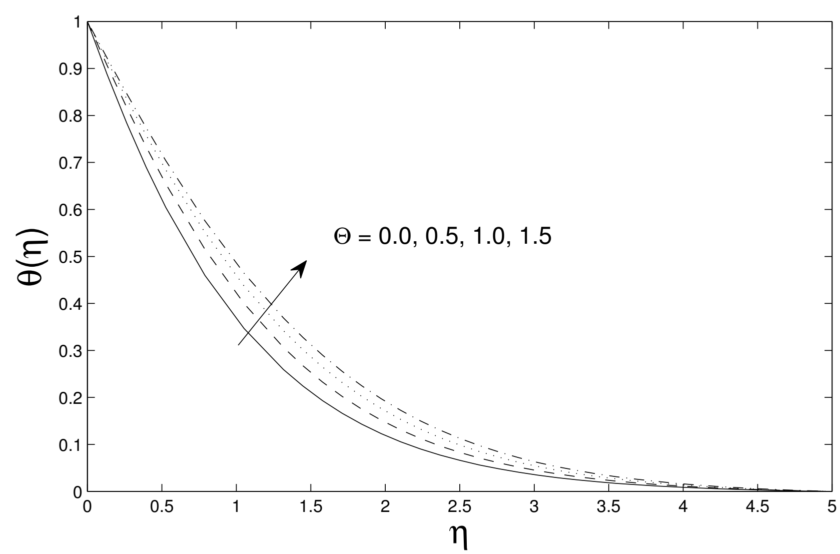

Figure 8.2: Impact of Θ on $\theta(\eta)$.

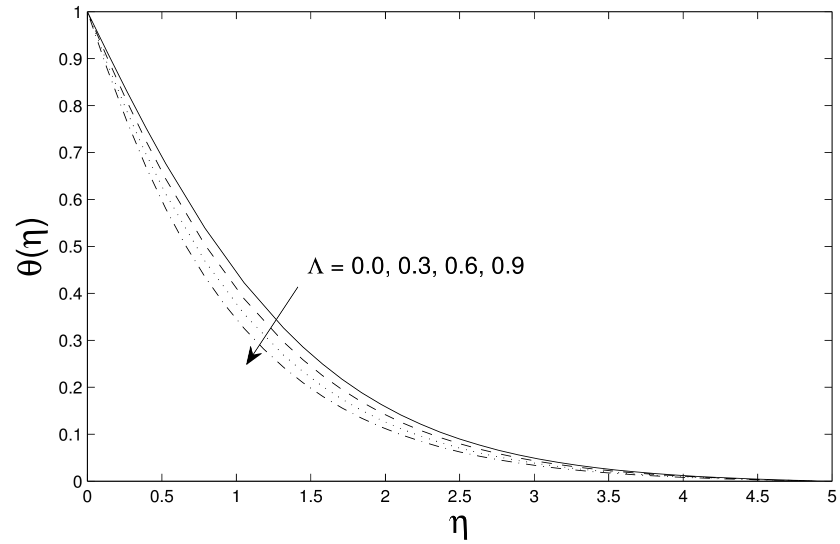

Figure 8.3: Impact of Λ on $\theta(\eta)$.

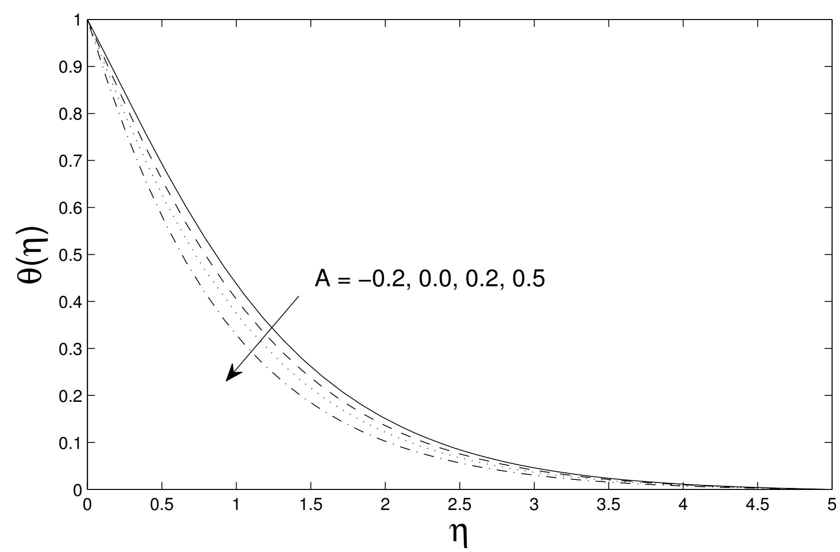

Figure 8.4: Impact of A on $\theta(\eta)$.

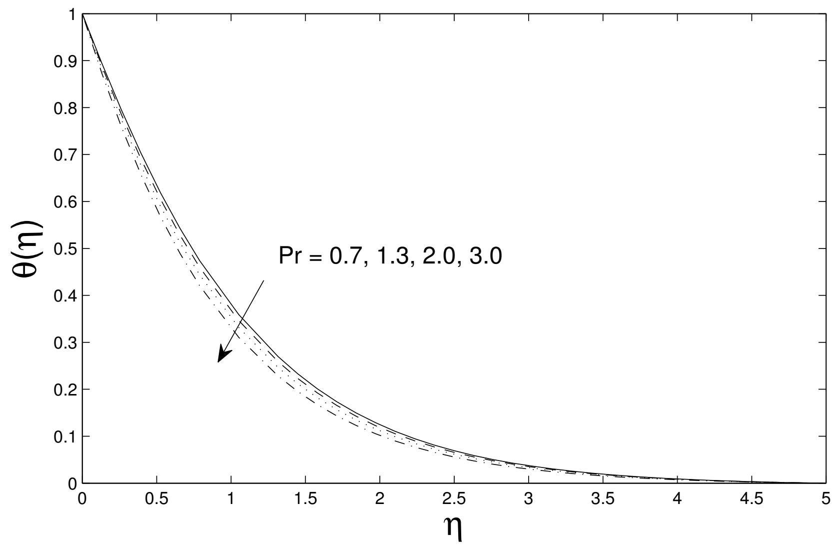

Figure 8.5: Impact of Pr on $\theta(\eta)$.

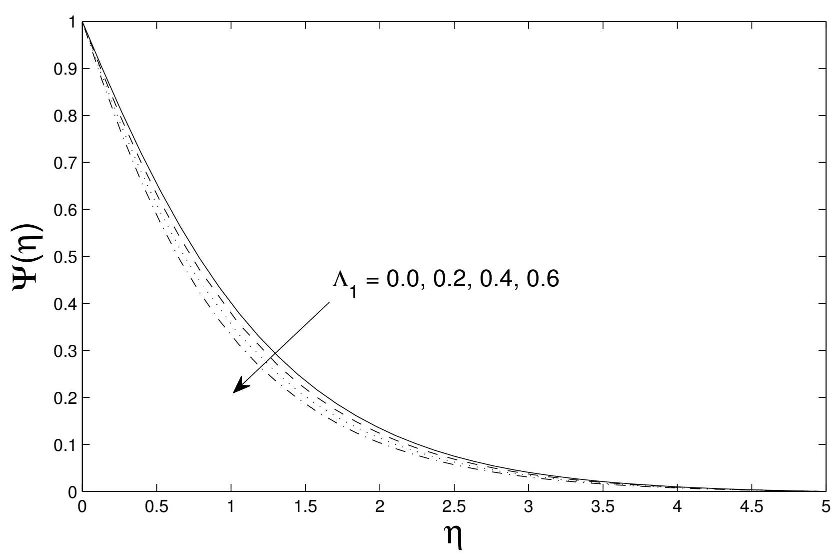

Figure 8.6: Impact of Λ_1 on $\Psi(\eta)$.

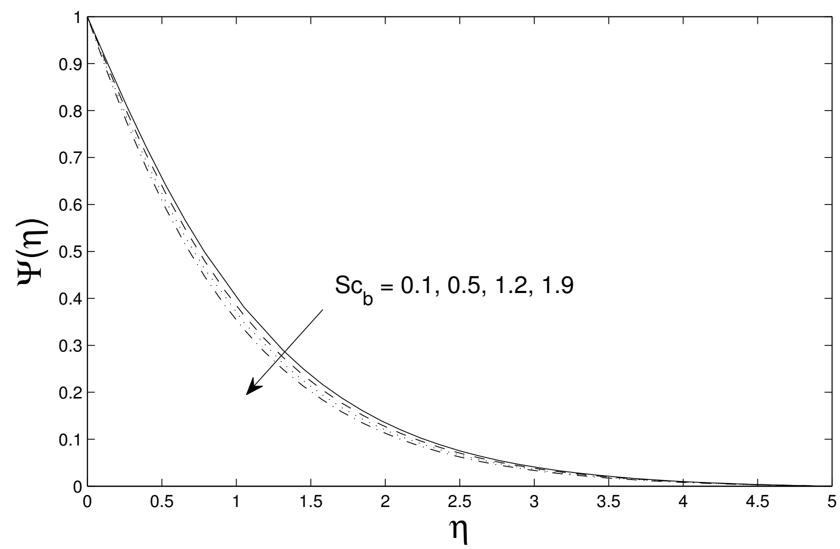

Figure 8.7: Impact of Sc_b on $\Psi(\eta)$.

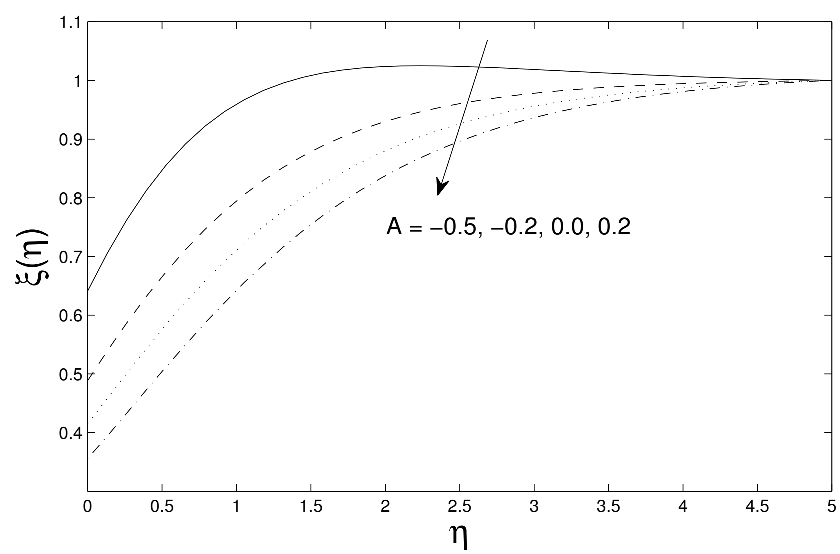

Figure 8.8: Impact of A on $\xi(\eta)$.

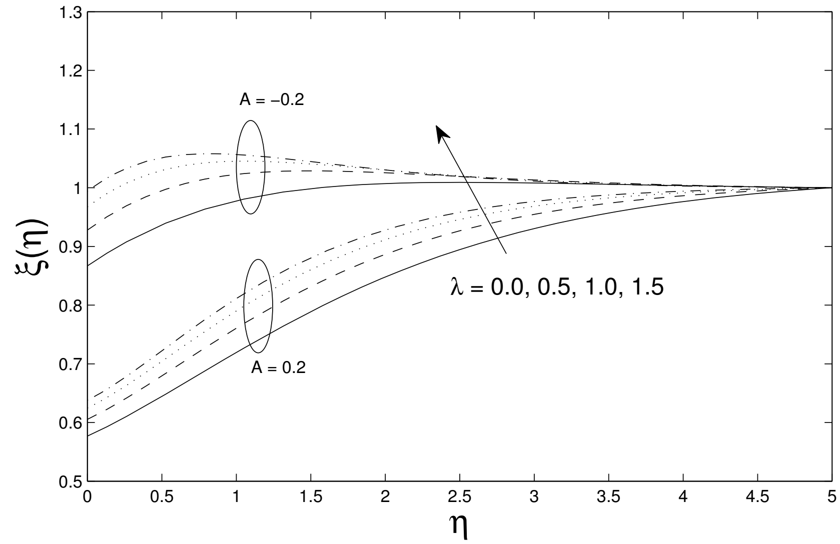

Figure 8.9: Impact of λ on $\xi(\eta)$.

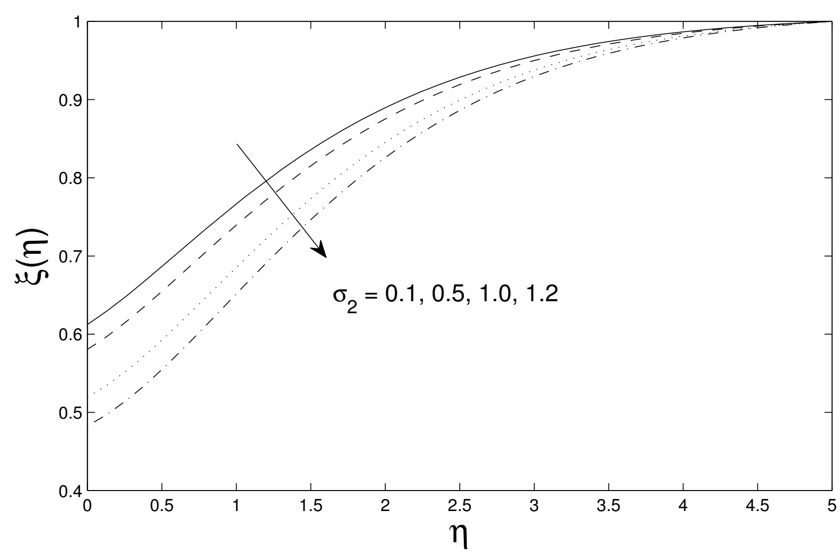

Figure 8.10: Impact of σ_2 on $\xi(\eta)$.

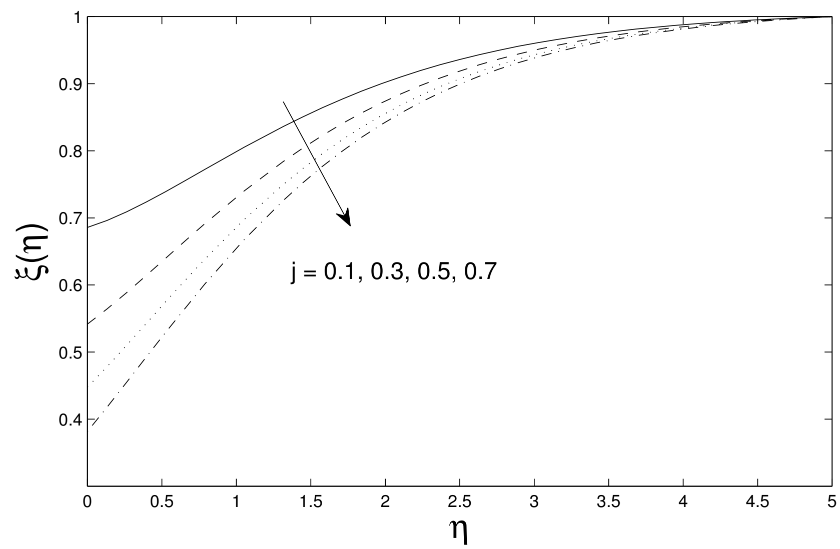

Figure 8.11: Impact of j on $\xi(\eta)$.

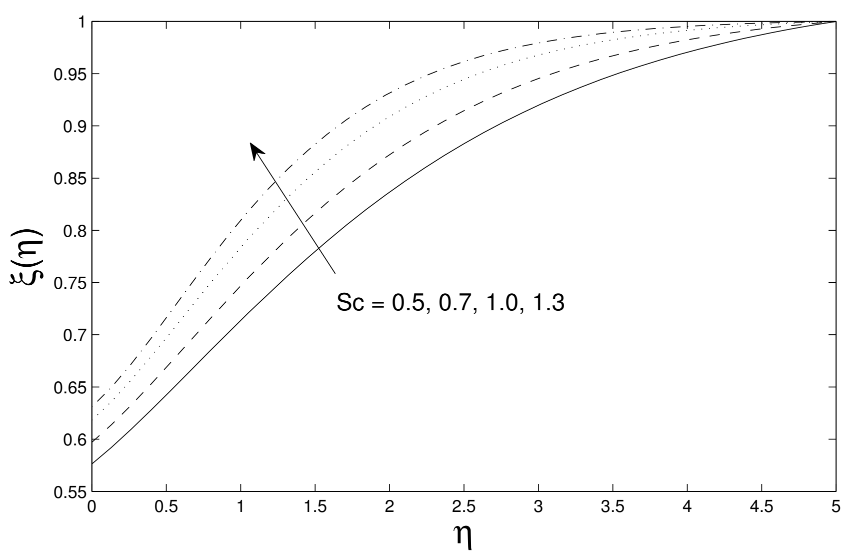

Figure 8.12: Impact of Sc on $\xi(\eta)$.

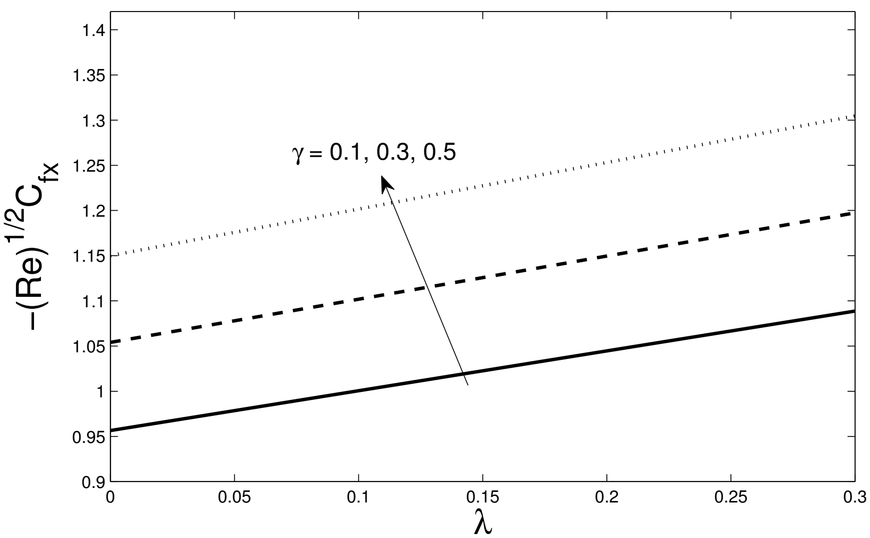

Figure 8.13: Impact of γ on skin friction along x direction.

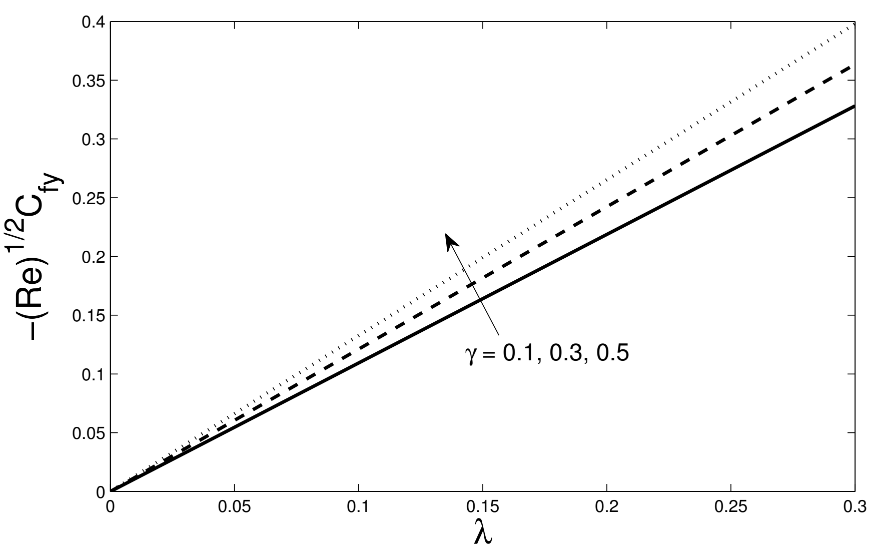

Figure 8.14: Impact of γ on skin friction along y direction.

Table 8.2: Effects of Skin friction C_f along x and y directions

γ	ε_1	λ	-$C_{fx}(\text{Re})^{\frac{1}{2}}$	-$C_{fy}(\text{Re})^{\frac{1}{2}}$
0.1	0.3	0.5	1.16825	0.586861
0.3			1.2831	0.648962
0.5			1.39664	0.709681
0.7			1.509	0.769324
0.3	0.1		1.29828	0.651543
	0.3		1.2831	0.648962
	0.5		1.26705	0.646268
	0.7		1.24973	0.643416
		0.0	1.05405	0.0
		0.1	1.10412	0.111622
		0.3	1.19743	0.363538
		0.5	1.2831	0.648962

8.3 Final Remarks

- Temperature becomes high for greater variable thermal conductivity.
- For non-Fourier's and Fick's laws, temperature and concentration are lesser as compared to classical Fourier's model.
- Temperature and concentration reduces when temperature and concentration relaxation parameters are increased.
- The flow resistance increments with the variation of as well as with , therefore, shear stress increases.
- With the larger values of reaction parameters, concentration distribution decreases.

Chapter 9

Further Study

There is a wide range of work for new exploration in the present field of research. We have exhibited formulation for problem and analytical/numerical solutions for hybrid nanofluid and non-Newtonian Eyring-Powell fluid inside this assortment of work. The properties of transfer of heat over a stretching sheet are examined theoretically. Surely there is a lot of study staying in this extremely intriguing new class of nanofluid called hybrid nanofluid and Eyring-Powell liquid model. Here we will talk about a few, however not all, of the numerous conceivable future extensions. Initially, it would be an intriguing extension to think about the heat transfer properties of hybrid nanofluid by taking different but suitable composite of nano particles with micropolar liquid over an exponentially stretched surface which have a lot of technological and industrial applications. However, there is a great deal of more examination that should be addressed in the field of Eyring Powell liquid. Forexample, study of Eyring Powell liquid in the context of unsteady flows over a wedge. no experimental examinations have yet occurred to the best of our information. Subsequently, the present piece of work obviously persuades the need for comprehensive experimental outcomes to think about for the comparison of this examination.

Bibliography

[1] S. Ostrach, Natural convection in enclosures, *J. Heat Transf*, 110 (1988) 1175–1190.

[2] L.J. Crane, Flow past a stretching plate, Z. Angew, *Math.Phys*, 21 (1970) 645-647.

[3] C.W. Wang, The three-dimensional flow due to a stretching flat surface, *Phys. Fluids*, 27 (1984) 1915–1917.

[4] W. Ibrahim and B. Shankar, MHD boundary layer flow and heat transfer of a nanofluid past a permeable stretching sheet with velocity, thermal and solute slip boundary conditions. *Comp. Fluids*, 75 (2013) 1–10.

[5] A.V Rosca and I. Pop, Flow and heat transfer over a vertical permeable stretching/shrinking sheet with a second order slip, *Int. J. Heat and Mass Transf*, 60 (2013) 355–364.

[6] R. Nazar, M. Jaradat, N. M. Arifin and I. Pop, Stagnation point flow past a shrinking sheet in a nanofluid, *Cent Eur J Phys*, 9(5), (2011)1195-1202.

[7] S.K Nandy and T.R Mahapatra, Effects of slip and heat generation/absorption on MHD stagnation flow of nanofluid past a stretching/shrinking surface with convective boundary conditions, *Int. J. Heat and Mass Transf*, 64 (2013) 1091–1100.

[8] V. Kumaran, A.K Banerjee, A. Vanav Kumar and I. Pop, Unsteady MHD flow and heat transfer with viscous dissipation past a stretching sheet, *Int. Comm. Heat and Mass Transf*, 38 (2011) 335–339.

[9] M. Turkyilmazoglu, Multiple solutions of heat and mass transfer of MHD slip flow for the viscoelastic fluid over a stretching sheet, *Int. J. of Thermal Sciences*, 50 (2011)2264–2276.

[10] A. Ishak, R. Nazar and I. Pop, Unsteady mixed convection boundary layer flow due to a stretching vertical surface, *Arab. J. Sci. Eng*, 31 (2006) 165–182.

[11] A. Ishak, R. Nazar and I. Pop, MHD boundary-layer flow due to a moving extensible surface, *J. Eng. Math.*, 62 (2008) 23–33.

[12] A. Ishak, R. Nazar and I. Pop, Magnetohydrodynamic (MHD) flow and heat transfer due to a stretching cylinder, *Energ. Convers. Manage*, 49 (2008) 3265–3269.

[13] K.L Hsiao, Numerical solution for Ohmic Soret-Dufour Heat and Mass Mixed Convection of Viscoelastic Fluid over a Stretching Sheet with Multimedia

Physical Features, *J. Aerospace. Eng.*, doi:10.1061/(ASCE)AS. (2016) 1943-5525.0000681.

[14] N.A Yacob, A. Ishak, I. Pop and K. Vajravelu, Boundary layer flow past a stretching/shrinking surface beneath an external uniform shear flow with a convective surface boundary condition in a nanofluid, *Nanoscale Res. Lett.*, 6 (2011) Article Number 314.

[15] M. Hussain, M. Ashraf, S. Nadeem and M. Khan, Radiation effects on the thermal boundary layer flow of a micropolar fluid towards a permeable stretching sheet, *J. Franklin Inst.*, 350 (2013) 194-210.

[16] M. K Laha, P. S Gupta, and A. S Gupta, Heat transfer characteristics of the flow of an incompressible viscous fluid over a stretching sheet, *Wärme−Stoffü bertrag.*, 24(1989) 151-153.

[17] M. E Ali, On thermal boundary layer on a power-law stretched surface with suction and injection, *Int. J. Heat Fluid Flow*, 16 (1995) 280-290.

[18] A. Ishak, K. Jafar, R. Nazar and I. Pop, MHD stagnation point flow towards a stretching sheet. *Physica A* (2009); 388: 3377-838.

[19] S. Nadeem, A. Hussain, and M. Khan. "HAM solutions for boundary layer flow in the region of the stagnation point towards a stretching sheet." *Communications in Nonlinear Science and Numerical Simulation*15.3 (2010): 475-481.

[20] Elbashbeshy, Heat transfer over an exponentially stretching continuous surface with suction, *Arch. Mech.*, 53, (2001) 643-651.

[21] S. K Khan and E. Sanjayanand, Viscoelastic boundary layer flow and heat transfer over an exponentially stretching sheet, *Int. J. Heat Mass Transfer*, 48, (2005) 1534-1542.

[22] M. Q Al-Odat, R. A Damseh and T. A Al-Azab, Thermal boundary layer on an exponentially stretching continuous surface in the presence of magnetic field effect, *Int. J. Appl. Mech. Eng.*, 11, (2006) 289-299.

[23] B. J. Gireesha, G. M. Pavithra and C. S. Bagewadi, "Boundary Layer Flow and Heat Transfer of a Dusty Fluid over an Expo- nentially Stretching Sheet," *British Journal of Mathematics & Computer Science*, Vol. 2, No. 4, (2012), pp. 187-197.

[24] S. Nadeem, S. Zaheer and T. Fang, Effects of thermal radiation on the boundary layer flow of a Jeffrey fluid over an exponentially stretching surface, *Numer. Algorithms*, 57, (2011) 187-205.

[25] E. Magyari and B. Keller, Heat and mass transfer in the boundary layers on an exponentially stretching continuous surface, *J. Phys. D : Appl. Phys.*, 32(1999) 577-585.

[26] S. Nadeem and C. H. Lee, Boundary layer flow of nanofluid over an exponentially stretching surface, *Nanoscale Res. Lett.*, 7(2012) article 94.

[27] S.U.S. Choi, Enhancing thermal conductivity of a fluids with nanoparticles, *ASME Int.* 66(1995) 99-105.

[28] T. Hayat, R. Sajjad, A. Alsaedi, T. Muhammad and R. Ellahi, On squeezed flow of couple stress nanofluid between two parallel plates, *Results Phys* 7 (2017) 553-561.

[29] T. Hayat, R. Sajjad, A. Alsaedi, T. Muhammad and R. Ellahi, On MHD non-linear stretching flow of Powell-Eyring nanomaterial, *Results Phys* 7 535-543.

[30] R. Ellahi, M. Hassan and A. Zeeshan, Aggregation effects on water base Al2O3. nanofluid over permeable wedge in mixed convection, *Asia Pac. J. Chem. Eng*, Vol. 11 (2), (2016) 179-186.

[31] G.S Seth and M.K Mishra, Analysis of transient flow of MHD nanofluid past a non-linear stretching sheet considering Navier's slip boundary condition, *Advanced Powder Technology*, 28(2) (2017) 375-384.

[32] G.S Seth, R. Sharma, M.K Mishra and A.J Chamkha, Analysis of hydromagnetic natural convection radiative flow of a viscoelastic nanofluid over a stretching sheet with Soret and Dufour effects, *Eng. Comp.* 34 (2) (2017) 603-628.

[33] R. Tripathi, G.S Seth and M.K Mishra, Double diffusive flow of a hydromagnetic nanofluid in a rotating channel with Hall effect and viscous dissipation: active and passive control of nanoparticles, *Advanced Powder Technology*, 28 (10) (2017) 2630-2641.

[34] M. Hatami, S. Mosayebidorcheh and D. Jing, Two-phase nanofluid condensation and heat transfer modeling using least square method (LSM) for industrial applications, *Heat and Mass Transfer* 53(6) (2017) 2061-2072.

[35] T. Hayat and S. Nadeem, Induced magnetic field stagnation point flow of nanofluid past convectively heated stretching sheet with Buoyancy effects, *Chin. Phys. B* 25, no. 11 (2016): 114701.

[36] T. Hayat and S. Nadeem, The effects of MHD and buoyancy on Hematite water-based fluid past a convectively heated stretching sheet, *Neural Comput Appl* (2017): 1-8.

[37] T. Hayat and S. Nadeem, Flow of 3D Eyring-Powell fluid by utilizing Cattaneo-Christov heat flux model and chemical processes over an exponentially stretching surface, *Results in Physics* 8 (2017): 397-403.

[38] H. Chen, S. Witharana, Y. Jina, C. Kim and Y. Ding, Predicting thermal conductivity of liquid suspensions of nanoparticles (nanofluids) based on rheology, *Particuology* 7 (2009) 151-157.

[39] M. Zhou, G. Xia, J. Li, L. Chai and L. Zhou, Analysis of factors influencing thermal conductivity and viscosity in different kinds of surfactant solutions, *Exp Therm Fluid Sci* 36 (2012) 22-29.

[40] K. Kwak and C. Kim, Viscosity and thermal conductivity of copper oxide nanofluid dispersed in ethylene glycol, *Korea Aust Rheol J Journal* 17 (2005) 35-40.

[41] A.E. Kabeel, T.A.E. Maaty and Y.E. Samadony, The effect of using nanoparticles on corrugated plate heat exchanger performance, *Appl. Therm. Eng.* 52 (2013) 221.229.

[42] S.M. Peyghambarzadeh, S.H. Hashemabadi, S.M. Hoseini and M.S. Jamnani, Experimental study of heat transfer enhancement using water/ethylene glycol based nanofluids as a new coolant for car radiators, *Int J Heat Mass Transf.* 38 (2011) 1283-1290.

[43] S.M. Peyghambarzadeh, S.H. Hashemabadi, M. Naraki and Y. Vermahmoudi, Experimental study of overall heat transfer coefficient in the application of dilute nanofluids in the car radiator, *Appl. Therm. Eng.* 52 (2013) 8-16.

[44] W. Duangthongsuk and S.Wongwises, Comparison of the effects of measured and computed thermophysical properties of nanofluids on heat transfer performance, *Exp Therm Fluid Sci* 34 (2010) 616-624.

[45] G. G. Momin, Experimental investigation of mixed convection with water-Al2O3 & hybrid nanofluid in inclined tube for laminar flow, *IJSTR.* 2 (2013) 195-202.

[46] S. Suresh, K. Venkitaraj, P. Selvakumar and M. Chandrasekar, Synthesis of Al2O3-Cu/water hybrid nanofluids using two step method and its thermo physical properties. *Colloids Surf.*, A 388 (2011) 41- 48.

[47] S. Suresh, K. Venkitaraj, P. Selvakumar and M. Chandrasekar, Effect of Al2O3-Cu/water hybrid nanofluid in heat transfer, *Exp Therm Fluid Sci.*, 38 (2012) 54 -60.

[48] S. Suresh, K. P. Venkitaraj, M. S. Hameed, and J. Sarangan, Turbulent Heat Transfer and Pressure Drop Characteristics of Dilute Water Based Al2O3-Cu Hybrid Nano fluids. *J. Nanosci. Nanotechnol.* 14 (2014) 2563-2572.

[49] J.B.J Fourier, Théorie Analytique De La Chaleur. Paris 1822.

[50] C. Cattaneo, Sulla conduzione del calore. Atti Semin Mat Fis Univ Modena Reggio Emilia.(1948); 3: 83-101.

[51] C.I Christov, On frame in different formulation of the Maxwell-Cattaneo model of finite-speed heat conduction, *Mech Res Commun.* 2009;36: 481-486.

[52] V. Tibullo and V. Zampoli, A uniqueness result for the Cattaneo-Christov heat conduction model applied to incompressible fluids, *Mech Res Commun.* (2011); 38: 77-79.

[53] B. Straughan, Thermal convection with the Cattaneo-Christov model. *Int J Heat Mass Transfer.* (2010); 53: 95-98.

[54] B. Straughan, Acoustic waves in a Cattaneo-Christov gas. *Phys Lett A*. (2010); 374: 2667-2669.

[55] B. Straughan, Gene-culture shock waves. *Phys Lett A*. (2013); 377: 2531–2534.

[56] S. Han, L. Zheng, C. Li and X. Zhang, Coupled flow and heat transfer in viscoelastic fluid with Cattaneo-Christov heat flux model. *Appl Math Lett*. (2014); 38: 87-93.

[57] M.A. Chaudhary and J.H. Merkin, A simple isothermal model for homogeneous heterogeneous reactions in boundary layer flow: I. Equal diffusivities, *Fluid Dyn. Res*.16. (1995); 311-333.

[58] N. Bachok, A. Ishak and I. Pop, On the stagnation point flow towards a stretching sheet with homogeneous–heterogeneous reactions effects, *Commun. Non−linear Sci. Numer. Simul*. (2011); 16: 4296-4302.

[59] W.A. Khan and I. Pop, Effects of homogeneous-heterogeneous reactions on the viscoelastic fluid towards a stretching sheet, *ASME J. Heat Transf*. (2012); 134: 064506 1-5.

[60] H. Zaman, Am. *J. Comput.Math*. 3 (2013) 313.

[61] A. Mushtaq, M. Mustafa, T. Hayat, M. Rahi and A. Alsaedi, *Z. Naturforsch.A* (2013) 68- 791.

[62] M. Jalil, S. Asghar and S.M Imran, *Int.J. Heat Mass Transfer* (2013) 65-73.

[63] M. Poonia and R. Bhargava *J.Thermophys.Heat Transfer*, (2014), 28-499.

[64] R.E Powell and H. Eyring, Mechanisms for the relaxation theory of viscosity. *Nature* (1944); 154:427-8.

[65] N.S Akbar and S. Nadeem, Characteristics of heating scheme and mass transfer on the peristaltic flow for an Eyring-Powell fluid in an endoscope. *International Journal of Heat and Mass Transfer* (2012); 55:375-83.

[66] A.V Rosca and I. Pop, Flow and heat transfer of Powell-Eyring fluid over a shrinking surface in a parallel free stream [J]. *International Journal of Heat and Mass Transfer*, (2014), 71: 321-327.

[67] T. Hayat and S. Nadeem, Aspects of developed heat and mass flux models on 3D flow of Eyring-Powell fluid, *Results in Physics*, (2017): 3910-3917 https://doi.org/10.1016/j.rinp.(2017).09.048.

[68] R. Ul Haq, S. Nadeem, Z.H. Khan and N.F.M. Noor, Convective heat transfer in MHD slip flow over a stretching surface in the presence of carbon nanotubes, *Physica B* 457 (2015) 40-47.

[69] O.D. Makinde , W.A. Khan and Z.H. Khan, Buoyancy effects on MHD stagnation point flow and heat transfer of a nanofluid past a convectively heated stretching/shrinking sheet, *International Journal of Heat and Mass Transfer* 62 (2013) 526-533.

[70] S. J. Liao, Homotopy analysis method in non-linear differential equations. Springer and Higher Education Press, Heidelberg (2012).

[71] L.F Shampine , I. Gladwell and S. Thompson, Solving ODEs with Matlab. Cambridge University Press: Cambridge; (2003).

[72] L.F Shampine, M.W Reichelt and J. Kierzenka, Solving boundary value problems for ordinary differential equations in MATLAB with bvp4c . http://www.mathworks.com/bvptutorial.

[73] S. Suriya Uma Devi and S.P Anjali Devi, *Can J Phys*. 94.5 (2016) 490.

[74] S. Mukhopadhyay and R.S.R Gorla, Effects of partial slip on boundary layer flow past a permeable exponential stretching sheet in presence of thermal radiation, *Heat Mass Transfer* (2012); 48:1773–81.

[75] S. Mukhopadhyay, Slip effects on MHD boundary layer flow over an exponentially stretching sheet with suction/blowing and thermal radiation. *Ain Shams Eng J* (2013);4:485–91.

[76] M. Mahmoodi and Sh. Kandelousi, Analysis of the hydrothermal behaviour and entropy generation in a regenerative cooling channel considering thermal radiation. *Nucl Eng Des* (2015);291:277–86.

[77] M.M Rashidi, N. Vishnu Ganesh, A.K. Abdul Hakeem and B. Ganga, *J. Mol. Liq*. 198, 234 (2014).

[78] T. Hayat and S. Nadeem, *Results in Physics* 7 (2017): 2317-2324.

[79] M. Khan, M. Irfan, W.A. Khan and L. Ahmad, Modeling and simulation for 3D magneto Eyring–Powell nanomaterial subject to nonlinear thermal radiation and convective heating, .*Results in Physics* , 7 (2017) 1899-1906.

[80] W.A. Khan, M. Irfan, M. Khan, A.S. Alshomrani, A.K. Alzahrani and M.S. Alghamdi, Impact of chemical processes on magneto nanoparticle for the generalized Burgers fluid, *J. Mol. Liq.*, 234 (2017) 201-208.

[81] M. Turkyilmazoglu, Determination of the Correct Range of Physical Parameters in the Approximate Analytical Solutions of Nonlinear Equations Using the Adomian Decomposition Method, *Mediterranean Journal of Mathematics*, 13 (2016) 4019-4037.

[82] M. Patel and M.G Timol, Numerical treatment of Powell-Eyring fluid flow using method of satisfaction of asymptotic boundary conditions (MSABC). *Applied Numerical Mathematics*, 59(10)(2009), pp.2584-2592.

[83] Y. Dong, B.Y Cao and Z.Y Guo, Generalized heat conduction laws based on thermomass theory and phonon hydrodynamics. *Journal of Applied Physics*, 110(6)(2011), p.063504.

[84] I.C Liu, H.H Wang and Y.F Peng, Flow and heat transfer for three-dimensional flow over an exponentially stretching surface. *Chemical Engineering Communications*, 200(2)(2013), pp.253-268.

[85] C.S.K Raju, N. Sandeep and S. Saleem, Effects of induced magnetic field and homogeneous–heterogeneous reactions on stagnation flow of a Casson fluid. *Engineering Science and Technology, an International Journal*, 19(2)(2016), pp.875-887.

[86] J. Sui, L. Zheng and X. Zhang, Boundary layer heat and mass transfer with Cattaneo- Christov double-diffusion in upper-convected Maxwell nanofluid past a stretching sheet with slip velocity. *Int.J.Thermal Sci.* (2016);104:461-8.